CHARLES UNIVERSITY OF PRAGUE

FACULTY OF PHYSICAL EDUCATION AND SPORT

HUMAN AXIAL SYSTEM: IDENTIFICATION OF CONNECTIVE TISSUES CHANGES

DIPLOMA THESIS

Academic advisor: Student:

Mgr. Šárka Panská   Bc. Jana Sacherová

Prague, 2013

UNIVERZITA KARLOVA V PRAZE

FAKULTA TĚLESNÉ VÝCHOVY A SPORTU

AXIÁLNÍ SYSTÉM ČLOVĚKA: MOŽNOSTI IDENTIFIKACE ZMĚN POJIVOVÝCH TKÁNÍ

DIPLOMOVÁ PRÁCE

Vedoucí diplomové práce: Vypracovala:

Mgr. Šárka Panská   Bc. Jana Sacherová

Praha, 2013

I confirm, I have written this thesis by my own with the use of literature mentioned in the bibliographic citation part. This work or its essential part has not been presented to obtain the same or another academic degree.

In Prague, ……………………………

<div align="right">Jana Sacherová</div>

Evidenční list

Souhlasím se zapůjčením své diplomové práce ke studijním účelům. Uživatel svým podpisem stvrzuje, že tuto diplomovou práci použil ke studiu a prohlašuje, že ji uvede mezi použitými prameny.

Jméno a příjmení:	Fakulta / katedra:	Datum vypůjčení:	Podpis:

ABSTRACT

Title: Human axial system: identification of connective tissues changes

Objectives: The main objective of this thesis was to compile a review of techniques and methods currently used in identification of connective tissues changes.

Methods: The method used in this thesis is a critical literature review – a study of research papers from available information sources accompanied by author's comments. Foreign sources are represented mostly by research papers accessible via electronic archives such as ScienceDirect, Pubmed, Springer, Wiley. Also other foreign publications were used. The theoretical part is focused on basic anatomy and physiology of the spine and states main methods of identification of connective tissues changes involved in this area. The main part describes particulars of researches dedicated to identification of functional and morphological characteristics of different spinal components.

Results: In addition to classic methods of spinal research, the thesis introduces also new developing techniques and methods. Procedures used in current research are described; their advantages and limits are explained.

Key words: spine, biomechanics, loading, intervertebral disc, method

ABSTRAKT

Název: Axiální systém člověka: možnosti identifikace změn pojivových tkání

Cíle: Hlavním cílem práce bylo sestavení přehledu technik a metod využívaných k identifikaci změn pojivových tkání páteře.

Metody: Práce je zpracována metodou kritické literární rešerše – zpracování literárních pramenů z dostupných zdrojů doplněné komentáři autora práce. Zahraniční zdroje využité v této práci jsou zejména odborné články z elektronických databází ScienceDirect, Pubmed, Springer, Wiley. Dále pak autor čerpal ze zahraničních odborných publikací. Teoretická část práce slouží k představení problematiky anatomie a fyziologie páteře a uvádí stručný přehled metod výzkumu těchto pojivových tkání. Hlavní část se věnuje popisu jednotlivých výzkumů, zaměřených na detekci funkčních a tvarových vlastností jednotlivých částí axiálního systému člověka.

Výsledky: Práce seznamuje čtenáře s již klasickými metodami výzkumu z této oblasti a doplňuje tento výčet o metody nové, teprve se rozvíjející. Práce popisuje, jaké techniky se používají v současných výzkumech a vysvětluje jejich přínos či nedostatky.

Klíčová slova: páteř, biomechanika, zátěž, meziobratlová destička, metoda

TABLE OF CONTENTS

1. INTRODUCTION

The Olympic logo *Citius, altius, fortius* (faster, higher, stronger) expresses the wish to be better and better in sports performances. Pressure on athletes in enormous due to the fact that sport is a part of business and entertainment in the society these days. No wonder we witness more injuries, microtraumatic illnesses and sudden heart attacks in professional sport. The reason is simple, the human body is not a machine and it has its musculoskeletal limitations.

On the other hand, our society is dealing with the decrease of physical activity in everyday life. Sedentary lifestyle begins in early childhood and is mostly connected to computer usage and other Hi-tech devices. Content of many jobs has also turned into sitting in front of the screen.

To sum up, meanwhile many people are dealing with a problem of absence of an exercise in their everyday life, professional athletes suffer from having too much exercise. We all agree both extremes are dangerous for human body.

How influenced is the axe of our body, the spine, by activities we pursue or we do not pursue during our lifetime? From little children with scoliosis, through adults with low back pain to elderly people with herniated disc; back problems occur all across the population and, of course, not necessarily in this order. Factors are countless – working position, genetics, sport, nutrition, sudden injury etc.

Changes in our spine may be divided into different categories according to the type of tissue. Intervertebral discs with its complex structure of peripheral fibrous ring, gelatinous centre and cartilaginous endplates may experience changes due to loading, ageing or injury. Bones (vertebrae, if the spine is discussed) are not there only to attach muscles; they work as a dynamic organ with network of nerves and blood vessels. During the lifespan bones are constantly changing and remodelling depending on external circumstances such as loading, injuries, immobility and nutrition.

The purpose of this thesis is to show different imaging and measuring methods used in identification of connective tissues changes of the spine in the last decade (after the year 2000). How the geometry of vertebrae may be determined? How to trace age-related changes in spinal components? How to develop artificial materials that could substitute overused human tissue? On the field of these broad terms and questions, this thesis will

be concentrated mainly on the "HOW"; it means what the techniques and methods used in spinal research are.

The expected contribution of this study is a formation of complex review of research methods, focused on the axial system, described and published in internationally recognized journals.

2. THEORETICAL BACKGROUND

2.1 The Spine

The *Spine Technology Handbook* (Kurtz and Edidin, 2006) describes the spine as a complex structure with hard and soft tissue constituents. The hard elements are the bones, the *vertebrae*, which protect the vulnerable spinal cord and nerves. The structure and function of the vertebrae slightly change along the length of the spine, but generally, each vertebral body has an anterior part designed for sustaining compressive loads and posterior part with elements for protection of the spinal cord and elements for anchoring the muscles. Between every two vertebral bodies is situated the intervertebral disc that provides a support and cushioning against mechanical loads together with ensuring an adequate flexibility. The whole spinal column is tied together by ligaments and actuated by muscles.

The spine is divided into 4 regions: *cervical*, *thoracic*, *lumbar*, and *sacral* (Figure 1). C1 – C7 (in the cranial-to-caudal direction) are seven *cervical vertebrae* of the neck. They provide maximum flexibility and range of motion for the head. The discs are designated based on their adjacent vertebral bodies (e.g., C1-C2 for the disc between C1 and C2). The *thoracic vertebrae* (T1 – T12) provide a support to the ribs and the organs that hang from them. Compared to the cervical region, the flexibility in the thoracic region is rather limited. The five *lumbar vertebrae* (L1 through
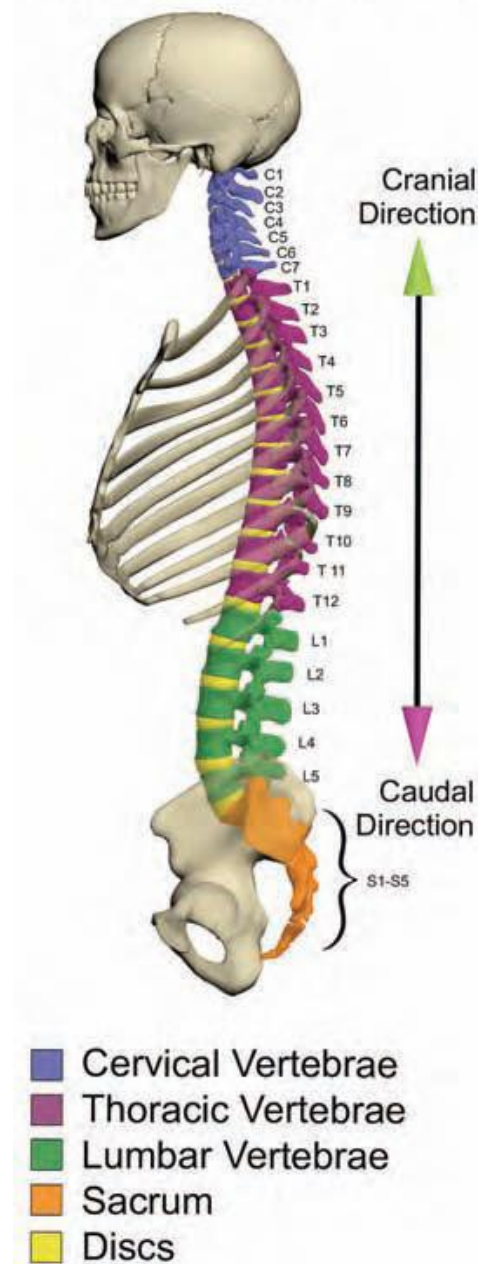

Figure 1 Cervical, thoracic, lumbar, and sacral regions of the spine (Courtesy of Christopher Espinosa, Exponent, Inc), (Kurtz and Edidin, 2006).

12

L5) are subjected to the highest loading of the spine therefore their bodies are the largest and strongest to ensure appropriate structural support. The *sacrum* is attached to the spine at L5-S1 joint and to the illiac bones of the pelvis at the sacroilliac joint. The coccyx, located inferior to the sacrum, is the most caudal region of the spine.

Spine joint needs to allow the rocking movements that are necessary if flexion and extension or lateral bending are to occur. Equally it has to bear the weight of the human body and has to assure stability of the joint (Bogduk, 2005). So a layer of strong but deformable soft tissue is indispensable: the intervertebral disc.

2. 1. 1 The Intervertebral Disc

The intervertebral disc (IVD) is a soft tissue structure situated between each of the 24 vertebrae of the human spine. There are a total of 23 discs in the entire length of the spinal cord. When the high of all the discs (approximately 8-10 mm in height and 4 cm in diameter) are considered, they comprise approximately 25% of the total height of the vertebral column (Shankar et al., 2009). IVD is the largest nonvascular structure of the human body. Additionally, the intervertebral discs are largely aneural (with nerve endings reaching only the periphery of the tissue), and the intervertebral discs are only sparsely populated with cells. The intervertebral discs vary in size and shape with spinal level. A small, round cross sectional shape in the cervical spine progresses to a larger, more kidney-like cross sectional shape in the lumbar spine to accommodate the mechanical requirements at different levels of the spine (Kurtz and Edidin, 2006) .
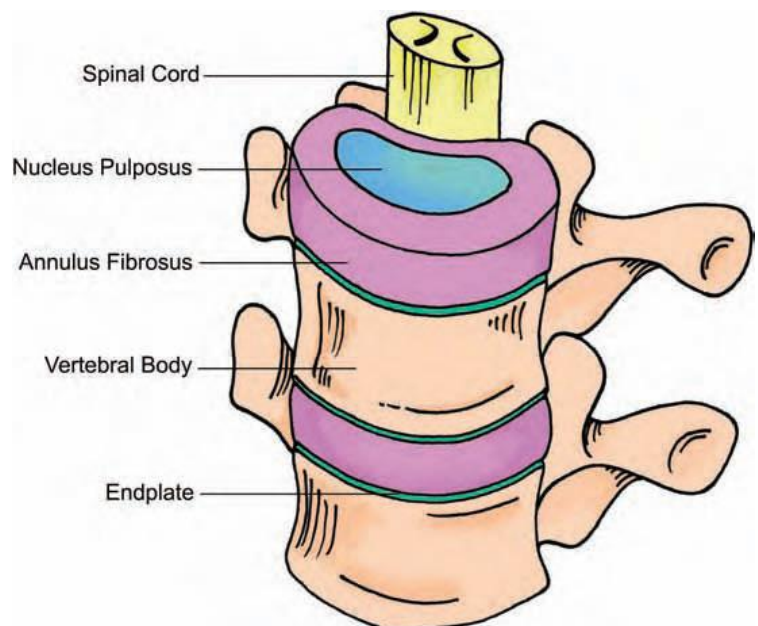
Figure 2. Spinal motion segment with intervertebral discs and spinal cord.(Kurtz and Edidin, 2006)

Unlike the size and shape, the general structure remains the same along the length of the spine and ensures the flexibility (allowing bending, flexion, extension and torsion) and

13

load-bearing capacity (transmitting loads from body weight and muscle activity through the spinal column).

The structure of each IVD has three main components: a peripheral fibrous ring (*annulus fibrosus*) which surrounds the gelatinous, hydrated centre of the intervertebral disc (*nucleus pulposus*) and the *end plates*, which are situated above and below each intervertebral disc, adjacent to the vertebrae (Figure 2) (Kurtz and Edidin, 2006).

2. 1. 2 Ligaments

Besides the muscles, the vertebrae are also held together by ligaments that join each of the components of the vertebrae except for the pedicles (the spinal nerves have to pass between these in the intervertebral foramina). Thus there are anterior and posterior longitudinal ligaments joining the front and back of the bodies, supraspinous and interspinous ligaments, itertransverse ligaments, ligamenta flava (which contain much elastic tissue and join the laminae) and capsular ligaments of the synovial joints between the articular processes (Faiz and Moffat, 2002).

2. 1. 3 Loading of the spine

Any load through the spinal column is transmitted to the intervertebral disc from the vertebral body. Under loading, the nucleus pulposus acts like a fluid-filled bag and swells under pressure due to the hydrophilic nature of the proteoglycans. In this manner, a circumferential tension is applied to the annulus, converting it to a load-bearing structure. The whole construct acts as a shock absorber for the spine such that there is no high-spot loading at any point. This also allows for complex motion to occur (Kurtz and Edidin, 2006)

2. 2 Age related changes and degeneration of the spine

Age related changes firstly appear at the biochemical level. The rate of synthesis and the overall concentration of proteoglycans in NP decrease. Collagen content of NP and AF increase with aging, but the concentration of elastic fibres in the annulus drops. Aging is associated also with decrease of water content in NP. Thus, the discs become drier with age, and with increase in collagen and the loss of elastin, they become more fibrous and less resilient. These biochemical changes affect the microbiomechanical and overt biomechanical properties of the spine.

Biomechanical changes are ultimately reflected in the morphology of different components of the spine and its patterns of movement.

2. 2. 1 Low back pain

Back pain can range from a dull, constant ache to a sudden, sharp pain that makes it hard to move. It can start quickly with a fall or with lifting something too heavy, or it can get worse slowly. The causes of back pain may be for example disc breakdown, spasms, tense muscles, ruptured discs or any kind of injury. Treatment for back pain generally depends on what kind of pain you experience: acute or chronic. Acute back pain usually gets better on its own and without treatment, with a help of medicaments to ease the pain. Exercises or surgery are not usually advisable for acute back pain. Treatment for chronic back pain may be an exercise or a surgery (http. 1).

2. 2. 2 Degenerative disc disease

Degenerative disc disease (DDD) brings alternations of the biomechanical properties of the disc and it is closely associated with low back pain. The causes of the disc degeneration might be a genetic predisposition, aging, overloading, underloading or loss of nutrition. Once degeneration sets in, the intervertebral disc goes through a cascade of degenerative changes that result in biomechanical alteration of load transfer through the disc, in turn causing changes in the mechanical properties and composition of the tissue. Structural disorganization of the intervertebral disc along with loss in proteoglycans stemming from degeneration causes the hydrostatic mechanism to fail. There are different ways a degenerated disc can lead to low back pain, depending on if the degeneration occurs in the nucleus pulposus or the annulus fibrosus. A degenerated annulus can have fissures, tears, concentric cracks, cavities, and radiating ruptures. Disc

bulging may occur due to decrease in the radial tensile strength of the annulus. Degeneration of the nucleus occurs following loss of water content leading to collagenation of the nucleus. This results in an increase of the elastic modulus of the nucleus. Nucleus degeneration combined with annular degeneration may cause disc herniation into the spinal canal, causing low back pain due to nerve pinching. Thinning of the disc and loss of disc height are also seen in a degenerated disc. This loss of disc height combined with gradual ossification of the end plate and protrusion of the disc tissue causes stenosis, which again leads to back pain (Kurtz and Edidin, 2006).
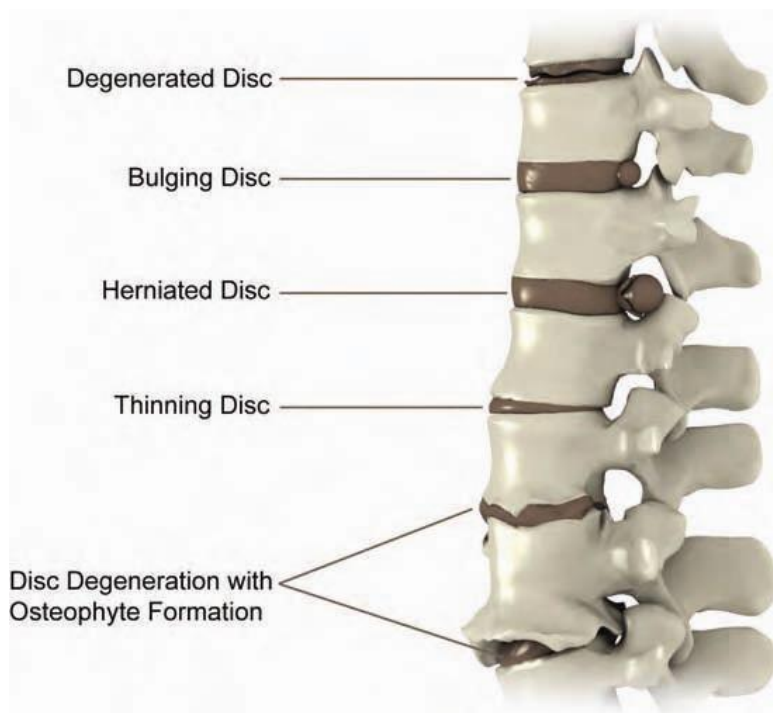
Figure 3 Intervertebral disc disease (Kurtz and Edidin, 2006)

For identification of the level of disc degeneration the Thompson grading scale (Thompson et al., 1990) is most frequently used. It is a five-category grading scheme (I – V) which distinguish various stages of degeneration according to its morphology. Different parts of intervertebral motion segment (nucleus pulposus, annulus fibrosus, endplate, vertebral body) are evaluated as shown in Table 1.

Grade	Nucleus	Anulus	End-plate	Vertebral body
I	Bulging gel	Discrete fibrous lamellas	Hyaline, uniformly thick	Margins rounded
II	White fibrous tissue peripherally	Mucinous material between lamellas	Thicness irregular	Margins pointed
III	Consolidated fibrous tissue	Extensive mucinous infiltration; loss of anular-nuclear demarcation	Focal defectsin cartilage	Early chondrophytes or osteo phytes at margins
IV	Horizontal clefts parallel to end-plate	Focal disruptions	Fibrocartilage extending from subchondral bone; irregularity and focal sclerosis in sub-chondral bone	Osteophytes less than 2 mm
V	Clefts extend through nucleus and anulus		Diffuse sclerosis	Osteophytes greater than 2 mm

Table 1 Description of the morphologic grades (Thompson et al., 1990).

2. 2. 3 Osteoporosis

To understand properly the notion of osteoporosis, it is necessary to explain terms Bone Mineral Content (BMC) and Bone Mineral Density (BMD) Bone mineral content represents the total grams of bone mineral within a measured region of bone meanwhile bone mineral density stands for the grams of bone mineral per unit of bone area scanned. This use of the term density is not technically correct; in physics, density is defined as mass per unit volume. The quotient of bone mineral content and area gives a two-dimensional picture and is therefore often described as an *areal density*. Bone mineral content is highly dependent on bone size, thus a larger person will have a greater value than a smaller person. When bone strength is increased through changes in size as well as in mineral content (as might be the case for physical activity during growth), BMD alone would not detect this, so these two measures are complementary (Hardman and Stensel, 2009).

Osteoporosis (literally meaning 'porous bones') is a skeletal disorder characterized by low bone mass and microarchitectural deterioration of bone tissue, with a consequent increase in fragility and susceptibility to fracture (Figure 4). Diagnosis relies on measurements of BMD at the hip as a proxy measure of bone strength. The World Health Organization (WHO) operationally defines osteoporosis as bone density 2.5 standard deviations below the mean for young white adult women, based on DXA scan results. Osteopenia (low BMD not reaching a threshold for diagnosis of osteoporosis) is identified when BMD is 1–2.5 standard deviations below this mean (Hardman and Stensel, 2009). The same authors give a list of risk factors for primary osteoporosis including female sex, age greater than 60 years, family history of osteoporosis, prolonged immobility, smoking, eating disorder etc. Possible treatment represents

bisphosponates (inhibitors of bone turnover) and calcium and vitamin D supplementation. Well known prevention of osteoporosis is a mechanical loading i. e. physical activity. Gormley and Hussey (2005) state that in general, studies have found an increase in the density of weight-bearing long bone with exercise training. However, the mechanism behind this observation is not well understood. This adaptation appears to be regardless of gender and age.

(a)   (b)
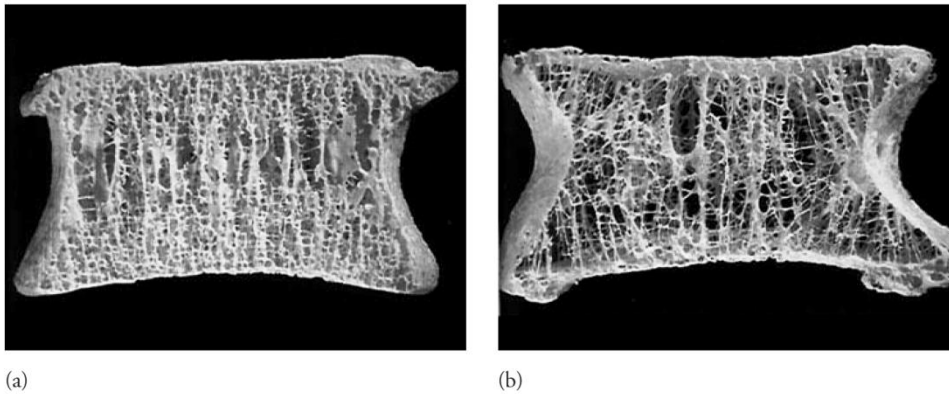
Figure 4 Osteoporotic changes in lumbar vertebrae. The strong vertebral bodies of (a) early adult life lose much of their structure and become prone to crush fractures as weight-bearing capacity diminishes (b) (Hardman and Stensel, 2009; source: L Mosekilde MD, DMSci).

2. 3 Treatment of the spine

The primary standard treatment for intractable back pain unresponsive to nonsurgical treatment is decompression and fusion, which consists of immobilizing the spine using bone graft, metal plates or rods, and screws. Because fusion is irreversible and stops all motion at the implanted level, it can be perceived as an end-stage procedure, naturally opening the door to many earlier-stage motion-preserving technologies for treating the diseased spine. Motion-preservation technologies cover a wide range of techniques, including nucleus repair, total disc replacement, and vertebral fracture repair. Novel motion-preserving technologies, many of which are still under design, will require innovative implants and instruments for deployment in the body (Kurtz and Edidin, 2006).

2. 4 Methods of identification connective tissue changes

2. 4. 1 Imaging methods

Imaging methods are non-invasive diagnostic tools for treatment of DDD and low back pain and also serve as resources of data for spinal research. Plain radiographs (X-ray), computed tomography (CT) ultrasound and magnetic resonance imaging (MRI) are widely used; further methods are relatively new and mostly derived from these basic ones. Main features including strong and weak points of each method are presented:

Radiography

Plain radiography is relatively cheap, fast and simple method of diagnosis based on the use electromagnetic radiation of X-rays to view objects with different density and composition. Mostly, it is used to detect bone fractures. Each screening involves low dose of irradiation. On the other hand the sensitivity of imaging is low and the result is usually a lateral and frontal static 2-D picture (Kjær et al., 2003).

For purposes of this thesis a *dual energy X-ray absorptiometry* (DXA) needs to be described in detail. DXA uses X-ray beams of two distinct energy levels to distinguish the relative composition of bone and non-bone compartments of the body. The measurements are based on the degree to which the X-ray beam is attenuated by the tissues and two measures derived are BMC and BMD. The main limitation of DXA is that, although it measures all bone within a given area, it does not assess bone architecture nor does it differentiate between trabecular and cortical bone. Advantages of DXA include the low level of radiation exposure and its accuracy and precision (Hardman and Stensel, 2009).

Computed tomography uses X-rays with higher radiation than conventional radiography to make tomographic images (or "slices") of specific areas of the human body. From these pictures a 3-D models can be reconstructed. Although contrast resolution is greater in computed tomography than conventional radiographs the spatial resolution is significantly less. Waiting time is longer and price higher than plain radiography(Kjær et al., 2003).

Ultrasound

The ultrasound systems work on the principle of sound waves and echo sound. They are capable of high-resolution imaging of superficial structures, particularly superficial

tendons, but also other soft tissues (muscles, fluid accumulation in joints, bursae). The ultrasound examination demands high skill of an investigator but it is relatively cheap(Kjær et al., 2003).

Bone scintigraphy

Bone scintigraphy is an atraumatic, easily applied and relatively inexpensive technique uses a radioactive pharmaceuticals and external detectors (gamma cameras) to show actual bone metabolism. This method detects stress fractures and vascularisation (Kjær et al., 2003). Pećina and Bojanić (2004) describe bone scintigraphy as highly sensitive method, but with low specificity.

Magnetic resonance imaging

Due to its multiplanar capabilities, lack of ionizing radiation and superior soft tissue contrast, MRI is an important adjunct to conventional diagnostic examinations such as plain radiography, bone scintigraphy and ultrasound in assessing the magnitude and extent of soft tissue injury. Compared to bone scintigraphy, MR imaging has superior spatial resolution in localizing soft tissue injury, yet does not provide a direct measure of bone turnover. As such, these imaging tests are often complementary, rather than mutually exclusive. Moreover MRI ranks among the more expensive imaging methods. MRI is founded on the principle that certain nuclear species, such as hydrogen, possess inherent magnetic properties. When placed in a high-strength external magnetic field in contact with radio waves a resonance phenomenon occurs(Kjær et al., 2003). Kurtz and Edidin (2006) state that the anatomical features such as disc height, tears in the annulus, fissures in the nucleus, and the level of hydration in the nucleus can be assessed in a MRI image. They also explain one of the major disadvantages of MRI: previously placed instrumentation may cause an imaging artefact due to the metal. In such cases myelogram with postmyelographic computed tomography (with contrast medium) can be used.

New imaging strategies

Haughton (2004) explains that although CT and MRI provide excellent anatomic imaging of the spine, they do not reliably identify the source of pain in patients with intervertebral disc degeneration. In his study, new and potentially useful imaging strategies could be found, p. e. dynamic computed tomography, dynamic magnetic

resonance imaging, functional magnetic resonance imaging, diffusion imaging (see below), and magnetic resonance spectroscopy.

With MR, the Brownian movement of water molecules can be tracked and measured. Because tissue structure determines the direction and magnitude of water diffusion, diffusion imaging may be used to examine the structure of spinal tissues. Diffusion-weighted imaging (that measures a relative amount of water diffusion occurring within a voxel[1]) and its more sophisticated form, diffusion tensor imaging (DTI, which indicates the direction and magnitude of water diffusion in 3 dimensions in each voxel) can be applied to the study of the spinal cord or intervertebral disc. Diffusion imaging of the spine may provide a means for demonstrating early intervertebral disc degeneration (Haughton, 2004).

2. 4. 2 Analyse of images

The Fourier Transform is an important image processing tool which is used to decompose an image into its sine and cosine components. The output of the transformation represents the image in the Fourier or frequency domain, while the input image is the spatial domain equivalent. In the Fourier domain image, each point represents a particular frequency contained in the spatial domain image. The Fourier Transform is used in a wide range of applications, such as image analysis, image filtering, image reconstruction and image compression. (http. 2)

2. 4. 3 Mechanical testing devices

In vivo loading is directly measured by load cells implanted into the spine. Simulation of loading of the spine during *in vitro* testing is done by variety of mechanical testing devices and machines such as screw driven machine, hemispherical indenter, hexapod robot, fibreglass rods, pendulum apparatus etc. Everyone serves to simulate certain type or types of motion or loading. To each of them belongs software for recording and analysing results.

2. 4. 4 Numerical techniques

The progress of computer technologies opened up a whole new field of medical research. The goal of numerical techniques is to predict the behaviour of the spinal

---

[1] voxel (volumetric pixel) is a volume element, representing a value on a regular grid in 3D space

21

segments under certain circumstances that cannot be reached by experimental approach. Nevertheless, it has many limitations; development of a single numerical model requires lot of time and resources. Afterwards this one model is not adequate to all individuals, so it is hardly useful in diagnostics and treatment.

The *finite element (FE) method* was applied to the human spine in 1970s and since then it has played an increasingly important role in improving our understanding of the fundamental biomechanics of the spine. The principle of this numerical technique is to convert a single very complex problem into many very simple problems (Kurtz and Edidin, 2006).

Above mentioned see a future of FE method in establishment of a "virtual clinic" serving like a bank of models representing patients with certain pathologies, more certainty in the broad applicability of a particular candidate device could be obtained. Nowadays, no such clinic exists, but developments in the generation of FE models allow the possibility of their existence in the immediate future predict authors.

3. OBJECTIVES AND METHODS

3.1 Aims

The main purpose of this thesis is to present different imaging and measuring methods used in the last decade to identify connective tissues changes of human axial system.

The reason for use of English language is a lack of translated resources and the possibility to employ the most recent papers.

3.2 Assignments

Particular assignments of this thesis were:

- → To research information about mentioned topic using key words, according to time period, that was done.
- → To sort out the information gained according to different thematic categories and to compare different research papers to select appropriate ones to illustrate each chosen theme.
- → To present and compare different research papers.
- → To add personal critical comments and to create well-arranged tables.
- → To summarize the results according to the aims of the thesis.

3.3 Hypotheses

1. Concerning identification of connective tissue changes, *in vitro* measurements prevail over *in vivo* testing.
2. The field of spinal research is rather spreading and looking for new approaches, technologies and devices, than only improving the existing ones.

3.4 Research questions

For the purposes of this thesis, the following questions were asked:

- → How are the geometrical parameters of vertebrae and IVD measured?
- → Which are the possibilities of simulated loading of axial system?
- → What technologies are used within in vivo and in vitro studies of biomechanical properties of tissues?
- → How to identify degenerated tissue?
- → What techniques and materials are used in fabrication of spinal implants?

3. 5 Methods

The method used in this work is a literature review, thus it is a theoretical thesis.

Planning

The preparatory phase includes consultations with teachers and advisors from the department of anatomy and biomechanics and the department of gymnastics. The procedure was chart, main field of interest, criteria, hypotheses and research questions were defined.

Afterwards skimming and scanning of literature followed. The access to databases of articles was enabled to look for convenient sources, sorting out articles respecting the criteria given.

Analysing

This phase is comprised of deep reading of chosen articles and selecting information relevant to the topic incl. figures and tables.

Summarizing results

Finally, after the author reviews chosen articles in each chapter, information gained are compared and commented. Answers to research questions should be found. Hypotheses are confirmed or disproved.

3.6 Criteria of the literature review

Basic criteria were determined to narrow the field of searching:

1) Language: English
2) Time period: after 2000 (exception only if necessary to further understanding)
3) Type of literature: Research papers published in scientific journals
4) Key words: loading, IVD, spine, biomechanics, method
5) Sources: Pubmed, ScienceDirect, Springer, Wiley

4. CRITICAL REVIEW

4. 1 Geometry of vertebrae and intervertebral discs

Information on the exact shape and geometry the spinal components are important for understanding the biomechanics and morphology of the spine. Data on the three-dimensional anatomy of hard and soft tissues of the vertebral column make groundwork for further research in the field of the clinical diagnosis and management of the spine including the replacement of the IVD. Furthermore the design of suitable orthopaedic artificial implants and instrumentation depends on such information.

In this chapter, you can find a review of methods used in last decade to measure vertebral geometry (cadavers, MRI, radiography, CT). Results are summarized, mostly in figures and calculations. The equations used in the studies of vertebral geometry are mentioned as well. Where methods are based on previously led measurements, a description of these is taken from the original study.

Author & Year	Method(s)	Region of spine	Dimensions measured	Summary of results	Additional
Eijkelkamp (2002)	MRI, X-ray	lumbar	intervertebral disc height (IDH) anterior (ADH) middle (MDH) posterior (PDH) wedge angle endplate depth	Wedge angle increases from T12-L1 to L5-S1. Endplate depth increases from T12 to L5 and S1 is flat. The maximal average depth of the vertebral endplate relative to the edge is 1.7 mm (range -1.1 to 3.67 mm).	
Tan et al. (2004)	Cadavers	cervical thoracic lumbar	endplate area/depth/width pedicle height/inclination/width spinal canal area/depth/width spinous process length transverse process width vertebral body height	All dimensions are lower for the population group measured in comparison to Caucasian specimens, especially spinal canal area and pedicle values.	study on Chinese Singaporeans
Houwen et al. (2010)	CT	lumbar	intervertebral disc height (IDH) wedge angle endplate depth/width/area	A comprehensive data set of quantitative anatomy of the vertebral endplate. The depth of the inferior endplate generally increases toward the lower lumbar region (with T12 as an exception).	

Table 2 Geometry of vertebrae and IVDs

4. 1. 1 Magnetic resonance imaging (MRI) and radiography

A study to determine the height, wedge angle of the IVD and concavity of the lumbar vertebral endplate was led as a part of the thesis *On the Development of an Artificial Intervertebral Disc* (Eijkelkamp, 2002).

Methods used in this study were X-ray (radiography) for the wedge angle (Figure 5) and MRI for wedge angle, IVD height and endplate concavity (Figure 6).
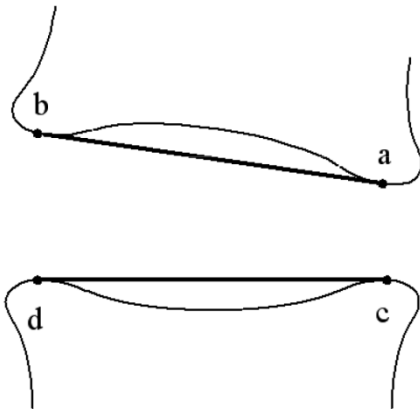
Figure 5 The measurement of the wedge angle of the lumbar vertebrae with X-ray. The angle between two lines drawn from the edges of the IVD was determined twice with software of the X-ray scanner and the mean was calculated for each two vertebrae. (Eijkelkamp, 2002)

Figure 6 Schematic design of the revised method of Brinkman: The anterior, middle and posterior disc height are determined by the rectangular distance to the middle line of the intervertebral disc. Note: The superior 'vertebra' is translated forward for a clearer view (Eijkelkamp, 2002) .

From the 3-D coordinates of 5 points on the surfaces in each scan of the MR were calculated the anterior (ADH), middle (MDH) and posterior disc height (PDH) of the IVD using a revised method of Brickmann (Frobin et al., 1997). The equations used were:
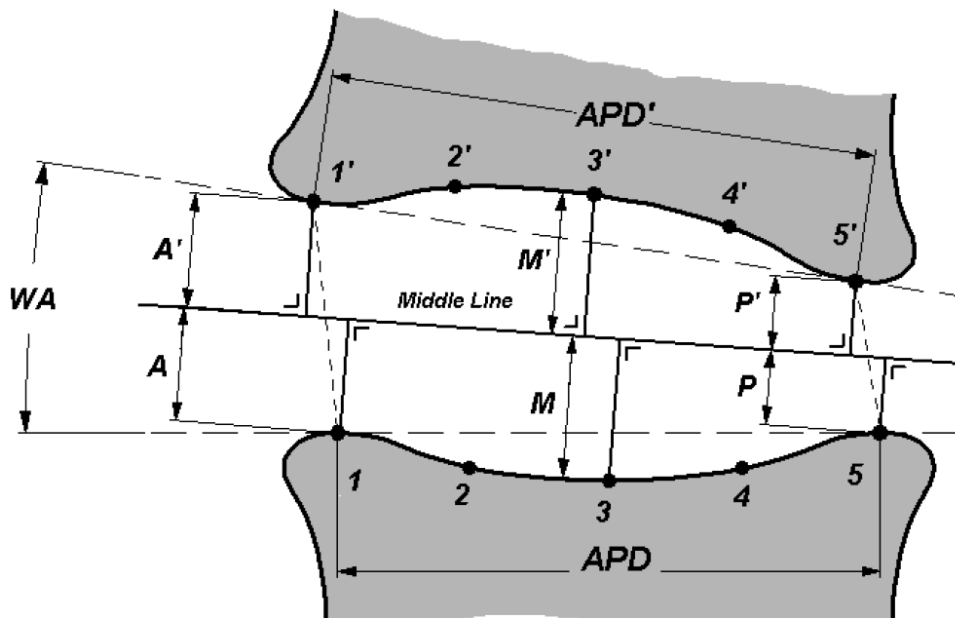
$$ADH = A + A'$$
$$MDH = M + M'$$
$$PDH = P + P' \quad \text{Equation 1}$$

The **wedge angle** of the IVD was calculated in Eijkelkamp's study in two ways:

1: MRI-normals method: The wedge angle of the intervertebral disc was calculated from the normals of the adjacent endplate planes.

2: MRI-heights method: The wedge angle was calculated from the posterior and anterior intervertebral disc heights using following equation (with WA the wedge angle):

$$WA = \sin^{-1} \frac{ADH - PDH}{\frac{1}{2}(APD + APD')} \quad \text{Equation 2}$$

The **concavity** of the vertebral endplate was determined using the method shown in Figure 7.
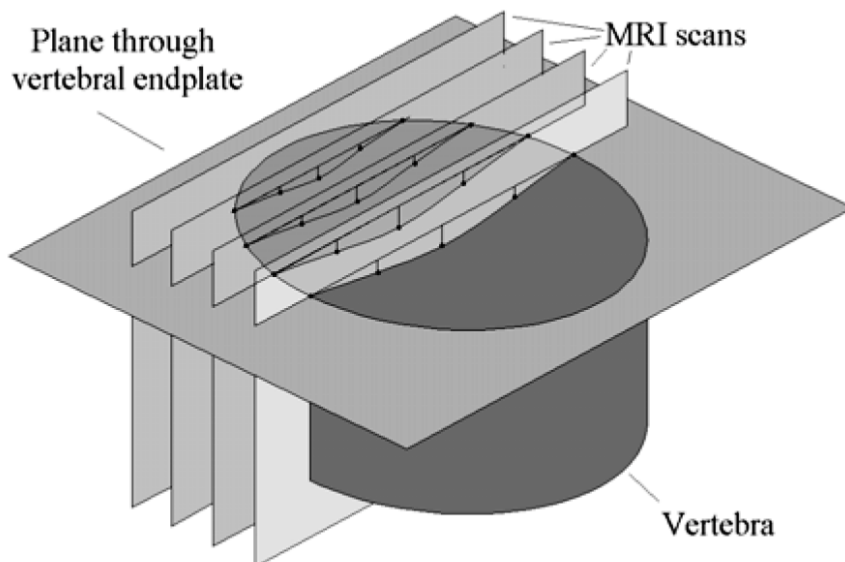
Figure 7 Schematic design of the method to determine the concavity (the depth) of the vertebral endplates. For each MRI scan, the perpendicular distance of the five points of the vertebral endplate to the endplate plane was calculated (Eijkelkamp, 2002).

Concerning results of the study, the **wedge angle** increases from T12- L1 to L5-S1. The wedge angle calculated with the MRI-normals method is slightly larger than the angle measured with the MRI-heights method as shown in Figure 8. The difference between the two methods to measure the wedge angle with MRI was limited. The differences of the X-ray method compared to the MRI method were within 20 percent.

Wedge angle of the Intervertebral Disc
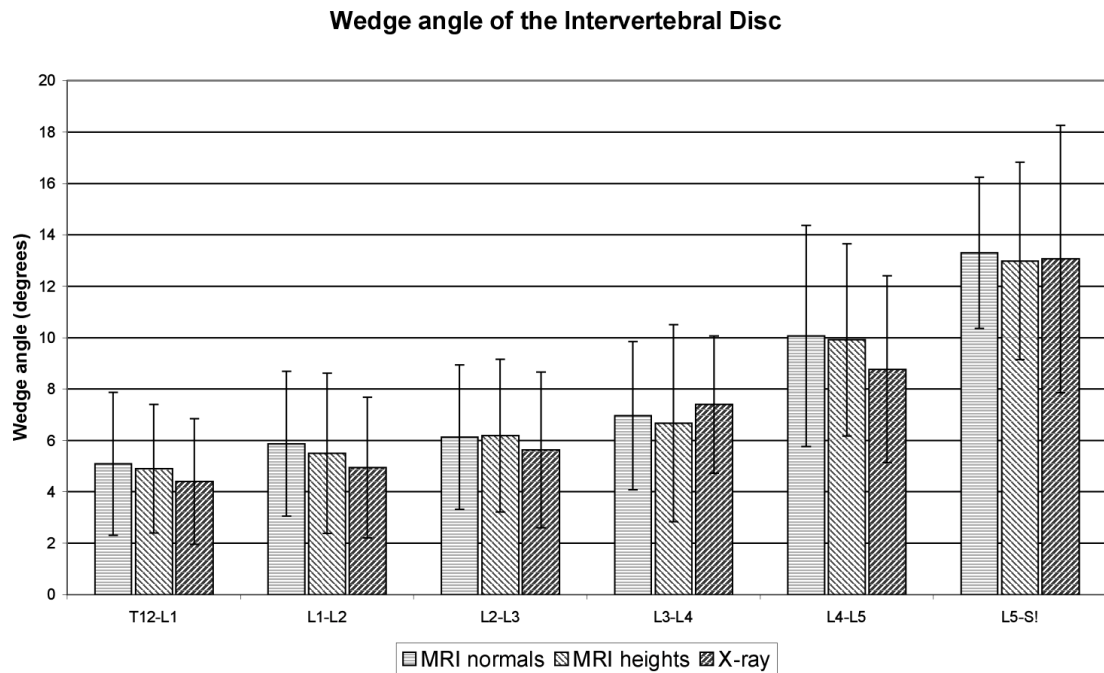
Figure 8 Wedge angle (with standard deviation) of the lumbar intervertebral discs in degrees with MRI-heights method, MRI-normals method and with X-ray measurements (Eijkelkamp, 2002).

Results of measurements of anterior, middle and posterior height of the IVD by MRI are summarized in Figure 9.

Intervertebral disc height
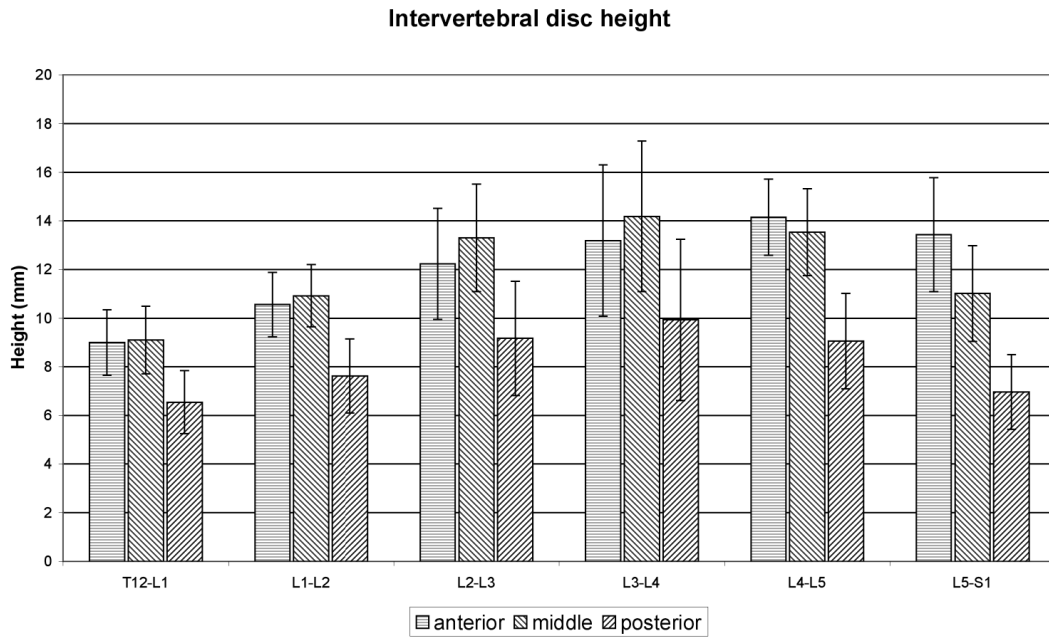
Figure 9 Anterior, middle and posterior height of the intervertebral disc (Eijkelkamp, 2002).

From results of Eijkelkamp´s study the average depth of the lumbar vertebral endplates in the middle of the disc is about 1.2 mm (range 0.1 to 1.8 mm). The maximum depth of the vertebral endplates is located at the posterior half of the vertebrae. More details are showed in Figure 10.

Depth of the endplates
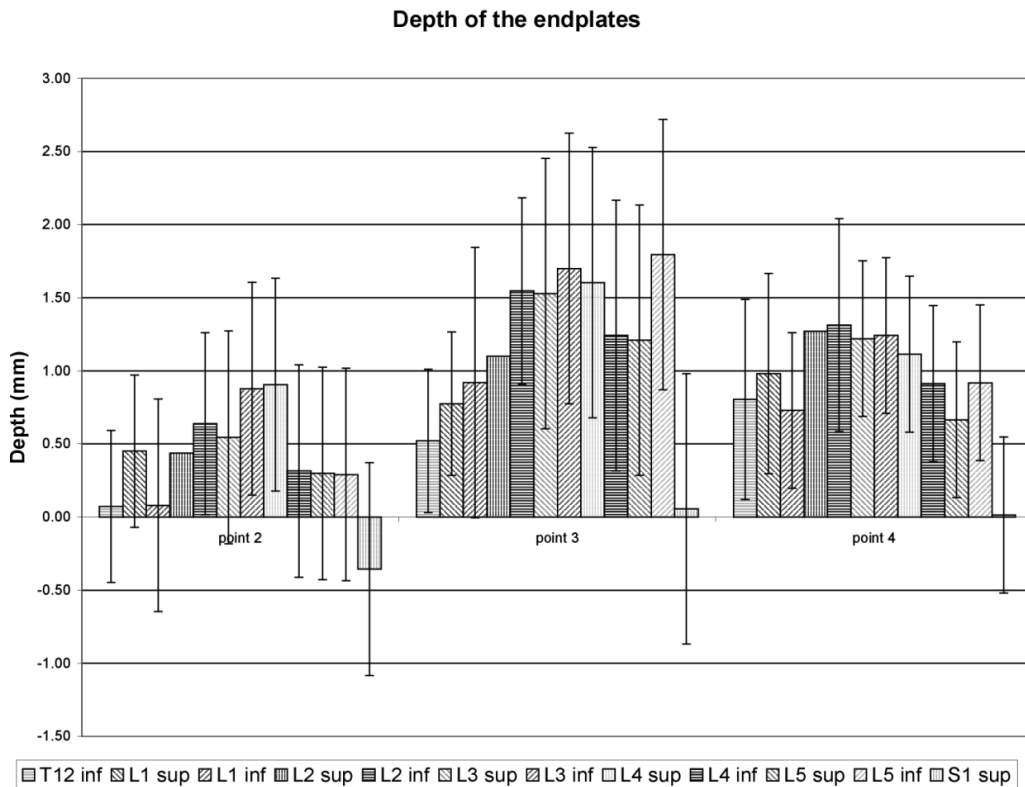
Figure 10 Depth (with standard deviation) of the lumbar vertebral endplates at 3 points (Eijkelkamp, 2002).

29

4. 1. 2 Study on cadavers

A series of three studies completed by Panjabi et al. details the quantitative three-dimensional surface anatomy of human vertebrae. The first study (Panjabi et al., 1991a) involves middle and lower cervical vertebrae, the second study (Panjabi et al., 1991b) describes thoracic vertebrae and the third study (Panjabi et al., 1992) details lumbar vertebrae. Data were measured on fresh autopsy spine specimens by a specially designed morphometer instrument. Marked points were identified and then measurements of three-dimensional coordinates of different points were taken and recorded directly into the computer. With these coordinates linear, angular and area dimensions were calculated, such as vertebral body height, endplate width, depth, area and inclination etc. (Figure 11). The purpose of their study was to provide information about geometry of particular vertebral components for constructing accurate mathematical models of human spine and also to help more precise clinical diagnosis and surgical management of spinal problems. This comprehensive data set may be as well used in designing of internal spine devices.

A decade later, a similar study was done on population of Chinese Singaporeans (Tan et al., 2004) and the data measured were put into comparison to Panjabi's study on Caucasian subjects. As a measuring instrument, a direct-contact, three-dimensional digitiser with an accuracy of 0.01 mm was used. The means and standard errors for linear, angular and area dimensions of the vertebral body, spinal canal, pedicle, spinous and transverse processes were measured for each vertebra.

The comparison with Panjabi (Table 3) revealed a difference between these two populations – the quantitative dimensions of vertebrae of Chinese Singaporeans are generally smaller than the respective values of the Caucasian specimens. Spinal canal area was smaller by 31.7% and researchers believe it may affect surgical management of the spine, especially low back pain in the lumbar spine, in the population of Chinese Singaporeans. Significantly smaller were also pedicle height and pedicle width values, the mean difference were -16.1% and 25.7%, respectively.

Comparison with studies measuring the pedicle length (Zindrick et al., 1987) (McLain et al., 2002) is shown in Figure 12. Based on the fact that the pedicles of Chinese Singaporeans are rather smaller, in this study by 22.1% on average, Tan et al. (2004) suggest the use of a transpedicle screw may not be suitable for this population.
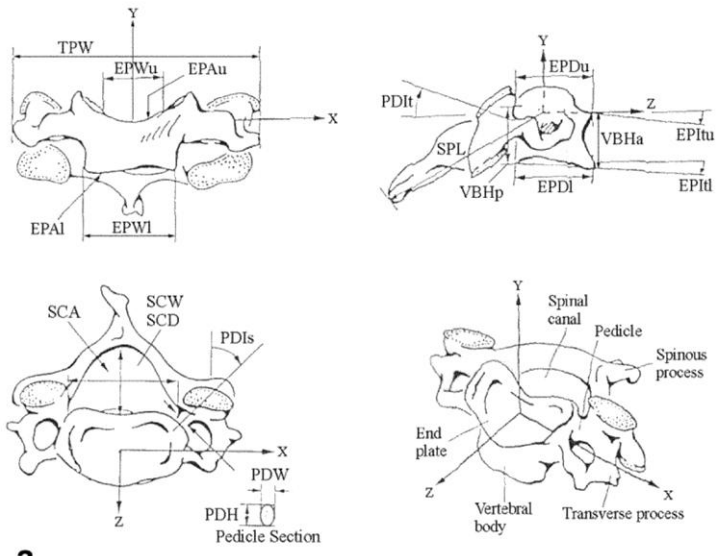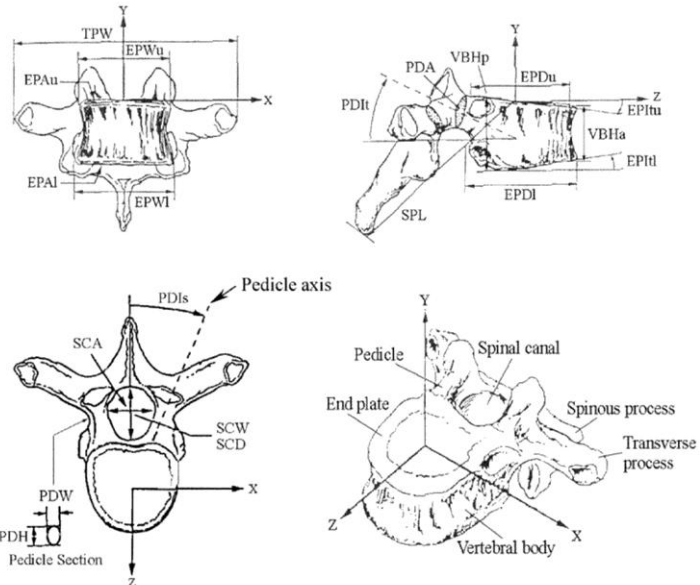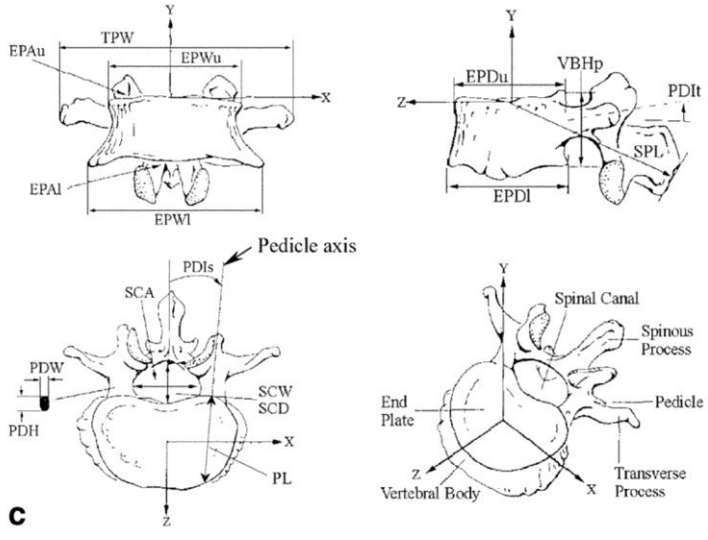
Abbreviations:

EPAl: lower end-plate area
EPAu: upper end-plate area
EPDl: lower end-plate depth
EPDu: upper end-plate depth
EPWl: lower end-plate width
EPWu: upper end-plate width
PDH: pedicle height
PDIs: left pedicle, sagittal inclination
PDIt: left pedicle, transverse inclination
PDW: pedicle width
SCA: spinal canal area
SCD: spinal canal depth
SCW: spinal canal width
SPL: spinous process length
TPW: transverse process width
VBHa: anterior vertebral body height
VBHp: posterior vertebral body height

Figure 11a–c Four views (front, side, top and isometric) of a cervical, thoracic and lumbar vertebra (Tan et al., 2004).

31

Parameter	Vertebral level																						Average
	C3	C4	C5	C6	C7	T1	T2	T3	T4	T5	T6	T7	T8	T9	T10	T11	T12	L1	L2	L3	L4	L5	
	Difference compared with Panjabi et al. (%)																						
EPWu	−12.7	−14.5	−14.9	−14.6	−12.8	+0.8	−5.2	−5.3	−8.2	−6.4	−9.5	−11.5	−12.2	−11.8	−9.7	−9.5	−11.5	−11.9	−10.3	−9.5	−9.9	−12.1	−10.2
EPWl	−16.9	−11.8	−18.0	−11.4	−13.2	−2.5	−9.0	−10.9	−3.5	−8.5	−12.1	−7.9	−8.5	−11.5	−9.9	−9.7	−13.5	−9.5	−9.0	−9.4	−8.5	−11.5	−10.4
EPDu	−9.3	−8.5	−5.9	−11.0	−16.6	−19.5	−16.8	−20.7	−18.9	−15.6	−16.1	−17.2	−16.5	−16.7	−16.7	−20.4	−18.6	−19.4	−18.2	−15.1	−13.2	−12.4	−15.6
EPDl	−3.2	−4.4	−15.6	−15.1	−7.1	−19.8	−18.1	−18.5	−18.4	−16.3	−14.5	−17.5	−16.0	−17.7	−17.1	−15.4	−17.1	−19.3	−16.3	−13.2	−10.6	−13.6	−14.7
VBHp	−3.4	−0.8	−0.8	+3.7	−7.8	−0.7	−2.6	−6.2	−2.5	+1.2	−2.3	−4.4	−4.8	−6.7	−5.5	−4.2	+0.9	−5.9	−4.9	−7.1	−10.4	−12.7	−4.0
SCW	−16.2	−21.9	−18.5	−20.7	−19.6	−18.8	−22.1	−22.4	−20.6	−20.5	−20.2	−19.7	−20.3	−20.7	−22.0	−21.1	−19.4	−18.1	−18.1	−20.2	−20.5	−13.7	−19.8
SCD	−36.4	−41.8	−40.8	−43.1	−27.6	−29.3	−23.5	−24.5	−27.2	−29.5	−29.7	−26.1	−25.2	−24.8	−23.2	−26.3	−31.5	−34.2	−35.7	−36.0	−39.8	−42.1	−31.8
PDHl	−6.9	−9.6	−13.7	−20.0	−13.3	−16.2	−19.0	−18.3	−26.2	−21.9	−25.0	−22.1	−15.2	−21.7	−14.7	−20.2	−15.5	−17.1	−12.8	−17.1	−14.5	−9.2	−16.8
PDHr	−10.5	−9.5	−11.9	−15.5	−18.7	−6.5	−13.5	−16.9	−21.9	−17.9	−24.2	−18.6	−19.2	−20.9	−11.6	−15.4	−15.2	−17.6	−15.3	−9.2	−14.7	−12.8	−15.4
PDWl	−16.7	−9.8	−7.9	−8.9	−13.9	−14.9	−22.8	−26.2	−41.4	−33.3	−26.7	−17.3	−35.8	−35.1	−38.1	−33.6	−9.3	−39.1	−26.4	−24.8	−38.1	−41.1	−25.5
PDWr	−24.1	−21.1	−19.7	−14.3	−13.6	−8.5	−31.0	−37.1	−29.1	−32.3	−28.3	−29.2	−29.9	−35.5	−28.9	−21.6	−17.1	−31.3	−20.5	−25.5	−35.8	−34.4	−25.9
SPL	−13.5	+0.0	+17.8	+18.4	+2.6	−3.6	−7.3	−5.2	−5.3	−4.4	−5.8	+2.6	−1.7	−0.4	+1.0	+6.1	+2.3	−23.0	−24.1	−19.7	−21.4	−25.9	−5.5
TPW	−17.7	−7.4	+2.6	−2.2	−19.2	−15.3	−17.2	−15.6	−12.5	−20.0	−18.1	−17.7	−20.2	−16.2	−22.3	−17.6	−12.6	−24.7	−15.5	−16.7	−14.7	−22.9	−15.6
EPAu	−8.7	−7.5	+2.5	−4.8	−20.7	+1.6	+4.4	−5.4	−1.9	−4.1	−6.4	−12.8	−8.6	−13.3	−11.8	−16.0	−16.6	−15.8	−13.4	−6.4	−7.0	−8.9	−8.3
EPAl	+13.7	+21.2	+16.3	+9.1	+21.2	−0.9	−0.3	−6.0	−5.4	−9.1	−8.2	−10.0	−8.1	−14.5	−14.2	−15.0	−14.3	−9.6	−8.9	−9.2	−5.8	−13.5	−3.3
SCA	−39.8	−41.2	−33.1	−38.6	−25.2	−20.5	−17.3	−19.2	−27.1	−29.6	−29.7	−27.6	−23.7	−27.0	−29.7	−32.3	−36.4	−37.5	−34.5	−40.7	−43.5	−43.3	−31.7

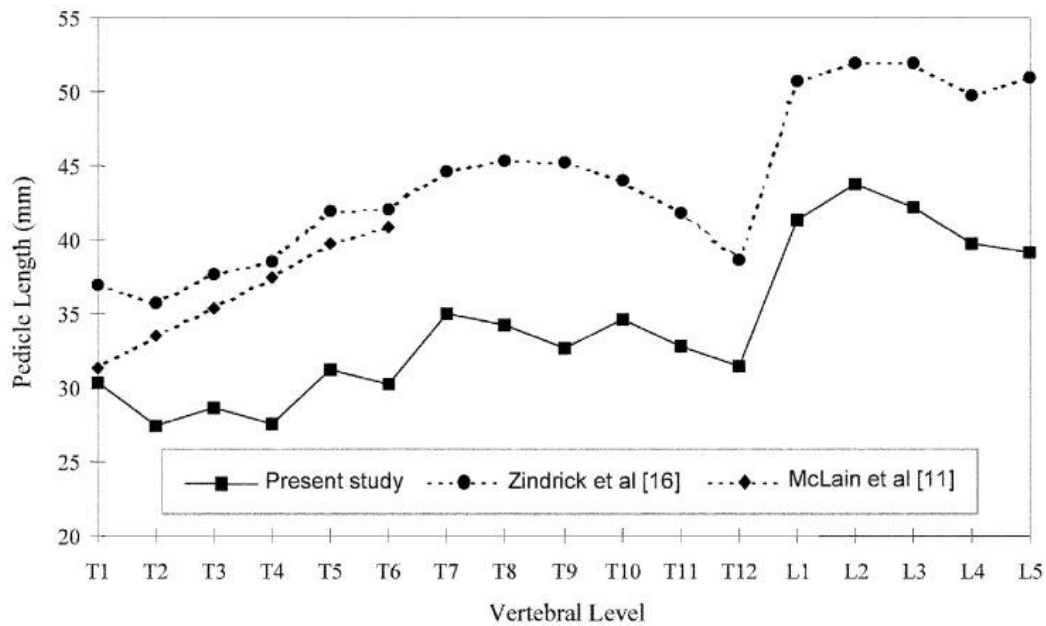Table 3 Comparison of measurements with those from Panjabi (Tan et al., 2004).

Figure 12 Comparison of the pedicle length of the present study, McLain et al. (2002) and Zindrick et al. (1987) (Tan et al., 2004).

4. 1. 3 Computed tomography (CT)

In Houwen´s study (2010), existing CT-scans of 77 patients of various age, health, and gender were analyzed with an aim to determine the vertebral endplate geometry of the lumbar region of the spine. The equipment used was *16 detector multi-detector CT scanner* (Siemens, Forchheim, Germany) and the CT-scans were visualized and analyzed using *Vitrea2 software* (Vital Images Inc., Minnetonka, Minnesota, US).

A total of 10 coordinates were measured on each endplate, five in the sagittal plane and five in the frontal plane. The endplate depths were calculated as the perpendicular distances from the surface coordinates to the best-fit plane from the three reference planes (sagittal, frontal and transverse). Distances between coordinates of the same number on opposite sides of the intervertebral disc space were used to yield the intervertebral disc height. The wedge angle (the angle between the planes of two adjacent endplates) was calculated using the 'heights method' (Eijkelkamp, 2002) for comparison to literature and to determine if the measurement points reflect realistic lumbar anatomy.

Results of this study are summarized in Figure 13. Depth profiles, endplates sizes and disc contour from the sagittal and frontal plane are described. Furthermore, it shows that the depth of the inferior endplate generally increases toward the lower lumbar region. The inferior T12 appears to be an exception to this trend, possibly because the depth

33

itself is smaller, and the measurement error has a larger influence here, or because T12-L1 is a common level of vertebral injury.

The accuracy of the measurement method was determined by comparing CT to vernier caliper measurements of real vertebra. Authors discuss gender and age dependencies, but the data on body weight and height was not available because CT-scans were retrospectively selected from Picture Archiving and Communication System. Results of this study are immediately put into comparison against literature (Eijkelkamp, 2002), (Lee, 2003) which leads to few comparative figures (Figure 14).
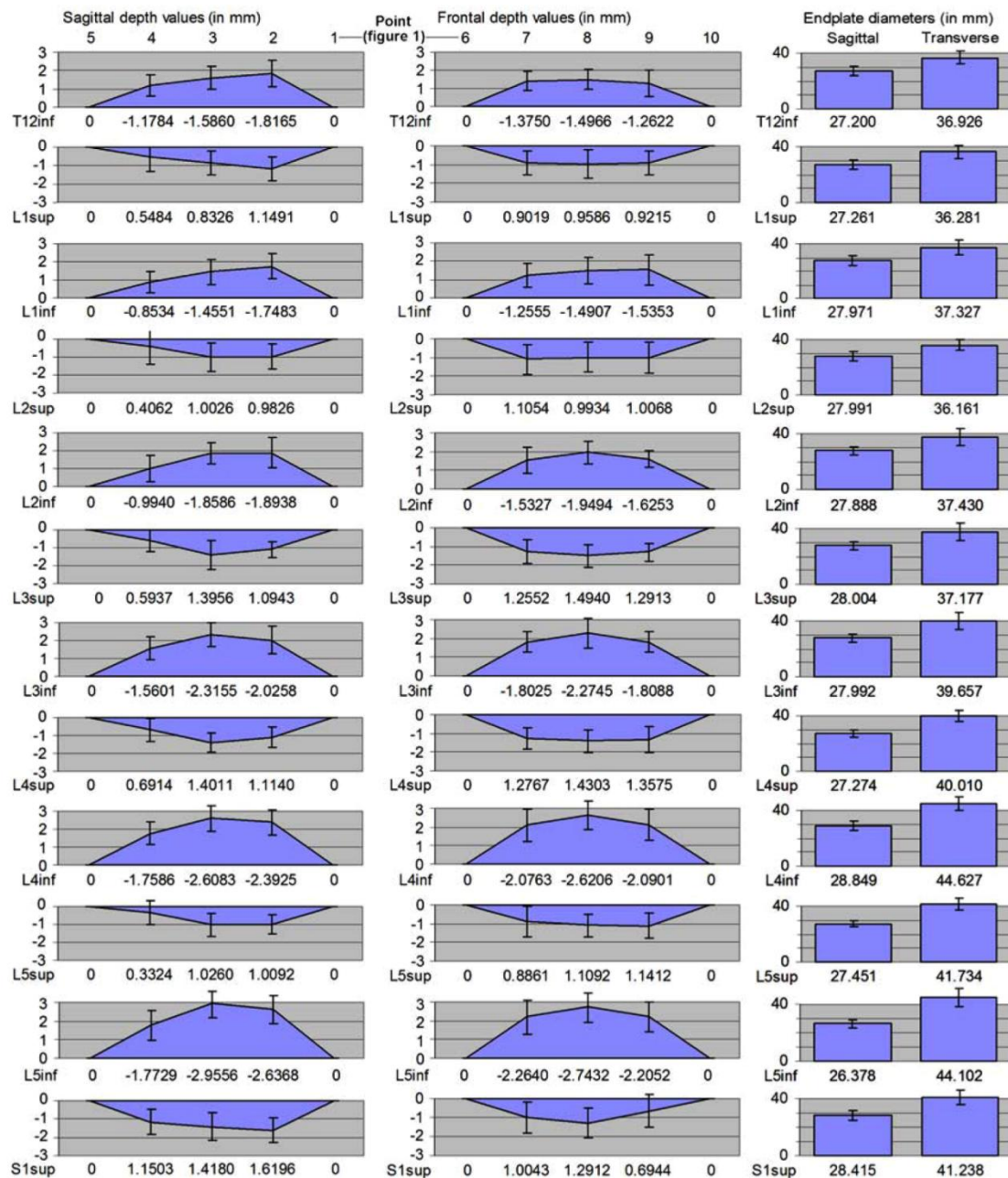

Figure 13 Depth profiles, endplates sizes and disc contour from the sagittal and frontal plane. All values are in mm. Standard deviations are depicted by error bars. (Houwen et al., 2010)
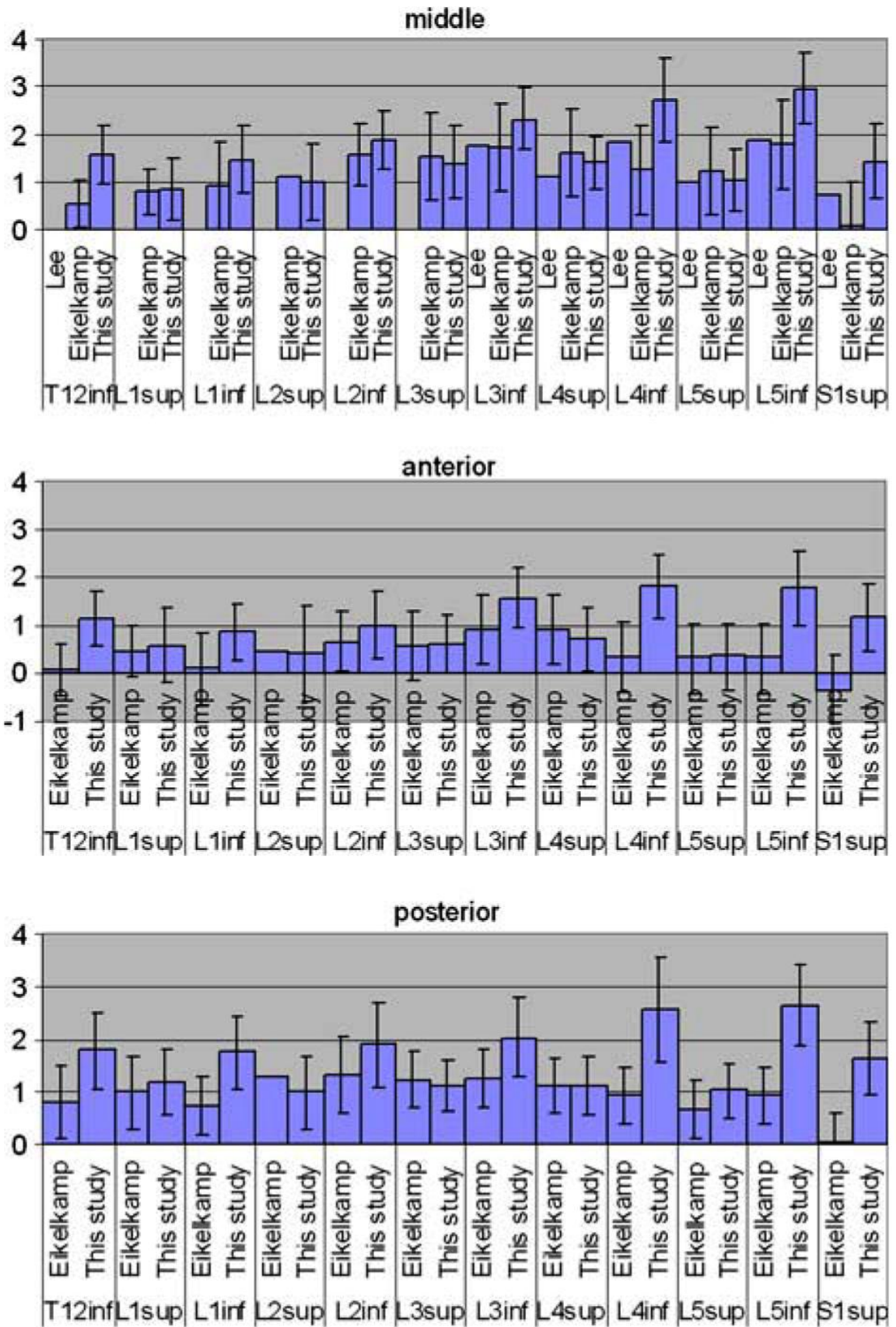
34

Figure 14 Comparison of endplate depth (mm) against literature (Eijkelkamp, 2002), (Lee, 2003), standard deviations depicted by error bars (Houwen et al., 2010).

4. 1. 4 Summary

Eijkelkamp´s study (2002), mixing two methods of measurement – X-ray and MRI, presents useful and comprehensive data as well as a description of measuring methods. The calculation of the wedge angle by 'height method' is then used in other studies (Houwen et al., 2010). For purposes of AID the study emphasises the importance of an availability of artificial discs in different wedge angles and in different heights (from 8 to 14 mm average disc height).

Concerning studies on cadavers of Panjabi at al. (1991a, 1991b, 1992) and Tan at al. (2004), the general difference in body size, the difference in size of vertebrae of Chinese Singaporeans and Caucasians is not surprising. The contribution of these studies could be seen in recommendations for surgical management in populations studied. Some of the geometrical data were significantly different. This fact could lead surgeons to different strategies and developers to adjustment of the tools used among each population. Accurate mathematical models could be constructed using the data of the surface anatomy thus it improves development of numerical techniques such as the finite element method.

Houwen et al. (2004) who focused on geometry of vertebral endplates compared his results obtained from CT-scans to the results of other studies that used X-ray and MRI methods, including Eijkelkamp (2002), and stated that CT could be used as a measuring technique. Figure 13 represents a great way how to visualized geometrical data. Houwen sees a future in custom-made implants, with for every person a perfect fit based on a pre implant measurement using of CT data.

4. 2 Biomechanical loading

The research focused on biomechanical properties of connective tissues is a broad field. This chapter summarize different approaches and methods used to determine changes in components of spine during specific loading activities (e.g. bending, flexion, compression etc.). All of the studies were executed on specimens of lumbar spine because this region is subjected to the highest loading. Parts of the spine subjected to loading were vertebrae, IVDs or only endplates depending on the type of study.

Author & Year	Methods	Type of study	Region	Specimens	Measurements
Hauerstock (2000)	load cells	in vivo	lumbar	sheep	average minimum and maximum axial loads
Fujiwara et al. (2001)	CT fibreglass rods (loading) VICON cameras (images)	in vitro	lumbar	human	foraminal width (maximum and minimum) foraminal height disc bulging thickness of ligamentum flavum cross-sectional area of the foramen
Stokes et al. (2002)	hexapod robot load cells	in vitro	lumbar	pork	stiffness matrix of a spinal motion segment
Grant et al. (2002)	DXA scans (BMD) digital camera (degeneration) 3 mm hemispherical indenter (loading)	in vitro	lumbar	human	bone mineral density disc degeneration endplate failure load endplate stiffness
Tsantrizos et al. (2005)	radiography wire grid and beads portable mechanical testing device	in vitro	lumbar	human	nucleus pulposus migration intradiscal strains
Keller et al. (2005)	X-ray quadrilateral element model	numerical technique	cervical thoracic lumbar	human	compressive load compressive stress shear stress
Costi et al. (2007)	radiography wire grid and beads hexapod robot	in vitro	lumbar	human	maximum shear strain of the IVD
Crisco et al. (2007)	pendulum apparatus	in vitro	thoraco-lumbar lumbar	human	bending stiffness damping coefficient
Roux et al. (2010)	DXA scans micro-computed tomographic (μCT) screw-driven machine	ex vivo	lumbar	human	bone mineral density bone volume/tissue volume trabecular thickness degree of anisotropy structure model index anterior cortical thickness anterior cortical radius of curvature
Schmidt et al. (2010)	Finite element method	numerical technique	lumbar	human	axial displacement fluid loss axial stress disc radial strain pore pressure disc collagen fiber strain
Dowthwaite et al. (2011)	DXA	in vitro	lumbar	human	bone mineral content areal bone mineral density vertebral width/depth/height bone mineral apparent density axial compressive strength fracture risk index

Table 4 Biomechanical loading

4. 2. 1 Load cells

In this *in vivo* study (Hauerstock, 2000) a miniature load cell (height of 5 mm and a diameter of 12.8 mm; A.L. Design, Buffalo, NY) and a radio transmitter were implanted in the L3-L4 space of the sheep spine to measure compressive intervertebral loads in a variety of activities (standing, lying prone, walking/trotting, and jumping). The radio transmitter with the transmission frequency of 913 MHz worked with the receiver and data acquisition software (Strainlink, Microstrain. Burlington, VT).

From total of four sheep, two were sacrificed during the experiment. Results for a range of activities were as follows: in walking at 1.5 m/s, average maximum and minimum loads were 461 N and 256 N, respectively; in walking at 2m/s, average maximum and minimum loads were 684 N and 303 N, respectively; in standing, loads averaged 161 N; and in lying prone, loads averaged 212 N. The highest loads were recorded in jumping, where the peak load was 1290 N.

4. 2. 2 Changes of intervertebral foramen

Fujiwara et al. (2001) led a study to examine the morphologic changes in the intervertebral foramen during flexion, extension, lateral bending, and axial rotation of the lumbar spine. They tried to correlate these changes with the flexibility of the spinal motion segments.

This *in vitro* study put 81 lumbar spine motion segments from human cadavers without signs of greater degeneration under examination. Concerning methods, each lumbar spine was divided into motion segments consisting of two vertebrae and the intervertebral disc with the ligaments. The motion segments were frozen and imaged with CT scanner (General Electric Medical System High-Speed Advantage 9800, Milwaukee, WI) with 1-mm thick consecutive sections.

For biomechanical testing, three markers reflecting infrared light were attached to the anterior, right, and left edge of the polymethylmethacrylate (PMMA) in which the superior portion of the superior vertebra was embedded. Similar procedure was done on the inferior vertebral body. The fibreglass rods were inserted anteroposteriorly and transversely through each vertebral body along the midline axis of the spine. Coupling forces were applied by hanging dead weights at the tip of the cords attached to the fibreglass rods and routed through pulleys so that a pure moment can be applied to the superior vertebra. Pure moments of flexion, extension, lateral bending, and axial

rotation were applied in six load steps (0.5, 1.6, 3.6, 4.7, 5.7, and 6.6 Nm). Rotational movements of the motion segment were measured using VICON cameras (Oxford Metrics, Ltd., Oxford, England) and Micro-Vax 3100 Workstation (DEC, Maynard, MA). Measurement accuracy and resolution of this system were 99.56% and 0.031 ± 0.074 mm with 95% confidence level, respectively. Three rotation angles of the superior vertebra with respect to the inferior vertebra in flexion–extension, lateral bending, and axial rotation were computed from the recorded marker position data in terms of Euler angles. After application of the last load, the specimens were frozen under load, and then CT was performed with the same technique described above. Six parameters of the intervertebral foramen were measured, including foraminal width (maximum and minimum), foraminal height, disc bulging, thickness of ligamentum flavum, and cross-sectional area of the foramen (Figure 15).

The results of this study are following: Flexion increased the foraminal width (maximum and minimum), height, and area significantly while significantly decreasing the disc bulging and thickness of ligamentum flavum ($P < 0.05$). However, extension decreased the foraminal width (maximum and minimum), height, and area significantly. Lateral bending significantly decreased the foraminal width (maximum and minimum), height, and area at the bending side, whereas lateral bending significantly increased the foraminal width (minimum), height, and area at the opposite side of bending. Likewise, axial rotation decreased the foraminal width (minimum) and area at the rotation side significantly while significantly increasing the foraminal height and foraminal area at the opposite side. The percent change in the foraminal area was found significantly correlated with the amount of segmental spinal motion except for the extension motion. At the end, researchers introduced an idea, that among segments with the same degree of foraminal stenosis, mechanical irritation to the spinal nerve root at the intervertebral foramen may be more severe in the segments that show more mobility or instability.
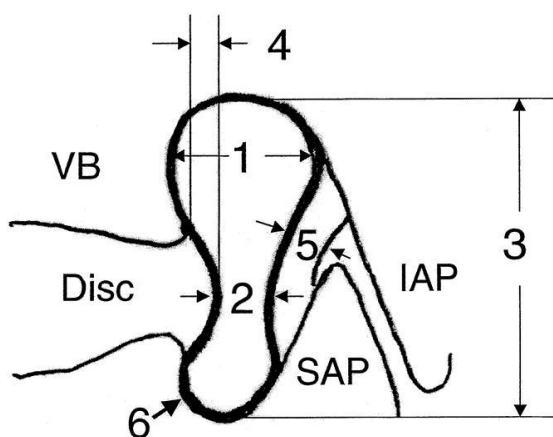

Figure 15 Measurement parameters. 1 = maximum foraminal width; 2 = minimum foraminal width; 3 = foraminal height; 4 = disc bulging; 5 = thickness of ligamentum flavum; 6 = cross-sectional area of the intervertebral foramen. VB = posterior vertebral body of vertebra; Disc = intervertebral disc; IAP = inferior articular process; SAP = superior articular process (Fujiwara et al., 2001).

4. 2. 3 Stiffness matrix

In his *in vitro* preliminary experiments, Stokes et al. (2002) measured stiffness matrix of a pig lumbar spinal motion segment consisting of two vertebrae and the intervening soft tissue. He simulated physiological conditions using axial preload and an isotonic fluid bath during testing. The testing machine (hexapod robot) consisted of a moving platform supported by six linear actuators mounted to a stationary base. The platform could be driven to any six-degree-of-freedom (6-DOF) position by controlling the actuator lengths (Figure 16).
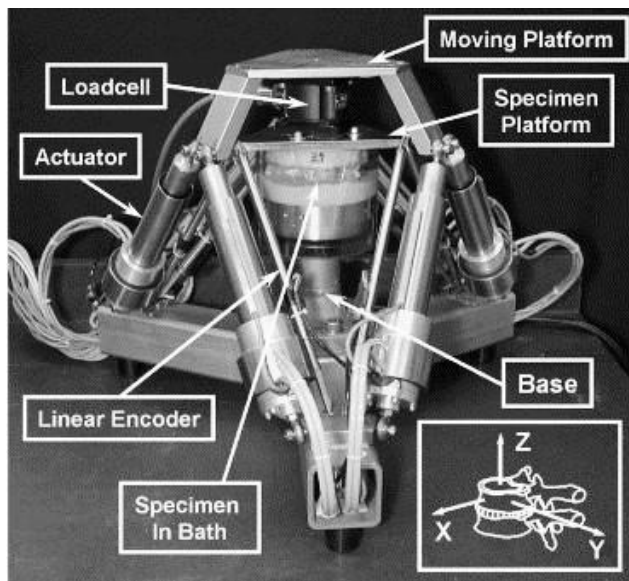

Figure 16 Photograph of the hexapod apparatus showing actuators, base pedestal, specimen mounting plate, linear encoders, moving platform, load cell and lumbar motion segment specimen that can be seen through the transparent bath surrounding it. Inset: the axis system convention (Stokes et al., 2002).

Test specimens were bolted rigidly to the testing machine through the use of screws and polymethylmethacrylate with a 6-DOF load cell (MC3A-6-500, Advanced Mechanical Technology Inc., Waltham, MA, USA) mounted below the moving platform. Specimens were surrounded by isotonic saline cooled to approximately 4°C.

An axial compressive preload of 500N was applied on each specimen for 3 hours. This value was based on knowledge of typical active in vivo quadruped loading (Hauerstock, 2000). After the preload, displacement tests followed. The displacements were ±3mm along the X-axis, ±1.5mm along the Y-axis, ±0.4mm along the Z-axis and ±4° about each axis. These ranges were selected to represent typical physiological ranges of displacements and forces. In post-processing, the forces and moments at the vertebral body centre were calculated from the load cell recordings by a rigid body transformation and the actual displacements of the centre of the superior vertebral body

41

were calculated from the six recorded encoder lengths using the testing machine geometry (Stokes et al., 2002).

Authors show that the loads and displacements are related by the linear relationship with a symmetric stiffness matrix using following equation:

$$[K] \{X\} + \{F_0\} = \{F\},$$ Equation 3

where [K] is a 6 x 6 stiffness matrix with 36 coefficients (21 independent coefficients due to symmetry), {X} is a 6 x 1 displacement vector of 3 translations followed by the three rotations, {F_0} is a 6 x 1 initial offset load vector (three forces and three moments), and {F} is a 6 x 1 load vector of the three resulting forces and three resulting moments.

Stokes et al. (2002) considered this methodology to be an efficient and direct way to obtain the load–displacement properties of a motion segment under physiological conditions of axial preload and in a physiological fluid medium. Results of testing with and without a 500N axial preload, showed a large stiffening effect with axial preload. This fact implies that spine analyses simulating in vivo loading should take this effect into account and avoid underestimation of the real values.

4. 2. 4 Failure load and stiffness of endplates

Grant et al. (2002) in an *in vitro* study confirmed a hypothesis that reduced bone density and developed disc degeneration result in changes to the structural property distributions of the lower lumbar endplates (L3 – L5). The BMD was recorded using lateral DEXA scans (LUNAR Corp., Madison, WI). The level of disc degeneration was determined according to the disc photographs taken with a digital camera (Nikon Coolpix 950, Nikon Corp., Tokyo, Japan) with a pixel count of 1600 x 1200. The testing device used was a custom-built 3 mm diameter hemispherical indenter that was pressed into the bone at 0.2 mm/s to a depth of 3 mm by a stepper motor-controlled electromechanical linear actuator (Dynact Model I-PP3-B5, Orchard Park, NY). The motor position and load through the indenter (Omega Model LCIOI-50 load cell, Omega Engineering, Stamford, CT) were recorded by a personal computer at 35 Hz.

The locations of the test sites of the endplate were determined using the dimensions of the endplate in order to standardize the results (Figure 17). The anterior-posterior (AP) dimension was divided into increments of 20%, while the lateral-lateral (LAT)

dimension was divided into increments of 15%. In each sample there was a minimum of 6 mm centre-to-centre between adjacent test sites and 4.5 mm between the centres of the outermost test sites and the edge of the endplate. Preliminary testing showed no interaction between tests separated by this distance. In most cases, 27 tests were done in each endplate, depending on actual endplate shape. Accurate movement between the test sites was secured by an *xy*-translating table. The specimens were levelled prior to testing using a mounting device with adjustable legs. A tripod bubble level (Grant et al., 2001) placed in the centre of the endplate was used to determine when the endplate was horizontal.
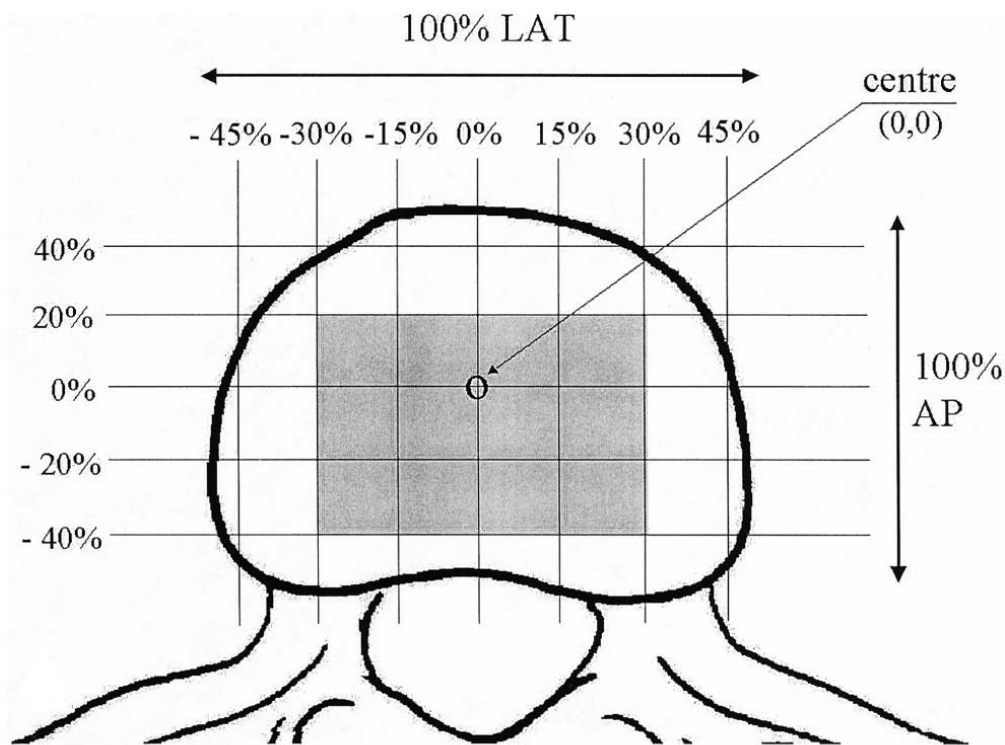

Figure 17 Test site layout based on endplate dimensions. Indentation tests were performed at the intersection points between the orthogonal lines. The shaded region identifies the area for which a complete AP-LAT statistical analysis was performed. AP is the anterior-posterior depth of the endplate and LAT is the lateral width of the endplate (Grant et al., 2002).

The load-displacement curves were generated at each test side and served for extraction of the failure load and stiffness values. The failure load was defined as the maximum load reached prior to a load decrease of greater than 5%. The stiffness was the slope of the linear region of the load-displacement curve based on a linear regression analysis of the data set. Three-way analyses of variance (ANOVA) were used to analyze the relationships between the data. All statistical analyses were performed using the STATISTICA 5.1H statistics software package (Statsoft Inc., Tulsa, OK). The structural

property distributions of the superior and inferior lumbar endplates were found to be significantly different therefore they were analyzed separately.

The results showed that the overall failure load decreased with bone mineral density (BMD) in the superior ($p < 0.0001$) and inferior ($p = 0.011$) lumbar endplates. In both endplates, the posterolateral regions were significantly stronger than more central regions. With increasing BMD, this difference became more pronounced in the superior endplates only ($p = 0.005$). Increased disc degeneration was associated with an overall failure load decrease in the inferior lumbar endplates ($p = 0.002$). The strength in the central regions of the superior endplates was reduced with increasing degeneration, but this was not observed peripherally ($p = 0.001$). Stiffness magnitude or distribution was not significantly affected by BMD or disc degeneration. The locations of the strongest regions of the endplate did not change with either bone density or disc degeneration.

4. 2. 5 Internal strains

Tsantrizos et al. (2005) study *in vitro* the effects of nucleus pulposus migration on the intradiscal strains experienced in the anulus fibrosus (AF) and transitional zone (TZ) during compressive and bending loads. Researchers worked with both healthy and degenerated IVDs from human specimens. Copper wires (0.170-mm diameter) were placed within each IVD and lead beads (0.5-mm maximal diameter) were glued to the external surface in the mid-transverse plane (Figure 18). 18 functional spinal units with beads and wires were subjected to compression, extension, flexion, and lateral bending using the portable mechanical testing device.
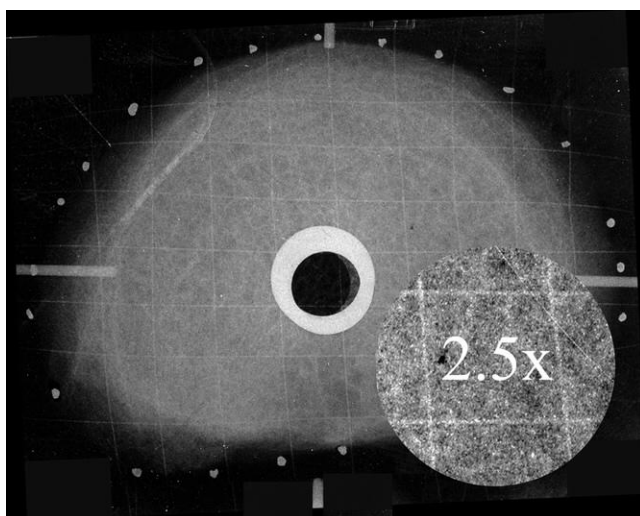

Figure 18 A craniocaudal radiograph depicting an intradiscal wire grid and surface beads fixed to the IVDs mid-transversal plane (Tsantrizos et al., 2005).

Circumferential strains defined as strains tangential to the annular lamellar orientation and radial strains defined as strains perpendicular to annular lamellar orientation (Figure 19) were defined. The remaining zones used the sagittal and transversal anatomic axis to define orientation angles. Strains subsequently were expressed for each IVD zone and region as mean circumferential and radial strains. A mean resultant displacement of 9 most central nodes in the central zone was included to define nucleus pulposus migration.
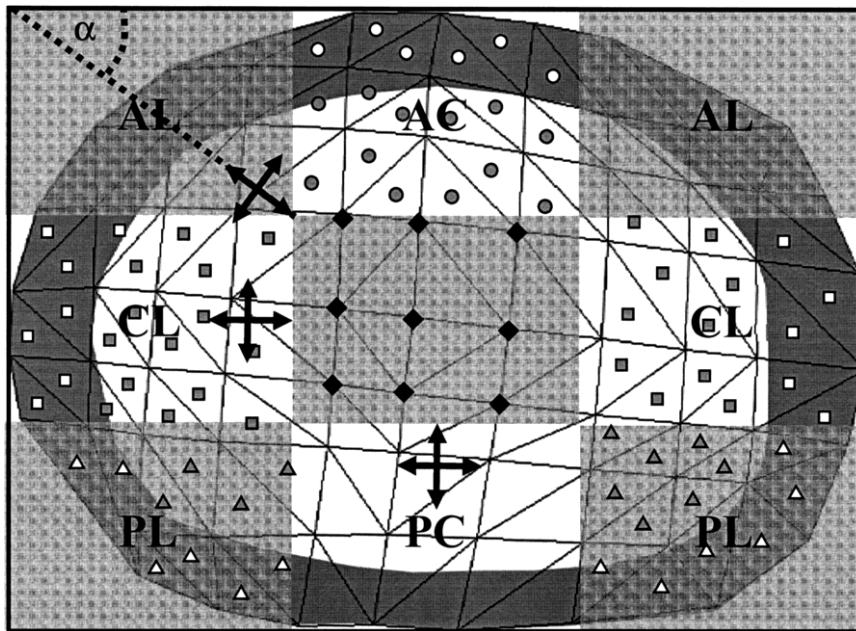

Figure 19 Elemental strains grouped into zones: AC, Anterior; AL, Anterolateral; CL, Lateral; PC, Posterior; PL, Posterolateral. The dark grey shaded band marks the anulus contour. Transparent and light grey shaded boxes depict zones. Elemental centroids are referred to with small white and grey symbols (*i.e.*, small circles, squares and triangles), depicting zones included in the study. White shaded symbols indicate centroids located within the AF region, while grey shaded symbols indicate centroids located within the TZ region. The arrow directions defined circumferential and radial strain directions. The angle α was used to transform elemental strains in the AL and PL zones into circumferential and radial strains. The nine nodes included in the study to represent the central zone NP are referred to with small black diamond symbols (Tsantrizos et al., 2005)

The wire and bead positions at unloaded and loaded steps were documented with craniocaudal radiographs (Ultra-Speed DF-49, Eastman Kodak Co., Rochester, NY). Craniocaudal radiographs documented nodal positions during the subsequent steps applied in this sequence: (1) unloaded, then 1000 N axial compression; (2) unloaded, then extension; (3) unloaded, then flexion; and (4) unloaded, then left lateral bending. All bending loads were of 10 Nm, with 500 N axial compression. A flatbed image scanner (DuoScan, AGFA Corp., Ridgefield Park, NJ) converted radiographs into digital images of 1000 dots/inch optical resolution, but the image resolution was interpolated to 2540 dots/inch to improve the appearance of nodes on a computer

monitor. Cartesian nodal coordinates were then obtained for all images using image analysis software (Scion Image 4.0.2, Scion Corp., Frederick, MD). The coordinates of markers can be measured with 0.042-mm precision. Then the IVDs were cut along their mid-transversal plane and digitally photographed. Finally, the IVDs were further cut along their mid-sagittal plane to obtain a Thompson degeneration grade (Thompson et al., 1990).

Circumferential and radial strains from the anterior, lateral, and posterolateral regions during load were compared between healthy and degenerated IVDs (Figure 20, Figure 21). Results of this study showed that the nucleus pulposus migrated to the opposite side of bending regardless of bending direction and significantly more in degenerated IVDs. The highest nucleus pulposus migration was observed during lateral bending and circumferential tensile strains were significantly higher in the posterolateral regions of degenerative IVDs during all load. Moreover degeneration significantly increased radial tensile and compressive strains during all bending loads.
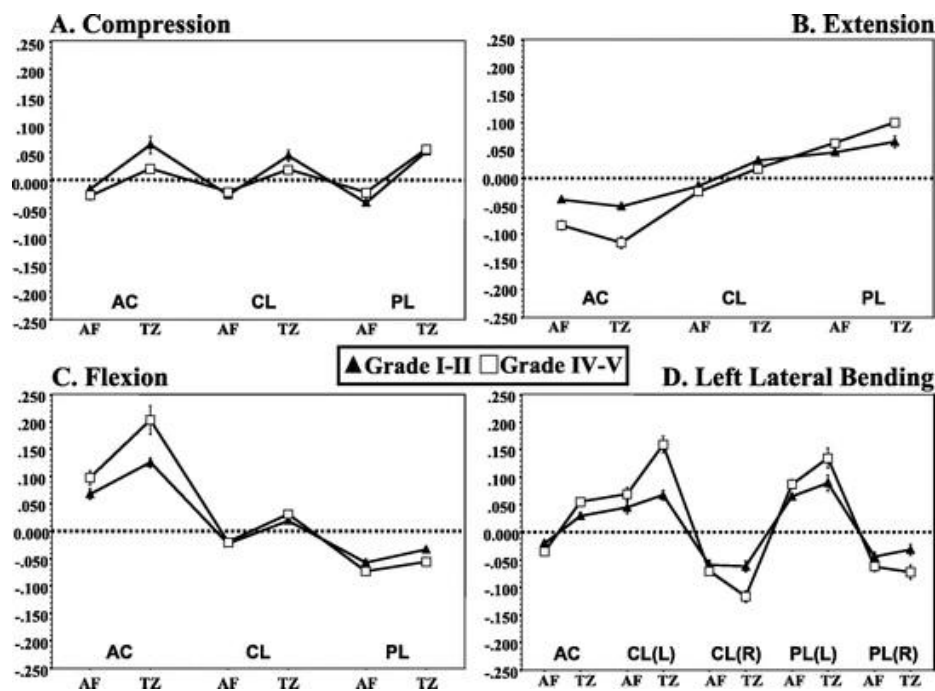

 Figure 20 Mean circumferential strains (in percent deformation) and standard errors of the mean experienced in response to compression, flexion, extension, and left lateral bending and calculated for the AC (Anterior), CL (Lateral) and PL (Posterolateral) zones and AF (anulus fibrosus), TZ (transitional zone) regions. L, Left; R, Right (Tsantrizos et al., 2005).
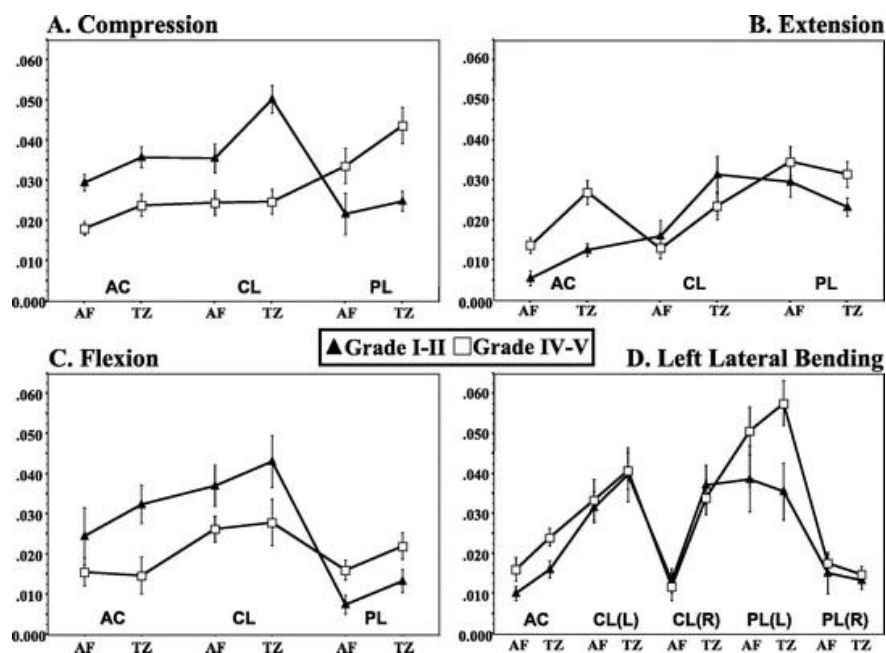
Figure 21 Mean radial tensile (+) and compressive (-) strains (in percent deformation) and standard errors of the mean experienced in response to compression, flexion, extension, and left lateral bending and calculated for the AC (Anterior), CL (Lateral) and PL (Posterolateral) zones and AF (anulus fibrosus) and TZ (transitional zone) regions. L, Left; R, Right (Tsantrizos et al., 2005)

Previous study (Brinckmann and Horst, 1981) confirmed that the axial stresses on the endplate are nonuniform and asymmetric during eccentric loading of the motion segment, and appeared to increase with degeneration. Tsantrizos et al. (2005) think that the increased nucleus pulposus migration patterns present in degenerative IVDs may explain why Horst and Brinckmann observed an asymmetry in axial stresses.

4. 2. 6 Postural loading model

Keller et al. (2005) subjected 67 asymptomatic young people (mean 26.7, SD 4.8 years) to a cross sectional study evaluating sagittal X-ray geometry and postural loading to investigate the influence of sagittal profile of the spine to spinal coupling and loads on spinal tissues. Morphological data (spine sagittal curvature and balance) were measured using digitized lateral full-spine X-ray images of neutral posture, upright standing subjects. X-Y coordinates of the anterior-superior, posterior-superior, anterior-inferior, and posterior-inferior corners of each vertebral body (VB) from C2-S1 were marked using a sonic digitizer (GP-9; GTCO CalComp, Columbia, MD) with the resolution of 0.125 mm. The digitized vertebral body coordinate data of each subject were used to create a quadrilateral element geometric model of the anterior spinal column (C2-S1), see Figure 22. Further description is available in Table 5. Measurements of anatomic angles of spine curvature were obtained from these models using a posterior tangent

technique (Harrison et al., 2000). The postural shear and compressive loads and stresses for each IVD segment were determined using a postural loading model developed by the same author in previous studies (Keller et al., 2003), (Keller and Nathan, 1999): "The two-dimensional spine model was idealized as a collection of 23 rigid vertebral bodies and 23 deformable intervertebral discs. Time-dependent height losses were modelled using axial compressive creep material properties based on in vitro measurements obtained from the literature."
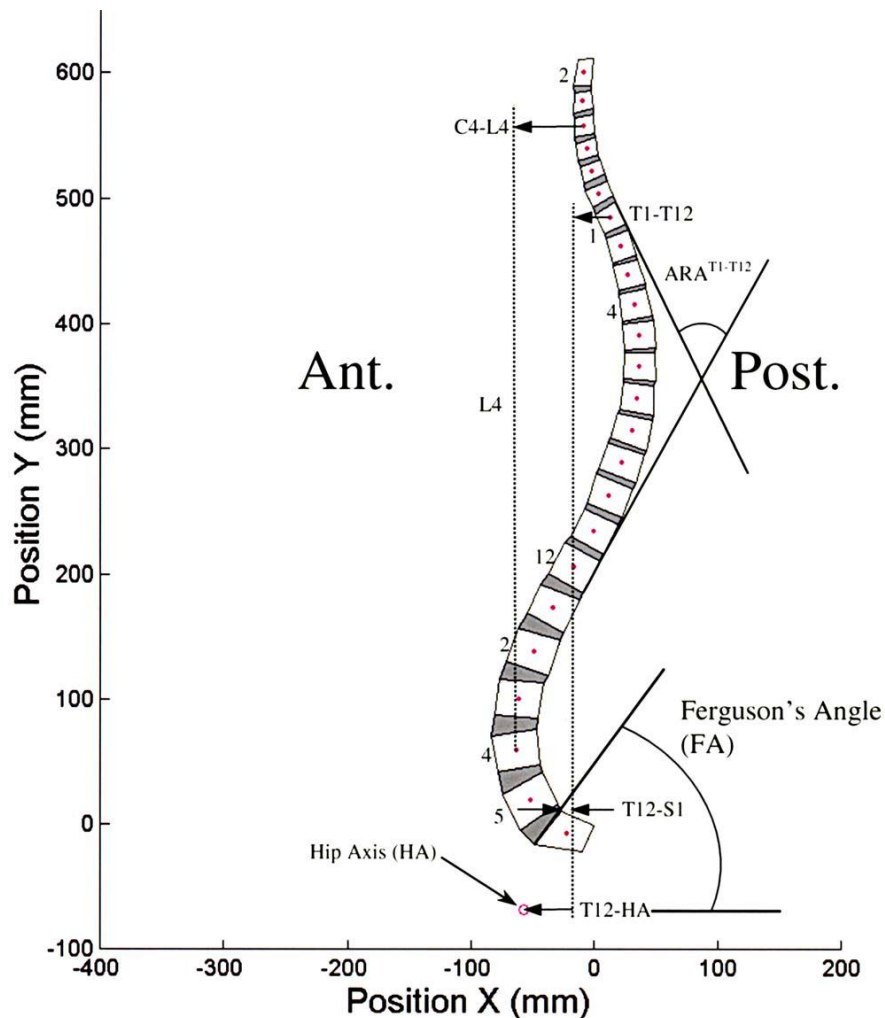
Figure 22 Quadrilateral element model (Subject 20) and posterior tangent spine curvature measurement technique after Harrison et al. (2000). Relative rotation angles were measured using a tangent line along the posterior margin of vertebral body for each vertebral segment and for the thoracic spine area (ARAT1-T12). Several sagittal balance parameters were measured, including C4-L4, C7-S1 (not shown), T1-T12, T4-S1 (not shown), T12-S1, HA-T4 (not shown), HA-T12, HA-S1 (not shown) (Keller et al., 2005).

Parameter	Abbreviation	Description
Sagittal alignment, C4-L4	C4-L4	Perpendicular distance between C4 (centroid) and L4 (centroid) plumblines (mm)
Sagittal alignment, T1-T12	T1-T12	Perpendicular distance between T1 (centroid) and T12 (centroid) plumblines (mm)
Sagittal alignment, T12-S1	T12-S1	Perpendicular distance between T12 (centroid) and S1 (posterior-superior VB corner) plumblines (mm)
Sagittal alignment, C7-HA	C7-HA	Perpendicular distance between C7 (centroid) and HA plumblines (mm)
Sagittal alignment, T4-HA	T4-HA	Perpendicular distance between T4 (centroid) and HA plumblines (mm)
Sagittal alignment, S1-HA	S1-HA	Perpendicular distance between S1 (posterior-superior VB corner) and hip axis (HA) plumblines (mm)
Sagittal alignment, C7-S1	C7-S1	Perpendicular distance between C7 (centroid) and S1 (posterior-superior VB corner) plumblines (mm)
Sagittal alignment, T4-S1	T4-S1	Perpendicular distance between T4 (centroid) and S1 (posterior-superior VB corner) plumblines (mm)
Thoracic kyphosis angle	ARA^{T1-T12}	Absolute rotation angle formed by posterior vertebral body tangent lines of T1 and T12 (degrees)
Lumbar lordosis angle	ARA^{T12-S1}	Absolute rotation angle formed by posterior vertebral body tangent lines of T12 and S1 (degrees)
Lumbo-sacral angle	ARA^{L4-S1}	Absolute rotation angle formed by posterior vertebral body tangent lines of L4 and S1 (degrees)
Ferguson's sacral base angle	FA	Angular measurement between horizontal and a line through the superior S1 end plate (degrees)
Pelvic tilt angle	PA	Angular measurement between horizontal and a line from the superior acetabulum of the posterior-inferior vertebral body of S1 (degrees)

ARA=absolute rotation angles; FA=Ferguson's angle; HA=hip axis; PA=pelvic angle; VB=vertebral body.

Table 5 Descriptions of the standing lateral radiograph sagittal balance (alignment) and sagittal curvature (angle) parameters (Keller et al., 2005).

To summarize the results, the neutral posture spine was characterized by following data: an average thoracic angle (T1-T12) = +43.7° (SD 11.4°), lumbar angle (T12-S1) = -63.2° (SD 10.0°), and pelvic angle = +49.4° (SD 9.9°). The greatest variance of the frequency distributions in sagittal curvatures was identified at the thoracic angle and the least variance at the pelvic angle. Concerning sagittal balance parameters, the best average vertical alignment showed C7-S1 and T1-T12 (5.3 mm and -0.04 mm, respectively). The comparison of anterior and posterior disc postural loads (Figure 23) showed greatest difference at L5-S1 IVD segment while at C4-C5 and T8-T9 the loads were balanced. Figure 24 shows that disc compressive stresses were greatest in the mid-thoracic region of the spine, whereas shear stresses were highest at L5-S1.
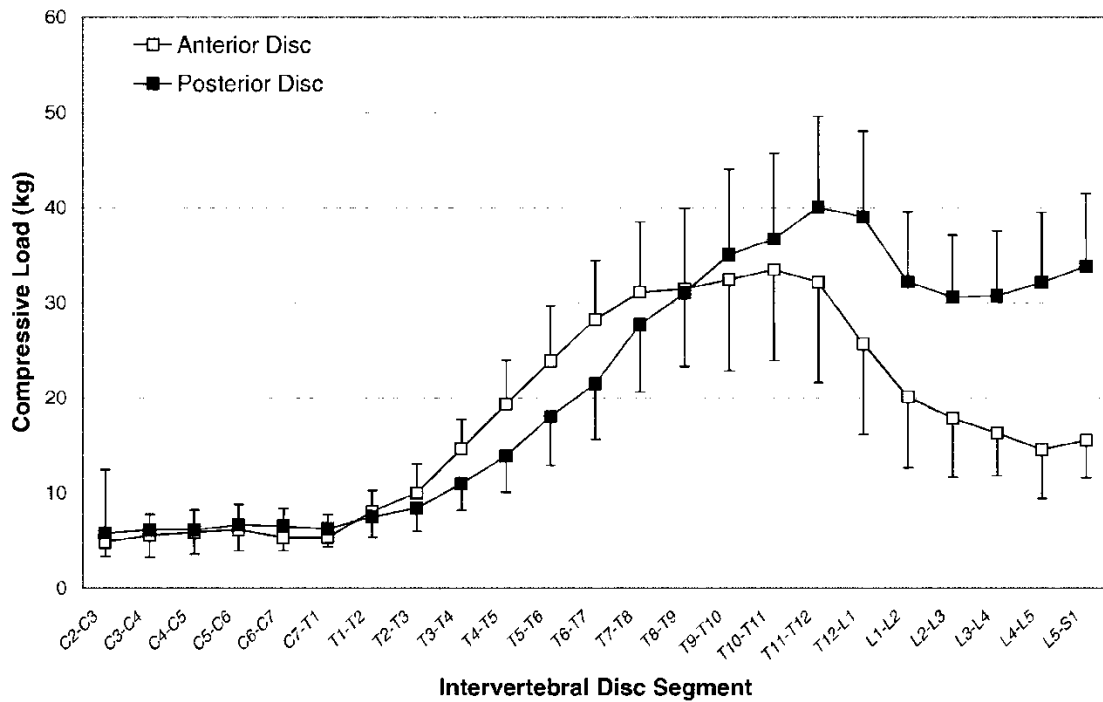
Figure 23 Distribution of anterior and posterior intervertebral disc compressive loads along the C2-S1 spine. Symbols and error bars represent mean and standard deviation, respectively, of the 67 subjects (Keller et al., 2005).

Figure 24 Distribution of intervertebral compressive and shear postural stresses along the C2-S1 spine (IVD centroids). Symbols and error bars represent mean and standard deviation, respectively, of the 67 subjects (Keller et al., 2005).

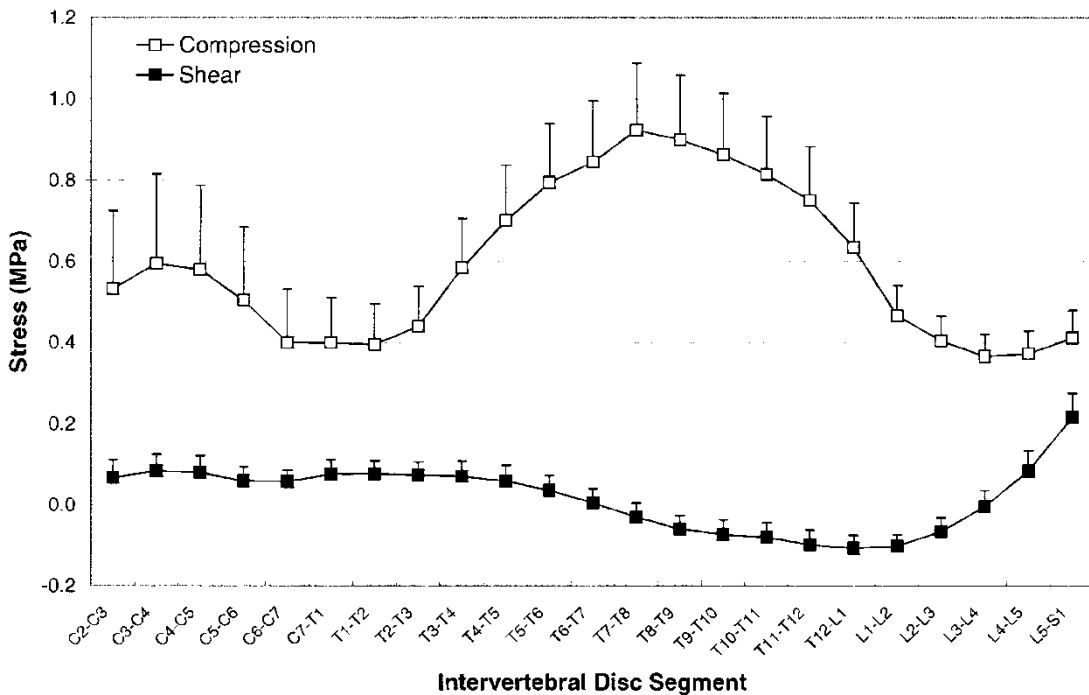Authors stated a good agreement with other experimental and analytical studies led by themselves (Keller et al., 2003), (Keller and Nathan, 1999) even though the effects of trunk muscle synergism (contribution of anterior muscles), passive spinal tissues

50

(ligament load sharing), and intra-abdominal pressure were not considered in this study. Above mentioned analyses suggest that sagittal spine balance and anatomic curvature influence postural loading and load balance of the intervertebral disc in healthy subjects. Specifically, the model predicted altered and increased loads as a result of variances in the ratio of distal lumbar lordosis to total lumbar lordosis, lumbar lordosis to thoracic kyphosis, and sagittal plane translations of the cervical and thoracic regions relative to the hip axis and sacrum. These deviations might prove to be undesirable for optimum spinal structure and function. They speculate that much of this variability is related to rotation and translation displacements in the thorax and head, which may be coupled to the variations in sagittal alignment observed in this and previous studies.

4. 2. 7 Maximum shear strain

Costi et al. (2007) tested human lumbar IVD specimens to determine the regions of largest maximum shear strain (MSS) experienced by disc tissues in each of three principal displacements and three rotations (6-DOF). They were also trying to identify the physiological rotations and displacements that may place the disc at greatest risk for large tissue strains and injury.

According to Thompson's criteria (Thompson et al., 1990) for disc grade, seven discs were grade 1 (excellent), and two were between grades 2 and 3 (the nucleus showed early signs of degeneration). Disc specimens were stored at − 80 °C until they were prepared for testing. Each disc and lower endplate was tagged with radiographic markers like is shown in Figure 25 and it was embedded in radiolucent cup with polymethylmethacrylate cement. Lead beads were fixed into position using cyanoacrylate. Wires were inserted through each disc by threading it with an 18G needle and needle-guide from one side to the other. Stereo-radiographs were taken before and after imposition of each loading.
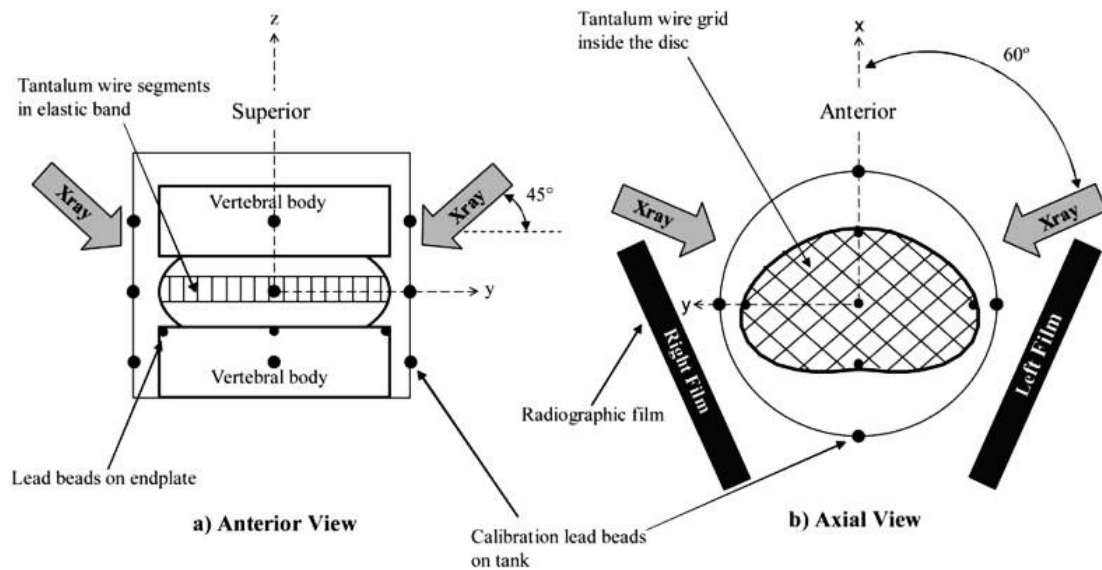
Figure 25 Schematic of the 3-D stereo-radiography displacement measurement set up. Anterior (a) and axial views (b) show the grid of tantalum wires in the disc, endplate and calibration lead beads, and tantalum wire segments in the elastic band stretched around the periphery of the disc. Specimen fixation cups are not shown and diagrams are not to scale (Costi et al., 2007).

For testing, each specimen was attached to the platens of a custom-made six degree of freedom hexapod robot (Stokes et al., 2002). The specimen was surrounded by a tank containing a 0.15M phosphate buffered saline bath at 4°C for the testing duration. Before testing, each specimen was equilibrated in the bath with a 100N compressive preload for 3 hours.

A sequence of 10 min ramp loadings consisting of displacements and rotations was applied to each specimen, with a 5-min dwell period at the datum position before stereo-radiographs were taken between each test. Axial compression was always the first displacement in the series, followed by axial rotation, anteroposterior shear, flexion/extension, lateral shear and lateral bending. The stereo-radiographs in each displaced position were made by use of a pair of X-ray tubes, each positioned at 60° to the mid-sagittal plane of the disc, and the tubes were raised and angled downwards at an angle of 45° (Figure 25).

The stereo-pairs of radiographs were scanned using a flatbed scanner at 600 dpi resolution (0.042 mm/pixel). The mean and 95% confidence interval precision root mean square (RMS) digitizing error was 0.045mm (0.016 mm), which was similar to that reported by Tsantrizos et al. (2005) (0.042 mm). Landmarks were identified in each film and manually digitized using software written in Matlab (The Mathworks Inc., Natick, MA, USA).

Methodology employed in this study has a number of limitations that researchers were aware of. Firstly, it was difficult to ensure that the specimen was potted perfectly parallel to the disc mid-plane to avoid coupling of forces and moments. Secondly it was not technically possible to place the grid of wires exactly in the true mid-plane of the disc, which could produce errors in strain measurement. Therefore the asymmetry of strains in axial rotation, lateral bending and lateral shear were attributed to small misalignment of the specimens in potting the specimens, and/or intradiscal wires not exactly in the mid-plane of the disc.

The use of beads to measure tissue deformation has been previously employed in 2-D radiography studies of internal disc motion (Krag et al., 1987; Seroussi et al., 1989). The method of using a wire grid in the disc has been extensively validated before (Tsantrizos et al., 2005).

Relative 3-D displacements of all coordinates (wires, endplate beads and circumferential markers) between displaced positions of the specimens were calculated and normalized by the respective input displacement (mm/mm) or rotation (mm/°). Maximum tissue shear strains were calculated from relative marker displacements and normalized by the input displacement or rotation. Lateral shear, compression, and lateral bending were the motions that produced the mean (95% confidence interval) largest mean MSS of 9.6 (0.7)%/mm, 9.0 (0.5)%/mm, and 5.8 (1.6)%/°, respectively, and which occurred in the posterior, posterolateral and lateral peripheral regions of the disc. After taking into account the reported maximum physiological range of motion for each degree of freedom, motions producing the highest physiological MSS were lateral bending (57.8 (16.2)%) and flexion (38.3 (3.3)%), followed by lateral shear (14.4 (1.1)%) and compression (12.6 (0.7)%).

This study has identified the lumbar segmental motions that produce physiological MSS comparable with the known failure strain of disc tissue and that may place the disc at greatest risk of injury. Lateral bending and flexion place the disc at greatest risk. The exact failure criterion for the intervertebral disc tissues is not known, and MSS was used because it has been shown that disc tears may be initiated by large interlamellar shear strains that dominate over radial and circumferential annular fibre strains.

4. 2. 8 Dynamic biomechanical properties

Crisco et al. (2007) used a novel unconstrained 3-D pendulum system to determine the dynamic, *in vitro* mechanical response of lumbar functional spinal unit (FSU).

Specimen included five thoracolumbar FSUs (three from level T12/L1, one from level L2/L3, and one from level L4/L5) obtained from four unembalmed human spines (average age 57.3±9.9 years). Both the superior and inferior vertebrae were cast in an urethane-molding compound within 89mm diameter cylindrical aluminium potting cups. To provide secure fixation while maintaining full range of motion of the facets, the vertebral bodies were potted to the pars interarticularis. Specimens were kept frozen until the day of testing, at which point they were completely thawed. During testing, the FSUs were kept moist with saline-soaked gauze.

Figure 26 shows a pendulum apparatus with the intervertebral disc of the FSU. The lower potted vertebra was rigidly fixed and a pendulum arm was fixed to the upper potted vertebra so that the intervertebral joint served as the fulcrum. The pendulum was an open rectangular shape (66 cm long x 23 cm wide) oriented in the frontal plane. This open shape permitted the pendulum to be mounted to the FSU with its weights directly below the FSU. The length of the pendulum (l) was fixed and the compressive load applied to the FSU was varied by changing the weight of the pendulum mass. The pendulum was set in motion by manually rotating it to 5° in extension and then releasing it. The three-dimensional motion of the pendulum (θ) was tracked using an infrared-emitting diode (IRED) markers and an Optotrak 3020 3-D motion tracking system (Northern Digital Inc., Ontario, Canada; RMS accuracy to 0.1mm and 3-D resolution to 0.01 mm). The relative motion of the upper FSU with respect to the lower FSU was calculated. For each test, the average period (τ), natural frequency (ω), dynamic bending stiffness (k), and coefficient of damping (Q) were calculated.
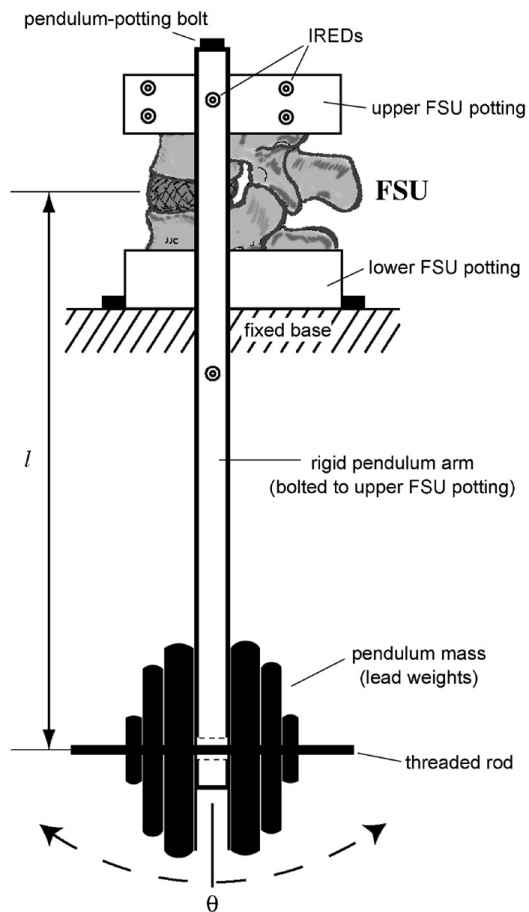
Figure 26 Schematic of the pendulum apparatus (Crisco et al., 2007).

All five FSUs were tested in flexion and extension under five axial compressive loads from 78 to 488N. The motion of the FSU after an initial rotation was characterized as an underdamped vibrating elastic system. Rotations in other directions occurred typically as the magnitude of an initial direction flexion/extension decreased or they appeared and then damped out as shown at Figure 27. Bending stiffness and coefficient of damping increased significantly as the compressive pendulum load increased (Table 6).
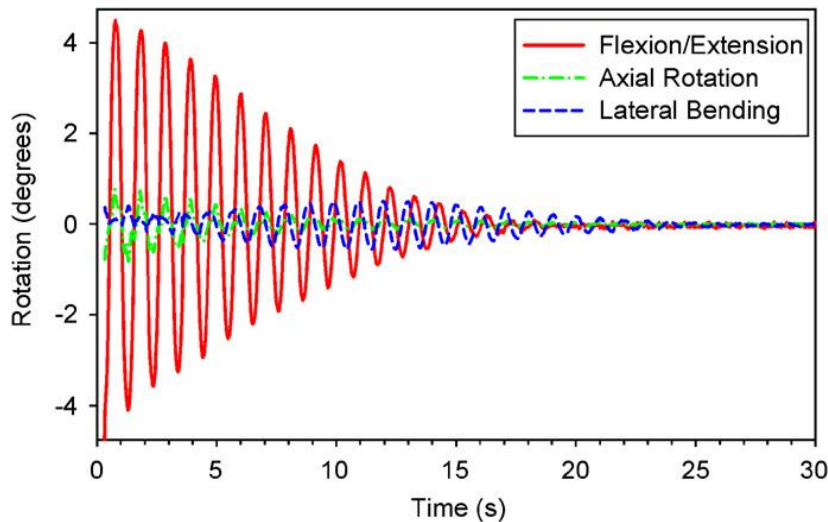
Figure 27 Typical relative rotations for an FSU with a compressive pendulum load of 385N and an initial rotation of 5° in extension (Crisco et al., 2007)

Compressive load (N)	Period (s)	Natural frequency ($2\pi/s^{-1}$)	Bending stiffness (Nm/°)	Coefficient of damping (Nm/s)
78	0.61 (0.09)	10.4 (1.6)	1.7 (0.7)	1.4 (0.9)
181	0.81 (0.07)	7.9 (0.8)	2.3 (0.8)	1.9 (0.3)
282	0.92 (0.06)	6.8 (0.5)	2.5 (0.6)	2.3 (0.4)
385	0.97 (0.06)	6.5 (0.4)	3.0 (0.7)	3.8 (0.5)
488	1.00 (0.05)	6.3 (0.3)	3.5 (0.8)	4.0 (0.8)

Table 6 Average (± one S.D.) response of the FSUs (n = 5) for increasing axial compressive pendulum loads (Crisco et al., 2007).

4. 2. 9 Contribution of bone components

Roux et al. (2010) in his *ex vivo* study tried to determine the relative contributions of bone mass, trabecular microarchitecture, cortical thickness and curvature to the mechanical behaviour of human lumbar vertebrae.

Bone mineral density (BMD) of the vertebral body was assessed by lateral dual energy X-ray absorptiometry (DXA, Delphi W, Hologic, Waltham, MA, USA) and 3D trabecular microarchitecture and anterior cortical thickness and curvature was assessed by micro- computed tomography (μCT, Skyscan 1076, Aartselaar, Belgium). 2D to 3D processing, analysis, and visualization were performed using Skyscan Ant software (Figure 28). The anterior cortical radius of curvature (Ct.Curv) measurement was expressed by the mean of three 2D slice-scans using Morpho Expert Explora Nova software (La Rochelle, France) (Figure 29).
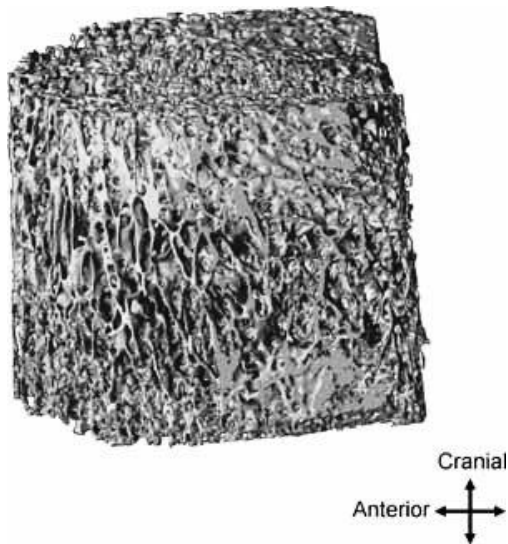
Figure 28 Vertebral trabecular bone compartment of a 75year-old male (Roux et al., 2010).
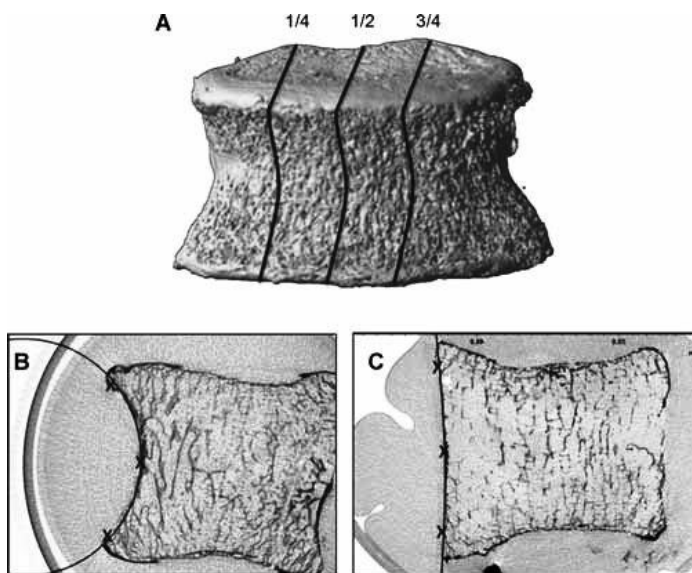

Figure 29 A) Three 2D slices were selected for measurement of the radius of curvature (1/4, 1/2, and 3/4 positions). The radius of curvature on the anterior cortical was expressed by the mean of these three measures. B), C) Anterior cortical radius of curvature measurement. Three points (superior, middle, and inferior) were positioned on the anterior cortex, and then a circle was automatically defined. B) A 54 year-old female, radius of curvature = 29.18 mm. C) An 86 year-old female, radius of curvature = 70.09 mm (Roux et al., 2010).

Then compressive stiffness, work to failure, and failure load were measured on the whole vertebral body with use of a screw-driven machine (Schenck RSA-250, Darmstadt, Germany). Results of measurements are shown in Table 7. The study showed that bone mass parameters (BMC, BMD, vBMD, and BV/TV) were strongly correlated with vertebral compressive stiffness and failure load, whereas only BMC and BMD were associated with work to failure (Table 8).

	Mean ± SD	Range
DXA measurements		
BMC (g)	6.6±1.69	2.96–9.68
BMD (g/cm^2)	0.62±0.11	0.36–0.80
vBMD (g/cm^3)	0.13±0.03	0.06–0.20
µCT measurements		
BV/TV (%)	15.31±5.05	7.17–25.85
Tb.Th (µm)	224±44	160–330
DA (n)	0.44±0.04	0.36–0.51
SMI (n)	1.83±0.24	1.26–2.25
Ct.Th (µm)	641±400	206–1983
Ct.Curv (mm)	33±15	12–70
Mechanical tests		
Failure load (N)	2644±1012	651–5481
Compressive stiffness (N/mm)	3072±1545	663–6741
Work to failure (N/mm)	1640±978	453–4158

DXA = dual energy X-ray absorptiometry; BMC = bone mineral content; BMD = bone mineral density; vBMD = volumetric bone mineral density; µCT = micro-computed tomography; BV/TV = bone volume/tissue volume; Tb.Th = trabecular thickness; DA = degree of anisotropy; SMI = structure model index; Ct.Th = anterior cortical thickness; Ct.Curv = anterior cortical radius of curvature.

Table 7 Descriptive Statistics of Measured Parameters (Roux et al., 2010)

	BMC	BMD	vBMD	BV/TV	Tb.Th	DA	SMI	Ct.Th	Ct.Curv	Failure load	Stiffness
BMD (g/cm^2)	0.86[***]										
vBMD (g/cm^3)	0.51[**]	0.64[***]									
BV/TV (%)	0.34	0.58[***]	0.70[***]								
Tb.Th (µm)	0.42[*]	0.35	0.08	0.37[*]							
DA (n)	−0.11	−0.18	−0.34	−0.59[***]	−0.42[*]						
SMI (n)	−0.27	−0.47[**]	−0.45[*]	−0.80[***]	−0.35	0.21					
Ct.Th[a] (µm)	0.61[***]	0.46[**]	0.09	0.29	0.68[***]	−0.09	−0.35				
Ct.Curv[a] (mm)	−0.60[***]	−0.50[**]	−0.27	−0.03	−0.36[*]	0.09	−0.14	−0.41[*]			
Failure load (N)	0.56[***]	0.70[***]	0.50[**]	0.47[**]	0.08	0.09	−0.58[***]	0.36[*]	−0.16		
Stiffness (N/mm)	0.45[*]	0.60[***]	0.61[***]	0.48[**]	−0.22	−0.02	−0.43[*]	0.01	0.06	0.75[***]	
Work to failure[a] (N/mm)	0.45[*]	0.55[***]	0.17	0.27	0.44[*]	0.07	−0.36[*]	0.61[***]	−0.36[*]	0.67[***]	0.14

BMC = bone mineral content; BMD = bone mineral density; vBMD = volumetric bone mineral density; BV/TV = bone volume/tissue volume; Tb.Th = trabecular thickness; DA = degree of anisotropy; SMI = structure model index; Ct.Th = anterior cortical thickness; Ct.Curv = anterior cortical radius of curvature.

a   Logarithmic transformation.
* $p < .05$;
** $p < .01$;
*** $p < .001$.

Table 8 Pearson Correlation Coefficients Between Bone Mass Parameters, Trabecular Microarchitecture Parameters, Cortical Parameters, and Mechanical Behaviour (Roux et al., 2010).

The data imply that measurements of cortical thickness and curvature may enhance prediction of vertebral fragility and that therapies that improve both vertebral cortical and trabecular bone properties may provide a greater reduction in fracture risk.

4. 2. 10 Finite element model

Schmidt (2010) developed a finite element model of the lumbar spine to analyze spinal response under dynamic physiological loading and unloading during diurnal activities. The model was constructed using data of 46-year-old male subject with no signs of degeneration.

The model (Figure 30) consists of eight distinct structural regions: namely cancellous bone, cortical bone, posterior bony elements, annulus, nucleus, cartilaginous and bony endplates plus seven major ligaments. The FE software ABAQUS 6.9 (SIMULIA, Providence, RI, USA) was used for simulations assuming fully saturated and incompressible phases. The 20-node, fully integrated elements with quadratic interpolation of displacement fields and linear interpolation of pore pressure were used for the annulus ground substance, nucleus, cartilaginous and bony endplates as well as cancellous and cortical bones. For the posterior structures, the fluid phase was neglected (Schmidt et al., 2010).
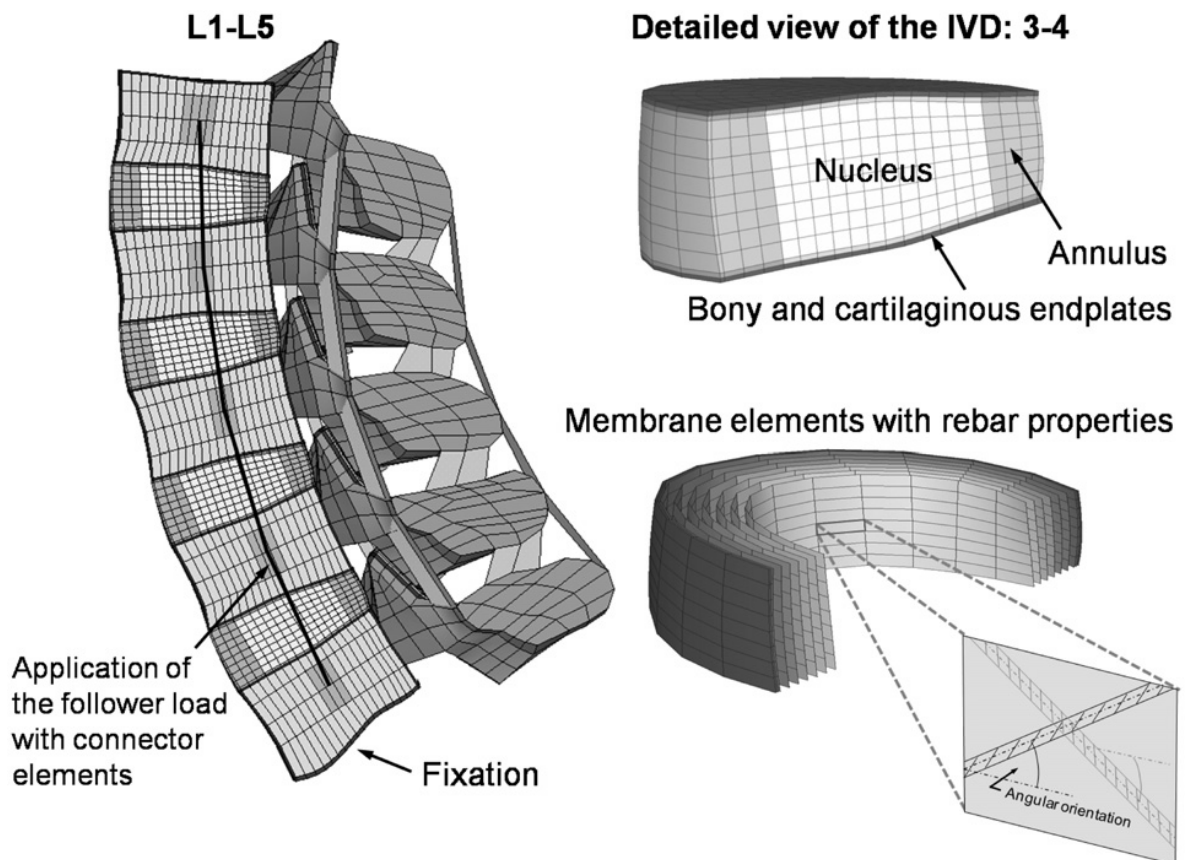

Figure 30 Finite element model of the whole lumbar spine L1–L5 depicting the follower loading. Top right: detailed view of the intervertebral disc (IVD: 3–4) used for data analysis. Bottom right: membrane elements with the rebar option simulating direction dependent non-linear stress–strain behaviour of the collagen fibres (Schmidt et al., 2010).

Time schedule for simulated loading describes Figure 31. Results showed faster recovery phase compared to the loading period, an increase in the axial displacement, fluid loss, axial stress and disc radial strain and a decrease in the pore pressure and disc collagen fibre strains. Authors of the study compared these computed results with experimental in vivo and in vitro studies and stated a fairly good agreement.

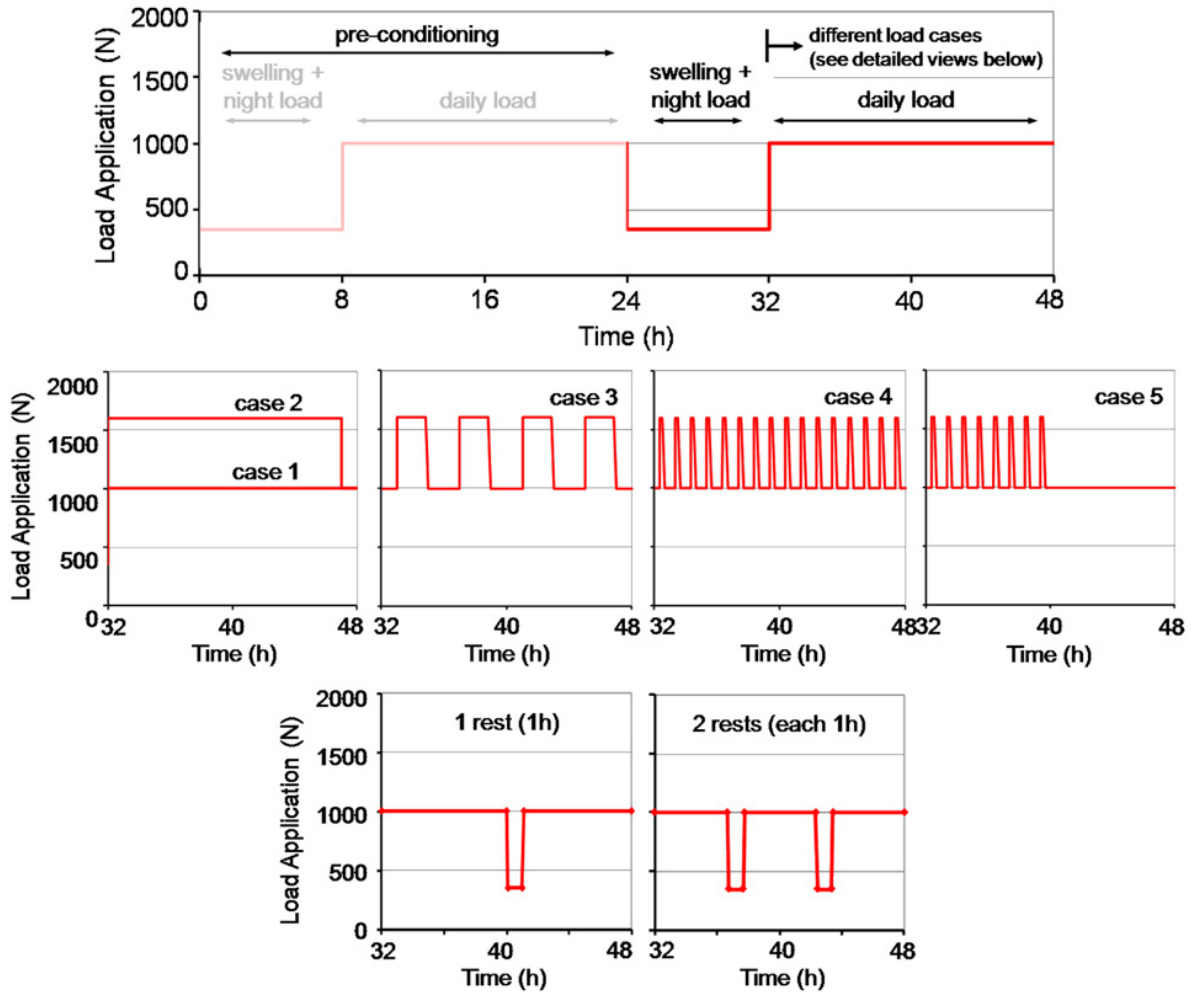Figure 31 Top: time history of the applied compressive force. After a pre-conditioning period (first 24 h), a second daily cycle was simulated consisting of an 8 h resting period, where fluid was imbibed due to swelling, followed by 16 h diurnal activity (middle). Bottom: in two additional simulations, the constant 1000 N load application was interrupted by one and two rests of 1 h (Schmidt et al., 2010)

4. 2. 11 Loading during growth

A study using dual-energy X-ray absorptiometry (DXA) to determine the relation between gymnastics exposure during growth and plane-specific advantages in vertebral body volumetric density, geometry and theoretical axial compressive strength was led by Dowthwaite et al. (2011).

Paired posteroanterior (PA) and supine lateral (LAT) DXA scans (Hologic Discovery A, software v.12.7.3.2:3) (Figure 32) of the third lumbar vertebra (L3) were taken for 114 females (60 ex/gymnasts and 54 non-gymnast athletes), post or pre-menarcheal. The reason for including only L3 data was to avoid an inclusion of rib and iliac crest overlap within the region of interest for L2 and L4.
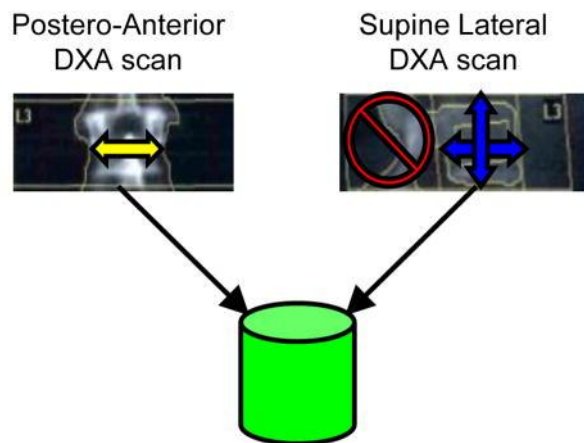
Figure 32 Simplified Geometric Model of Lumbar Vertebral Body L3: Mean width derived from the PA DXA scan is combined with mean height and mean depth derived from the Lateral DXA scan, yielding a three-dimensional model of the L3 vertebral body (elliptical cylinder). Using this model, mean width, depth and height are allowed to vary independently (Dowthwaite et al., 2011).

Vertebrae of females exposed to gymnastic training threshold during growth had shorter, wider vertebral bodies and showed greater areal BMD (aBMD) (Figure 33) and vertebral compressive strength (IBS = index of structural strength in axial compression) (Figure 34). Despite there was no bone mineral apparent density (BMAD) advantage, the vertebrae fracture risk (FRI = fracture risk index) was lower and cross sectional area (CSA) was greater than in group of non-gymnasts.
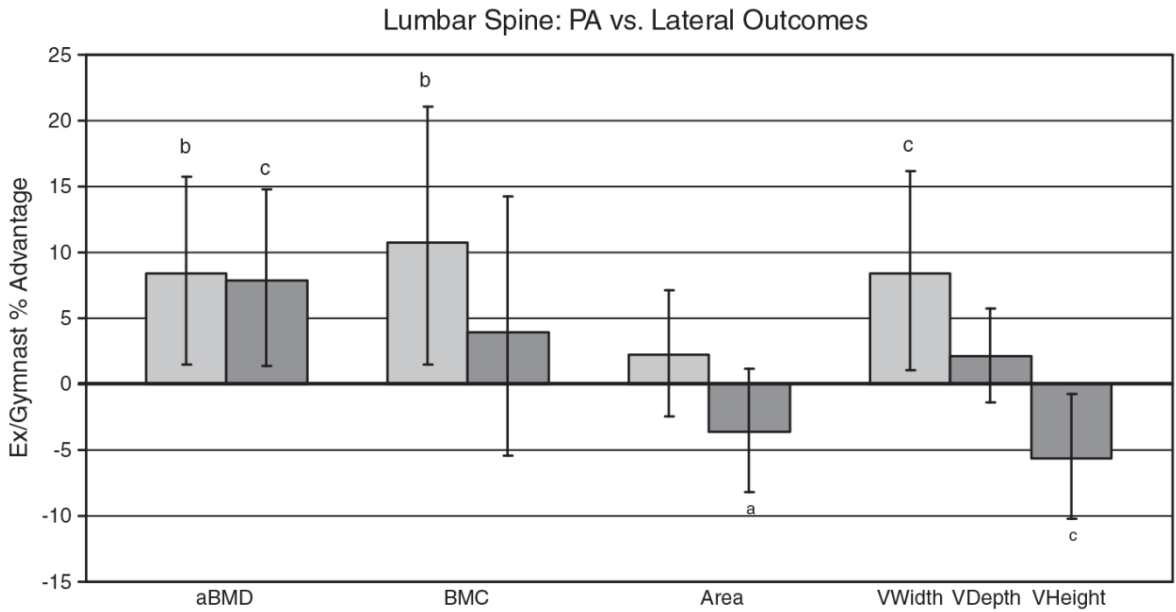
Figure 33 Percent advantages are presented for ex/gymnasts relative to non-gymnasts in graphical form. The zero line represents the mean for non-gymnasts. Reported outcomes account for the main effect of menarche status, the interaction between menarche status and gymnastic exposure, and the effects of age and height. Pale gray bars represent PA values; dark gray bars represent Lateral values. a = p<0.05; b = p≤0.01; c = p≤0.001 (Dowthwaite et al., 2011).
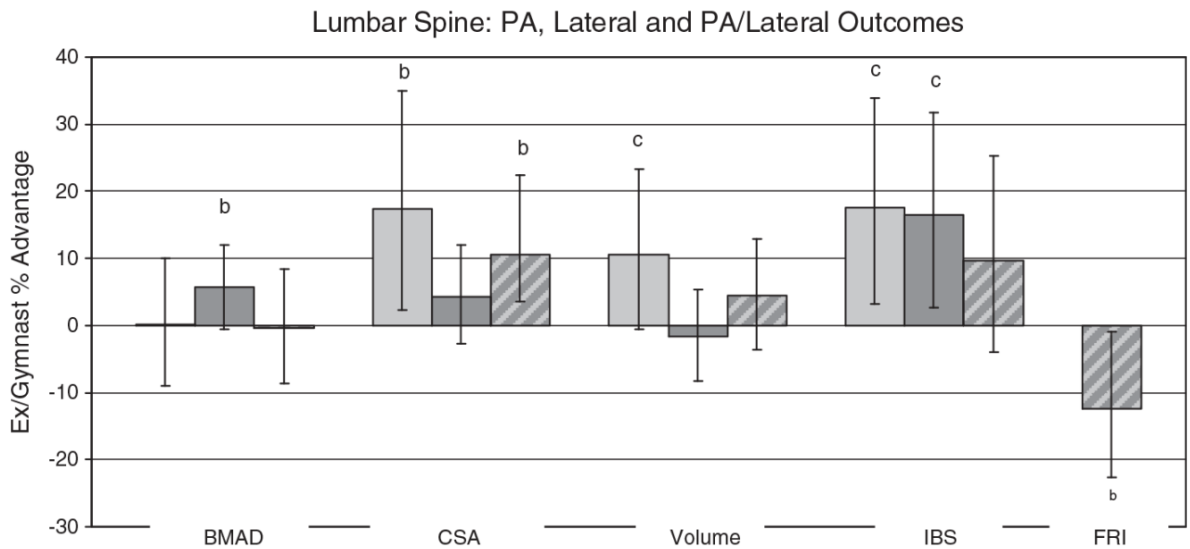
Figure 34 Percent advantages are presented for ex/gymnasts relative to non-gymnasts in graphical form. The zero line represents the adjusted mean for non-gymnasts. Reported outcomes account for the main effect of menarche status, the interaction between menarche status and gymnastic exposure, and the effects of age and height, except for FRI which is adjusted only for age. Pale gray bars represent PA values; dark gray represents lateral scan values; striped bars represent PALAT (paired scan) values; scan outcomes are placed in this order from left to right. a=pb0.05; b=p≤0.01; c=p≤0.001 (Dowthwaite et al., 2011).

4. 2. 12 Summary

Hauerstock´s study (2000) was the first one to demonstrate the magnitude of in vivo axial loads in the sheep lumbar spine. Anyway the fact, that only two animals were used during the measurements (after the two others died) shows the problems and demands of in vivo studies. Following researchers are using the data for testing animal specimens in vitro (Stokes et al., 2002) or for testing spinal implants. The above mentioned uses data from Hauerstock´s measurements despite different species involved (sheep and pigs) and presumes analogous loading stereotype in these quadruped animals. The load cells used in these two researches are different given the character of each study (in vivo/in vitro). Stokes et al. (2002) emphasize the importance of preloading during simulation of in vivo loading.

Fujiwara et al. (2001) combined anatomical and biomechanical measurements. It is possible to find previous studies of morphologic changes in the intervertebral foramen during flexion and extension; however this study examined also changes during lateral bending and axial rotation. Also no previous study confirmed the relationship between spinal motions and changes in intervertebral foraminal dimensions. According to the authors further studies are needed to assess the dynamic changes in the intervertebral foramen in vivo and to examine the relationship among the severity of foraminal stenosis, segmental instability, and radicular symptoms.

During load testing, the common substance for embedding or fixing samples emerges to be a polymethylmethacrylate (PMMA)[2]. For instance, Fujiwara et al. (2001), Stokes et al. (2002) and Costi et al. (2007) used PMMA in the studies reviewed in this work.

Results of testing the failure load and stiffness of vertebral endplates (Grant et al., 2002) revealed that the strongest regions of the endplate do not change with either bone density or disc degeneration. This information implies that implants designed using the basic structural property maps for the L3-L5 endplates are suitable even for patients with a wide range of pathologies.

---

[2] Polymethylmethacrylate (PMMA) is biologically compatible with human tissue and it has been used as a bone cement in the spine since the 1940s. PMMAs contain methylmethacrylate which polymerizes and hardens, achieving high compressive strength compared to cancellous bone. The compressive strength of PMMAs is typically 70MPa or more, while the compressive strength of vertebral cancellous bone is generally 5 to 10MPa. PMMAs are less able to resist torsion or shear loads compared to compressive loads, but are successfully used inside the vertebral body, where the torsion and shear loads are also low(Kurtz and Edidin, 2006).

The results of Tsantrizos at al. (2005) study of NP migration may provide an explanation to the segmental instability observed in degenerated segments as well as the associated annular tears present in the posterolateral region before IVD failure. His method of using a wire grid was used afterwards (Costi et al., 2007) to measure maximum shear strains experienced by disc tissues. The above mentioned also used a 6-DOF hexapod robot described in Stokes et al.´s study (2002) for his testing. Evidently, using already validated method saves time and enables comparison of results. The results of these in vitro studies provide better understanding of disc behaviours under loading and may also contribute to validating finite element models.

Two numerical techniques are presented in this chapter, quadrilateral element model (2D) was used to determine how sagittal profile of the spine (derived from X-ray scans) influence spinal coupling and loads (Keller et al., 2005) and finite element model of spine (Schmidt et al., 2010) was developed to analyze dynamic loading and unloading during diurnal activities. Numerical techniques individualize the process of measuring anatomical and morphological changes in human spine using personal data of each subject. Of course, imaging techniques like X-ray, MRI and CT are necessary to obtain input data. This field is still quite new in spine research and its development is quite fast. Many numerical techniques are in process of validation.

Crisco et al. (2007) introduced a novel technique of mechanical in vitro loading – a pendulum apparatus, which appears to be attractive providing a realistic simulation of in vivo loading conditions without constraining the kinematics of the joints. The study was led only on 5 samples of FSU and for those no level of degeneration was determined. Considering the average age of human spines (57.3±9.9 years) it is very likely some age or disease-related signs of degeneration could have been found. These potential changes could have affected biomechanical properties of tested tissue.

Even though Roux et al. (2010) describe their study as ex vivo, bone specimens were maintained frozen at – 20°C before µCT and mechanical testing, so we could not speak about loading fresh specimens. Authors presented a way of prediction of vertebral fragility, which may be useful in our aging society, where osteoporosis and its consequential vertebral fracture is a real threat for elderly people. Measurements of cortical thickness and curvature could contribute to early identification and treatment of patients at risk of vertebral fracture. Combining modern imaging techniques and

mechanical loading brought interesting correlations between structural properties of the bone tissue and mechanical behaviours of vertebrae.

Dowthwaite et al. (2011) used DXA to determine BMD, BMC and geometrical data of human vertebrae. Their research contributes to a discussion about pros and cons of professional sport training and its health issues, especially in gymnastics. Their results indicate that due to specific adaptation of vertebrae to mechanical loading during growth, gymnasts have shorter and wider vertebral bodies that show greater axial compressive strength and lower fracture risk. In the study, detailed subject characteristics could be found including BMI, percent body fat and physical activity of tested subjects. Comparison of pre and post menarche women has limitations because it does not involve the same individuals.

As could be seen, biomechanical loading experiments vary a lot and often only a small part of a spine is under examination. Afterwards, such partial information must be assembled for the purpose of fabrication of spinal implants and chirurgical management of degenerative diseases of the spine.

4. 3 Degeneration and age-related changes of the spine

Articles, chosen to this chapter, are trying to illustrate a range of different age-related changes of the spine and possibilities of their detection. Fundamental changes appearing at biochemical level influence biomechanical properties of the tissue. Finally, this phenomenon is reflected in the morphology of different components and its patterns of movement (Bogduk, 2005).

Combination of imaging and loading methods appears with intention to determine the relationship between degeneration and biomechanical functions of the spine. Also relatively new imaging method is presented: Diffusion tensor imaging (DTI). A numerical technique is shown to determine fibre reorientation of degenerated annulus fibrosus. To present a research on biochemical level, analysis of extracellular matrix is described.

Author & Year	Methods	Type of study	Region	Specimens	Measurements
Tanaka et al. (2001)	MRI cryomicrotome fibreglass rods Vicon cameras	in vitro	lumbar	human	Relationship between degenerative changes of IVD and biomechanical functions of the spine
Guerin and Elliott (2006)	camera, computer software, FFT (Fast Fourier transform)	in vitro	lumbar	human	Fibre reorientation of degenerated AF tissue
Singh (2009)	chemical assays comparative Western blotting	ex vivo	lumbar	human	Age-related changes in ECM of IVD
Zhang (2012)	DTI (Diffusion tensor imaging)	in vivo	lumbar	human	Age-related degenerative changes in IVD

Table 9 Degeneration and age-related changes of the spine

4. 3. 1 Biomechanical properties and degeneration

The purpose of the current study (Tanaka et al., 2001) was to investigate the relationship between degenerative grades of the lumbar intervertebral disc and three-dimensional biomechanical characteristics of the motion segment under multidirectional loading conditions.

114 specimens, lumbar motion segments from T12–L1 to L5–S1 taken from 47 fresh human cadaver spines, were imaged on a GE Signa 1.5-Tesla MR unit (General Electric, Inc., Milwaukee, WI) with a 12.7-cm-diameter send and receive solenoid coil. T1- and T2-weighted axial and sagittal images were obtained with a spin-echo sequence. On the basis of the T2-weighted midsagittal MR images, discs were graded for the severity of degeneration from grade I to V according to Thompson's grading system (Thompson et al., 1990).

Before biomechanical testing, the superior and inferior vertebrae of the motion segment were embedded in polymethylmethacrylate (PMMA). Fibreglass-threaded rods of 0.95 cm diameter were inserted anteroposteriorly and transversely into the vertebral bodies along the midline axis of the spine to obtain rigid fixation between the vertebrae and PMMA. On each PMMA structure, three nylon balls (0.64 cm diameter) were attached as reflective markers (Figure 35). Positioning of the markers was following: one in front of the PMMA structure and the other two on the

Figure 35 The motion segment for biomechanical testing; the superior and inferior vertebrae were embedded in PMMA, and reflective nylon balls were attached on the PMMA (Tanaka et al., 2001).

sides of the structure so that the midpoint of these markers could be located approximately at the centre of the vertebra. Loads were applied by cords attached to the fibreglass rods embedded in the PMMA superstructure and routed through pulleys to dead weights. The loads were applied perpendicularly to each of two rods in opposite directions to produce the six load steps from 0.5 to 5.7 Nm applied in flexion, extension, left and right lateral bending, and left and right axial rotation. There was five minutes pause between each load step and the order of application was randomly changed so

that any type of load could be the last. As the loads were applied to each motion segment, the positions of each reflective marker in 3-D space were measured by VICON cameras (Oxford Metrics, Ltd., Oxford, England) and recorded in the Micro-Vax 3100 workstation (DEC, Ltd., Maynard, MA).

Afterwards the motion segments were sectioned in the sagittal plane with a cryomicrotome (a tool used to cut extremely thin slices of frozen material; model 2250, PMV, Bromma, Sweden). Sections were obtained at 1-mm intervals, and a photograph was taken of the surface at every slice. The photographs of the midsagittal section were used to grade the gross morphology of the intervertebral disc from I to V.

Both cryomicrotome sections and MR images (Figure 36) were graded independently by three observers and no statistical difference was found between the grades based on the two types of images. When the MR images were graded, 2 segments had grade I disc degeneration; 45, grade II; 20, grade III; 26, grade IV; and 21, grade V. When the cryomicrotome sections were graded, 14 segments had grade I disc degeneration; 31, grade II; 22, grade III; 26, grade IV; and 21, grade V. However, 13 of 14 discs that were assigned to grade I based on cryomicrotome sections were assigned to grade II based on MR images. These findings suggest that MR images reflect the morphologic changes in degeneration of the intervertebral disc except for early grades I and II.
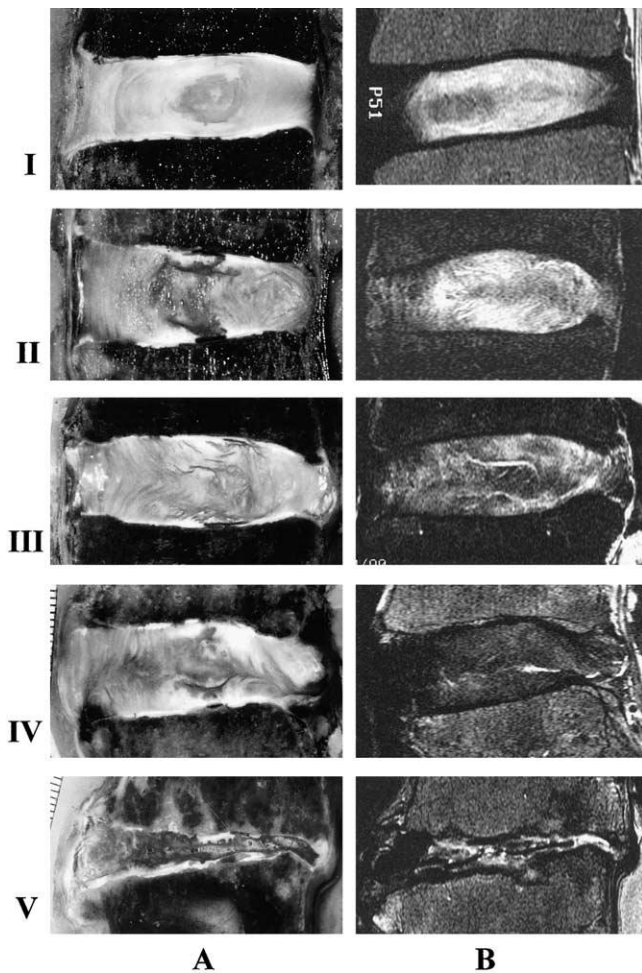

Figure 36 A) Photographs of the midsagittal cryomicrotome sections of the IVD with disc degeneration from grades I to V. B) T2-weighted midsagittal MR images of the IVD with disc degeneration from grades I to V (Tanaka et al., 2001).

Segments from the upper lumbar levels (T12–L1 to L3–4) tended to

have greater rotational movement in flexion, extension, and axial rotation with disc degeneration up to grade IV, whereas the motion decreased when the disc degenerated to grade V. In the lower lumbar spine at L4–5 and L5–S1, motion in axial rotation and lateral bending was increased in grade III. These results suggest that biomechanical functions of the lumbar spine are related to disc degeneration. Greater motion generally was found with disc degeneration, particularly in grades III and IV, in which radial tears of the annulus fibrosus are found. Disc space collapse and osteophyte formation as found in grade V resulted in stabilization of the motion segments.

4. 3. 2 Annulus fibrosus fibre reorientation

Guerin and Elliott (2006) confirmed their hypothesis that fibre tissue of degenerated AF reorient less than tissue of non-degenerated AF. Uniform, rectangular-shaped samples of dissected outer annulus fibrosus of IVD were mechanically tested in custom-designed grips (Instron 5542, Instron, Canton, OH) in circumferential (x1) uniaxial tension (see Figure 37).
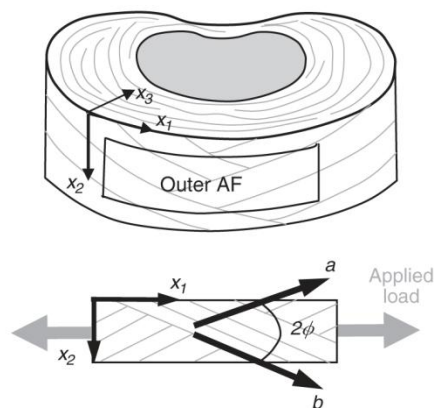

Figure 37 Sample location and loading orientation (Guerin and Elliott, 2006).

A high-resolution CCD camera (Kodak, Rochester, NY) coupled to a stereomicroscope (Leica Microsystems, Bannockburn, IL) was used to capture the sample images during testing in a resolution of approximately 1000 pixels/mm. Authors (Guerin and Elliott, 2006) describe the process of analysing each image to determine fibre angle:

Using Adobe Photoshop and Image Processing Tool Kit add-in software (Reindeer Graphics, Asheville, NC) original images (Figure 38a) were cropped, processed using contrast adjustment and the Sobel direction edge detection operator, and thresholded to emphasize fibre populations (Figure 38b). A custom-written Matlab image analysis program was used to determine fibre angle from these processed images (Figure 38c).
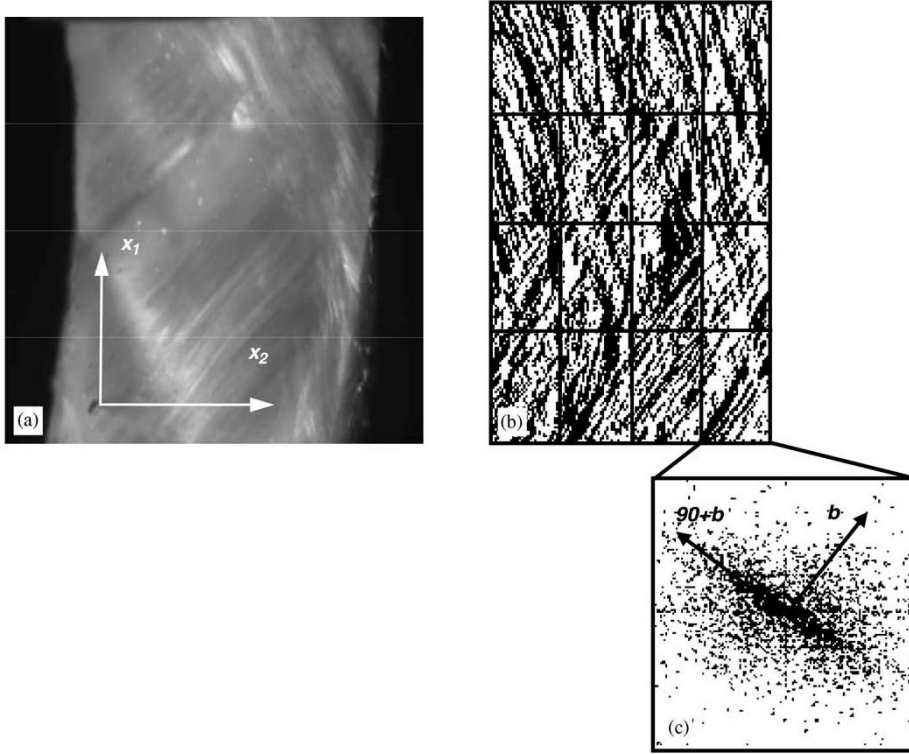
Figure 38 Image processing and FFT analysis: (a) Original image with axis. (b) Processed image with representative analysis regions. (c) FFT power spectrum (inverted) of one analysis region showing preferred orientation corresponding to fibre population b (Guerin and Elliott, 2006).

Each analysis region was padded with blank pixels to form a square image, and Fast Fourier transform (FFT) analysis was applied to the square analysis region. A two-dimensional discrete Fourier transform (DFT) was applied to each analysis region:

$$F(k,l) = \frac{1}{N^2} \sum_{i=0}^{N-1} \sum_{j=0}^{N-1} f(i,j) \mathrm{e}^{-i2\pi\left((ki/N)+(lj/N)\right)}, \qquad \text{Equation 4}$$

where F(k, l) are the pixel values of the transformed image, N is the number of rows and columns of the original and transformed images (which must be square), and f (i, j) represents the analysis region of the original image. The FFT transformed the analysis region into frequency space, where each pixel has a complex value. The power spectrum, the log of the magnitude of each pixel in the frequency space, provided a visual interpretation of the FFT (Fig. 2c). In the power spectrum, frequency was represented by distance from the origin. The orientation of the maximum intensity region in the power spectrum was found by summing the pixel intensity values along 175-pixel long radii spaced 1° apart, yielding an accuracy of 0.5°. Fibre orientation in each analysis region was then calculated by subtracting the 90° offset from the angle of maximum intensity in the power spectrum.

This newly applied image processing technique was validated for quantification of AF fibre reorientation in the study. Results showed AF fibres reorient toward the loading direction. Moreover degeneration significantly decrease fibre reorientation; the fibre reorientation parameter was $m_{FFT}= -1.70°/\%$ strain for non-degenerated and $-0.95°/\%$ strain for degenerated tissue.

4. 3. 3 Biochemical analysis

In Singh et al.'s study (2009) the IVD specimens were received within 24 hours of death, Thompson (Thompson et al., 1990) degeneration grades were obtained from MRI and only those classified as Grade 1 or 2 were further analysed. Then the IVDs were dissected to three parts: inner annulus fibrosus (i-AF), outer annulus fibrosus (o-AF) and nucleus pulposus (NP). Weighted and freeze-dried samples underwent a PicoGreen DNA assay (Molecular Probes, Eugene, OR), a measurement by a spectrofluorometer (emission 415nm, excitation 365nm) and DNA contents were calculated using a standard curve calibrated using calf thymus DNA.

The extracellular matrix of IVD tissues underwent a biochemical analysis to determine the total proteoglycan content by the Dimethylmethylene blue assay and the total collagen content using a the HPLC-based assay (Petit et al., 1996). The small proteoglycan protein levels in tissue extracts were analyzed by comparative Western blotting (Gruber and Hanley, 2002).

As shown in Figure 39 and Figure 40 total proteoglycan and collagen contents in both AF and NP decreased with aging. The small non-aggregating proteoglycan concentrations do not show the same tendency in this study: in the o-AF decorin levels decreased while biglycan and fibromodulin levels increased with age. In the i-AF and NP samples, biglycan demonstrated a significant increase with aging. However the functional significance of these changes is yet not clear.
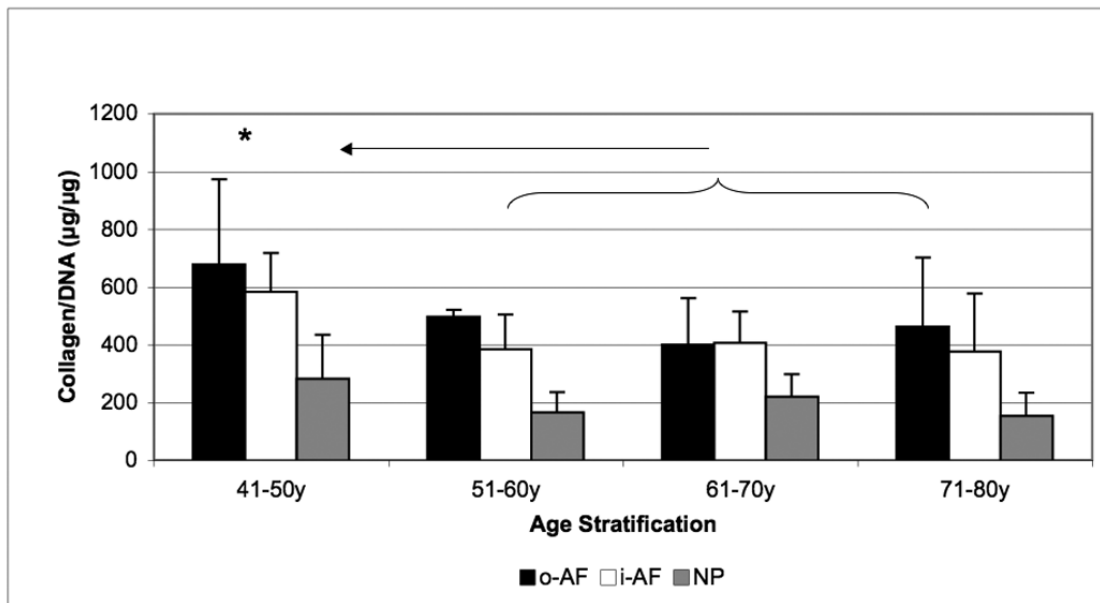
Figure 39 Age-related changes in collagen content of the outer-AF (black bars), inner-AF (white bars) and NP (gray bars) of human intervertebral discs. Data normalized to DNA content in each case. (* p<0.05) (Singh et al., 2009)
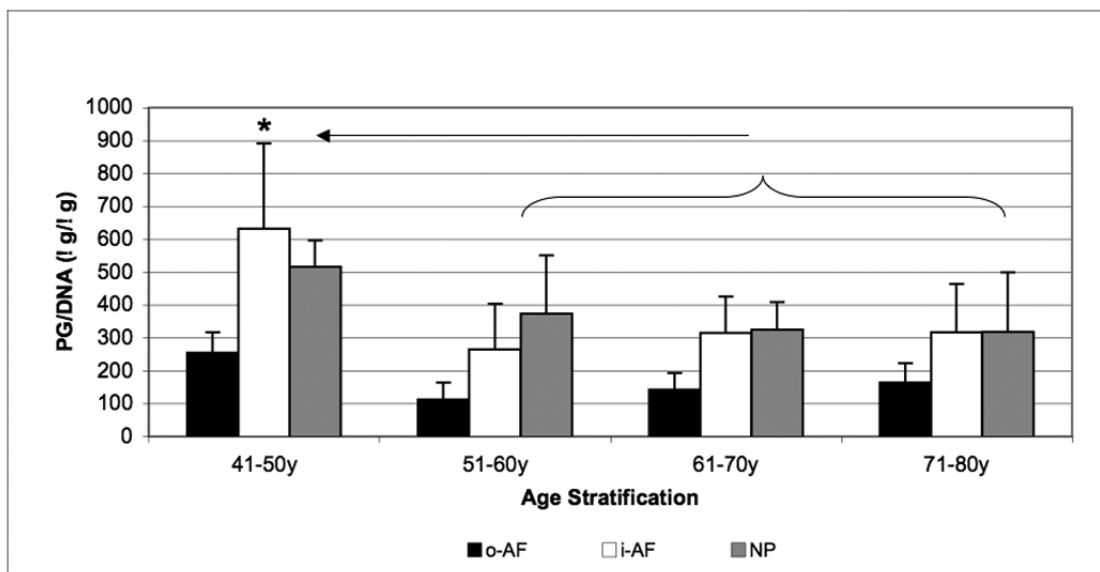
Figure 40 Age-related changes in proteoglycan content of the outer-AF (black bars), inner-AF (white bars) and NP (gray bars) of human intervertebral discs. Data normalized to DNA content in each case. (* p<0.05) (Singh et al., 2009)

4. 3. 4 Diffusion tensor imaging

A pilot study to determine whether age-related changes in human lumbar IVD can be quantitatively accessed by DTI-derived metrics was led by Zhang et al. (2012). In the study on thirty asymptomatic volunteers (age range 25 – 67 years) researchers performed DTI with reduced field of view at a Philips 3 T MRI Achieva scanner (Philips Healthcare, Best, the Netherlands).

DTI data were processed using a custom written program in Matlab (Mathworks, Natick, MA, USA). For each voxel, the three eigenvalues (λ1, λ2, λ3) and their corresponding eigenvectors were calculated (Basser and Pierpaoli, 1996). Then the mean diffusivity (MD), which represents the average diffusion rate in a biological tissue, and fractional anisotropy (FA), which is related to the extent of diffusion anisotropy, were calculated from the eigenvalues:

$$MD = \frac{1}{3}(\lambda_1 + \lambda_2 + \lambda_3),$$

Equation 5, 6

$$FA = \sqrt{\frac{3}{2} \cdot \frac{(\lambda_1 - MD)^2 + (\lambda_2 - MD)^2 + (\lambda_3 - MD)^2}{\lambda_1^2 + \lambda_2^2 + \lambda_3^2}}.$$

After an analyse of these DTI-derived metrics by a histogram analysis (which allows objective quantification of diffusion properties of the disc), a Mann-Whitney test was used to compare the two subject groups, young and elderly (48 years and more), with respect to each of the two diffusion metric means. All statistical computations were carried out using commercially available software (SPSS version 18.0.0, Chicago, IL, USA).

The study yielded significant age-related changes in the samples of each group (Figure 41). Results showed decrease of MD (11%, P<.001) and increase of FA (20%, P<.001) which demonstrate the possibility to measure the degenerative-related changes by DTI-derived metrics. Researchers suggest that it would be worthwhile to validate the relationship between DTI metrics and the actual degenerative status of IVDs using extracted disc samples and to extend it to studies on patients with degenerative discs in order to further explore the clinical usefulness and relevance of DTI (Zhang et al., 2012).
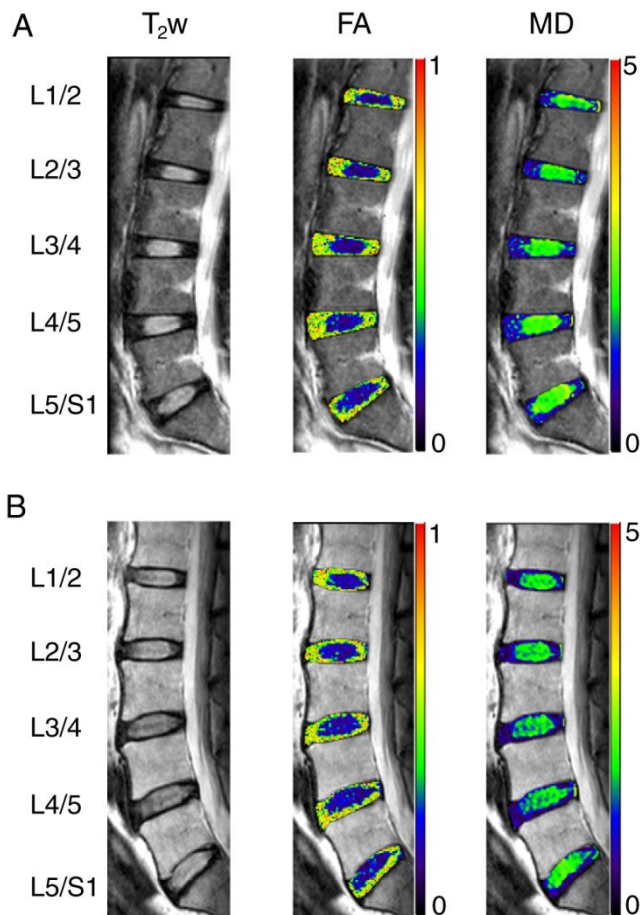
Figure 41 Representative colour maps illustrating the spatial variation of FA (dimensionless) and MD (unit: $\mu m^2/ms$) at the middle slice. A) Twenty-five years old, female; B) 58 years old, female. All disc levels were healthy (degenerative disc disease=0) (Zhang et al., 2012).

4. 3. 5 Summary

Tanaka et al.´s (2001) research to prove the effects of IVD degeneration on biomechanical functions of the lumbar spine touches the topic of previous chapter (biomechanical loading) and also introduces the topic of current chapter: degenerative changes in IVD. Thompson's grading system (Thompson et al., 1990) is put in practice to evaluate the level of degeneration. Generally greater motion and instability was related to grades III and IV of degeneration: this fact may explain the tendency to disc bulging and herniation. But the highest grade (V) was on contrary associated with a significant decrease in motion, which could be explained by disc space collapse and osteophyte formation. Methods similar to Fujiwara et al. (2001) are used in his experiments: motion segment embedded in PMMA, three reflecting markers, fibreglass rods, vicon cameras. Also six load steps values applied are almost similar: 0.5, 1.6, 3.6, 4.7, 5.7, 6.6 at Fujiwara et al. (2001) and 0.5, 1.6, 2.7, 3.6, 4.7, 5.7 at Tanaka et al.

(2001). Knowing the fact the institutions involved are the same and that some people in these two research groups are the same, it is no wonder.

Guerin and Elliott (2006) present a better understanding of mechanical behaviour of AF and the changes linked to degeneration in this particular area. The explanation how AF fibres reorient under tensile load may provide useful information for development of artificial intervertebral disc or its parts. Using the Fourier transform (DTF and its algorithm FFT) as an image processing tool was presented and immediately validated. Mathematical computation methods constitute another technique in spine research and help to widen the knowledge in this field.

Singh et al. (2009) were analysing age related changes in the extracellular matrix of IVD from the biochemical point of view. The trend determined by this study is a general decrease in collagen and proteoglycan content with aging. On the other hand, several small proteoglycans (biglycan, fibromodulin) are increasing during aging. As written by authors, the functional significance is to be determined. May these proteoglycan molecules counterbalance some of the age-related changes in the IVD tissue? What results would show samples classified as grade IV or V i.e. discs with signs of advanced degeneration? It seems that this research brings more questions than responses.

Diffusion tensor imaging is frequently used in brain and spinal cord research and treatment. It is matter of course to test other fields where it could be useful. Zhang et al. (2012) introduced this technique to the world of IVD degeneration by this pilot study and revealed the possibility to measure degenerative changes by DTI. To the proper testing: the line drawn between the tested volunteers (48 years) was set only based on ages of the subjects in the sample with no further explanation. So it should not be considered as a well-founded dividing point between "elderly" and "young".

4. 4 Replacement of IVD

This chapter present and discuss the topic of replacement of the degenerated natural IVD by a spinal implant which may be an alternative to traditional methods of treatment, such as spinal fusion. Although the height of the FSU is restored by fusion, it brings limited motion and an adjacent segment disease may occur as well.

This limitations force scientists to search for another options. One possibility is represented by revelation of artificial materials suitable to form a convenient AID compatible with human tissue that posses the biomechanical properties of natural IVD or its parts. Another way goes through tissue engineering: isolated and cultivated cells are inserted into scaffolds to create new functional tissue, afterwards an implantation follows.

Thus, the research in this field comprises development of artificial intervertebral discs, artificial FSU or tissue engineered structure. Moreover it includes biochemical and biomechanical testing of these materials and implants. Following articles present both, development and testing of chosen structures of spinal replacement.

Author & Year	Method	Type of the implant	Material
Mizuno et al. (2004, 2006)	tissue engineering	NP and AF scaffold	polyglycolic acid, polylactic acid
Bron et al. (2009)	plastic compression	NP scaffold	collagen
Broek et al. (2012)	biomimetics	AID	ionized hydrogel, fibre jacket
Daniels et al. (2013)	total spinal segment replacement (TSSR)	Flexuspine	cobalt chrome, silicone

Table 10 Replacement of IVD

4. 4. 1 Tissue engineered composites

Mizuno et al. (2004) constructed an IVD structure consisting of scaffold from polyglycolic acid and polylactic acid with anulus fibrosus cells and nucleus pulposus cells inside. The tissue cells were gained from sheep spine and after 3 weeks of nourishing in culture, they were seeded into implants. Then these IVD implants were placed in the spine of mice for 4, 8 and 12 weeks. Afterwards implants were analysed to determine the level of proteoglycans, hydroxyproline and DNA content. As shown in Figure 42, within 12 weeks the tissue-engineered samples gained histological and biochemical characteristics of native discs.
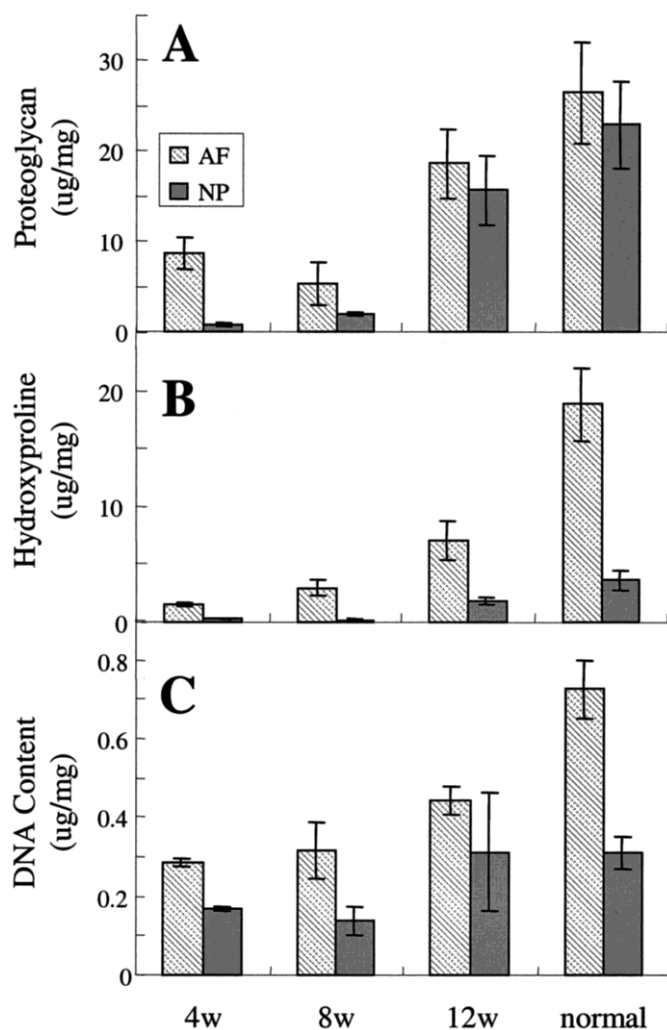
Figure 42 Biochemical composition of tissue-engineered disc constructs compared to native discs. A) Glycosaminoglycan (GAG) content of the tissue-engineered discs. B) Hydroxyproline (HYP) content of the tissue-engineered discs. C) DNA content of the tissue-engineered discs. All data are represented as mean ±SD for n = 3 samples (Mizuno et al., 2004)

Questions remaining for further research are mechanical properties of such implants and integration with surrounding tissues of the spine. The same authors (Mizuno et al.,

2006) examine almost identically prepared implants after 16 weeks in mouse spine to determine biomechanical properties of the samples. The values for the equilibrium modulus (49.0±13.2 kPa) and hydraulic permeability (5.1±1.7 x 10^{-14}m^2/Pa) were specified for implants at 16 weeks.

4. 4. 2 Dense collagen scaffolds

Researchers (Bron et al., 2009) aim their study to characterize the viscoelastic properties of the NP and to develop dense collagen scaffolds with similar properties. They also assessed the effects of a standard sterilization treatment – Gamma irradiation, which is considered as the most reliable method available of sterilizing collagen biomaterials (Friess, 1998). In the study a novel technique was used: a plastic compression technique to develop collagen I-based scaffolds with varying concentrations and viscoelastic properties (Brown et al., 2005). Before the rheological measurement took place, half of the collagen scaffold samples with four densities (0.5, 3, 6, and 12%) of collagen underwent treatment with 15 kGγ γ-irradiation according to medical implant sterilization protocol in The Netherlands. The mechanical behaviour of the collagen samples and the NP samples of a goat was assessed using a stress-controlled rheometer *(Paar Physica MCR501; Anton Paar, Graz, Austria)* in parallel plate configuration (40 mm diameter, 3,5 mm gap for scaffolds; 20 mm diameter, 2 – 3 mm gap for NP samples). Three types of rheological measurements were performed in the following order: time sweep, frequency sweep, and amplitude sweep.

Because collagen density of the samples was not higher than 12%, the stiffness equal to the stiffness of NP could not be reached. Researchers propose the stiffness of the NP should be matched by a scaffold containing 22.7% collagen. This study showed that a standard sterilization treatment of scaffolds with 15 kGγ γ-irradiation results in an over twofold increase of elastic modulus (G´) and also a significant increase of viscous modulus (G"). More importantly it showed that the resistance to high amplitude strains decreases dramatically. And the swelling capacity of the samples was significantly reduced by γ-sterilization as summarized in Figure 43.
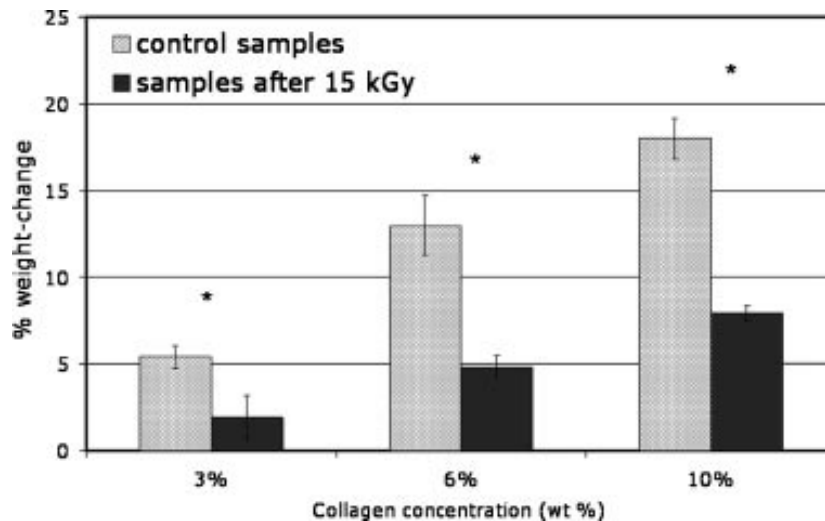
Figure 43. Statistically significant reduced (*p < 0,05) swelling capacity of the γ-irradiated samples compared to controls. Each bar represents the mean of five measurement (Bron et al., 2009).

4. 4. 3 Biomimetic AID

Broek et al. (2012) introduced the first prototypes of a new biomimetic AID, mimicking the fibre-reinforced, osmotic, viscoelastic, and deformation properties of the IVD. Their concept is based on the hypothesis that the better the material structure of the IVD is mimicked, the better its functionality is mimicked. This initial study was led to evaluate the strength and durability of the biomimetic AID and demonstrate whether its axial deformation behaviour is similar to that of a natural disc.

The AID comprises a swelling, fixed-charge, hydrogel core (the nucleus) and a surrounding 5-layer fibre jacket (the annulus), see Figure 44. The gel for the core was polymerized in a water bath (45°C), inside a mold filled with a polyurethane foam (MCF.03, Corpura B.V., Etten-Leur, The Netherlands), soaked by a monomer solution. The jacket was a knitted stocking (Varodem, Saint-Léger, Belgium) of fibres (Dyneema Purity fibre, type UG 165dtex, DSM, Geleen, The Netherlands), with a Young's modulus of 126 GPa, using 6.3 stitches per centimetre. Novel AIDs were manufactured by first wrapping the membrane around the hydrogel and then putting it inside the jacket. The open end of the jacket was twisted, and the jacket was turned inside out again around the core. Then, for both sides, the jacket was folded around the end plates. After twisting and folding once more, the opening of the jacket was sewn with Dyneema Purity fibre. The nominal lateral and sagittal diameters of the AIDs were 48 and 35 mm, respectively. The nominal height was 12 mm at 200-N preload.
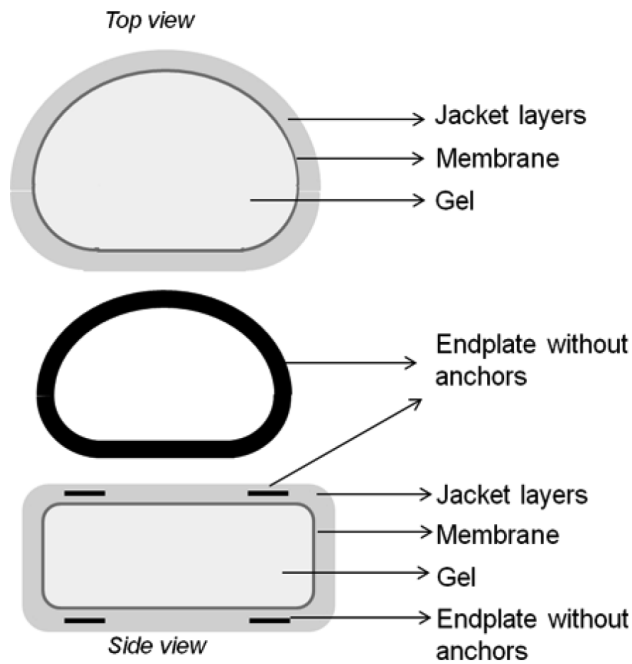
Figure 44 Schematic cross sections of the artificial intervertebral disc (Broek et al. 2012).

During mechanical loading, eighteen AIDs in total were tested in axial compression. Six were evaluated for strength. Six were tested in fatigue (600–6000 N). Another six were used to characterize the axial creep and dynamic response (0.01–10 Hz). Creep and dynamic response were also determined for four AIDs after fatigue loading. The device used was a material test system (858 Mini Bionix II, MTS Systems Corporation, MN), in 0.15 M NaCl solution at 37°C, except the creep experiments, which were performed at room temperature.

Results showed that the AIDs remained intact up to 15 kN and 10 million cycles. The creep and dynamic behaviour were similar to the natural disc behaviour, except for hysteresis, which was 20% to 30% higher. After fatigue, creep decreased from 4% to 1%, stiffness increased 2-fold, and hysteresis was reduced to that for a normal disc.

4. 4. 4 Total spine segment replacement

The replacement of the whole damaged FSU is possible with technique called Total Spinal Segment Replacement (TSSR) for which the device Flexuspine® (Pittsburgh, PA) may be used (Figure 45).

Figure 45 Total Spinal Segment Replacement device (Flexuspine®, Pittsburgh, PA). Composed of an interbody disc component with a metal-on-metal cobalt chromium articulation (Core) and posterior pedicle screw-based dynamic resistance component (Dampener) (Daniels et al., 2013).

Flexuspine's FSU Total Spinal Segment Replacement was designed to provide an alternative to fusion by reestablishing mobility to an affected segment of the lumbar spine. It is a comprehensive device composed of an interbody disc component *(Core)* and posterior dynamic resistance component *(Dampener)* that was designed as a system to replace the natural kinematics of the motion segment. The unique Cobalt Chrome metal-on-metal articulating design features two paired halves, which facilitate placement on each side of the dural sac intended to allow ample endplate coverage and natural kinematic motion. The Core is the foundational support for the FSU device. It features strength in compression while providing shear resistance intended to prevent overloading of the posterior dampening component. The combination of converging inferior endplate anchors, teeth on the superior surface, and Titanium Plasma Spray coating was designed to resist migration and provide short and long-term fixation. The Posterior Dampener component includes a Cobalt Chrome alloy pedicle screw and sliding rod assembly with silicone dampeners. The rod and screw assemblies are implanted bilaterally after facet removal. The silicone dampeners are designed to provide resistance to flexion-extension, lateral bending, and axial rotation motions. Dual silicone dampeners and sliding rod design provide physiological resistance (non-linear and direction-specific stiffness) which allows for some forgiveness in the alignment of the Dampeners to the Core component (http. 3).

Daniels et al. (2013) tested biomechanical properties using the pendulum system described above (Crisco et al., 2007) for the purpose of comparing the dynamic stiffness and energy absorption of the native FSU to TSSR device. Five human lumbar FSU were

individually tested on a pendulum apparatus as described previously (Crisco et al., 2007) with almost identical axial compressive loads (181 N, 282 N, 385 N, and 488 N). Energy absorption was measured by counting number of cycles to equilibrium of the pendulum apparatus. After the testing, the FSUs underwent Flexuspine TSSR implantation and they were re-tested on the pendulum apparatus with the same loading protocol. Those with implanted TSSR were found to have similar dynamic bending stiffness, but absorbed energy at a more rapid rate (Figure 46) than human functional spinal units during cyclic loading.
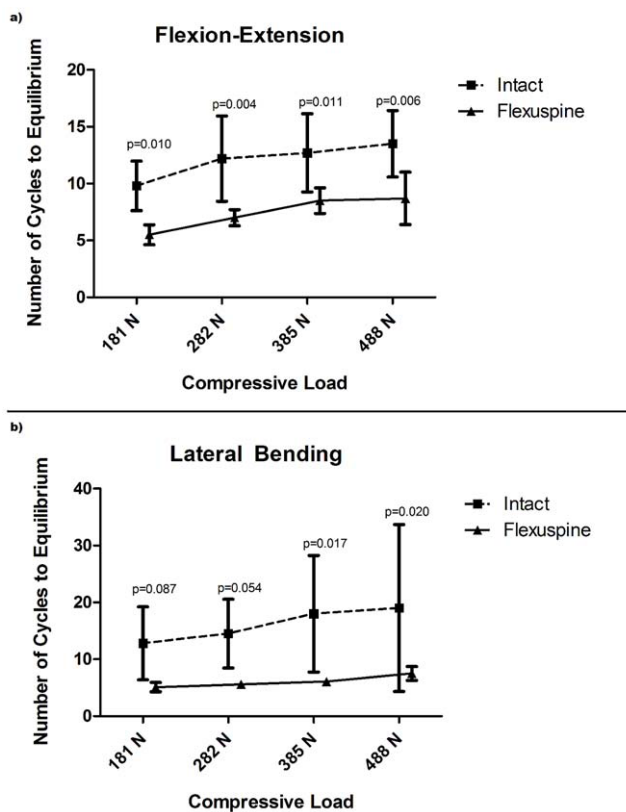

Figure 46 Pendulum testing results for mean cycles to equilibrium. Flexion/Extension (4a). Lateral bending (4b). Significantly fewer cycles to equilibrium for the TSSR indicate more rapid energy absorption for the TSSR compared to the intact FSU (Daniels et al., 2013).

4. 4. 5 Summary

Mizuno et al. (2004) present a study to characterize histological and biochemical properties of a constructed scaffolds with implanted cells. After proving that the content proteoglycans, hydroxyproline and DNA of the tissue engineered cells tend to equalize the natural disc content, Mizuno et al (2006) turned their attention also to the biomechanical characterization of such IVD structure. Tissue engineering is a field that combines biology and engineering to produce substitutes with similar functions as a human tissue or whole organ. Fabrication of scaffolds is illustrated in following paper of Bron et al. (2009). Their study did not determine exactly which collagen density matches to the viscoelastic properties of the human NP, but researchers calculated it should be a collagen concentration of approximately 23%. Anyway, they achieved a close biomechanical imitation of the NP with dense collagen matrices and for future they intend to investigate the effects of adding other proteins, such as proteoglycans. Furthermore, it clearly shows that sterilisation of scaffolds (in this case by γ-irradiation) could have an important effect on their mechanical and rehydration capacity. Thus, these factors should be considered to prevent unequal results of in vitro studies and clinical applications.

An initial study of biomimetic AID biomechanics (Broek et al., 2012) showed that a strong and durable AID was developed and manufactured. Its parts, a "nucleus" and "annulus" created a structure similar to that of natural IVD. More tests and are needed, as well as some manufacturing adjustments. However, closer behaviour of a natural disc was reached, including swelling, viscoelastic properties and shock absorption capacity. Authors think their novel implant may be a suitable alternative to ball-and-socket-type prostheses.

Daniels et al's (2013) research illustrates the possibility of total substitution of FSU using a pendulum apparatus to evaluate biomechanical properties of a device of total spine segment replacement. Unlike Crisco et al. (2007), samples of FSU in Daniels et al. (2013) study underwent radiographic screening to eliminate specimen with previous surgery, trauma or pathologies. Such comparison provides further insight into the level of development of the implant device and its possible in vivo behaviour.

It would be impossible to present all types of replacing devices and structures in this work, because there is number of them. For example, Broek et al. (2012) state that

current clinical AIDs, that is, the CHARITÉ (DePuy Spine, Inc., Raynham, MA, USA), Prodisc (Synthes, Inc., West Chester, PA, USA), and Maverick (Medtronic, Inc., Minneapolis, MN, USA), provide reasonable results, at least in the short term. Anyway, it is obvious, that most of the spinal implants have not reached the top of their function possibilities.

5. CONCLUSION

The aim of this literature review was accomplished: different imaging and measuring methods used in the last decade to identify connective tissues changes of human axial system were assembled and presented. As a secondary source the thesis does not report any original experimental work, nevertheless it may help to obtain an overview of the discussed subject and it may provide context for further studies. For this purpose, the review is divided into specific chapters that facilitate the search of particular field of interest.

Considering the countless number of research papers available, the chosen ones that were presented in this thesis should have illustrated the variety of methods used in spinal research. On the grounds of limited capacity of the thesis, chapters chosen by author do not cover the whole field of research (e. g. research on animal samples). Some studies are based on methodology previously tested and used, others are pilot studies; the reason is the same as mentioned before – to present a wide range of methods.

Geometrical parameters of vertebrae could be measured by X-ray, MRI, CT or in vitro on cadavers. Data from review studies were used for diverse reasons: comparison between populations, designs of artificial vertebral discs, clinical diagnosis and surgical management of the spine.

The possibilities of simulated loading appear to be various: custom made mechanical devices (such as hexapod robot, hemispherical indenter, screw-driven machine or pendulum apparatus) or numerical models (quadrilateral element model, finite element model). Simultaneous measurements of loading may be taken by X-ray, CT, DXA, cameras. In vivo studies of biomechanical loading appear to be enormously demanding and their number in sources view by author was much lower in comparison to in vitro studies. This fact confirms the first hypothesis that in vitro measurements prevail over in vivo measurement, as it concerns biomechanical loading.

The degenerated tissue identification depends on the level of apparition (biochemical level, biomechanical properties or morphology changes). According to this level, adequate imaging or measuring method may be used. Research question was not specific enough. There is significant difference between identification of degenerated tissue using in vitro measurements (chemical assays, cryomicrotome, loading devices

etc.) and identification of degenerated IVD or vertebrae of living patient during spinal treatment, where mostly imaging methods need to be used.

The spinal implants currently fabricated are various: artificial IVD scaffolds, tissue engineered materials or devices replacing the whole functional spinal unit. This field of research seems to have a great potential; new materials and methods are in the phase of validation.

Author tends to agree with the second hypothesis; spinal research is spreading and looking for new approaches, technologies and devices. Sometimes it could find a convenient method in a next door field like in the case of DTI frequently used in brain and spinal cord research and treatment.

The assumption that sources necessary to this study may not be available in Czech language was right and it only confirms the essential role of English on the field of research and new technology development. Further work with data from the main part is expected, so all the figures and tables are in the best quality available.

REFERENCES:

1. Basser PJ, Pierpaoli C. 1996. Microstructural and physiological features of tissues elucidated by quantitative-diffusion-tensor MRI. Journal of Magnetic Resonance B 111:209-219.

2. Bogduk N. 2005. Clinical anatomy of the lumbar spine and sacrum: Elsevier/Churchill Livingstone.

3. Brinckmann P, Horst M. 1981. Measurement of the distribution of axial stress on the end-plate of the vertebral body. Spine 6:217-232.

4. Broek PR, Huyghe JM, Ito K. 2012. Biomechanical behavior of a biomimetic artificial intervertebral disc. Spine 37: 367-73.

5. Bron JL, Koenderink GH, Everts V, Smit TH. 2009. Rheological characterization of the nucleus pulposus and dense collagen scaffolds intended for functional replacement. Journal of Orthopaedic Research 27:620-626.

6. Brown RA, Wiseman M, Chuo CB, Cheema U, Nazhat SN. 2005. Ultrarapid Engineering of Biomimetic Materials and Tissues: Fabrication of Nano- and Microstructures by Plastic Compression. Advanced Functional Materials 15:1762-1770.

7. Costi JJ, Stokes IA, Gardner-Morse M, Laible JP, Scoffone HM, Iatridis JC. 2007. Direct measurement of intervertebral disc maximum shear strain in six degrees of freedom: Motions that place disc tissue at risk of injury. Journal of biomechanics 40:2457-2466.

8. Crisco JJ, Fujita L, Spenciner DB. 2007. The dynamic flexion/extension properties of the lumbar spine in vitro using a novel pendulum system. Journal of Biomechanics 40:2767-2773.

9. Daniels AH, Paller DJ, Koruprolu S, Palumbo MA, Crisco JJ. 2013. Dynamic Biomechanical Examination of the Lumbar Spine with Implanted Total Spinal Segment Replacement (TSSR) Utilizing a Pendulum Testing System. Plos one 8:e57412.

10. Dowthwaite JN, Rosenbaum PF, Scerpella TA. 2011. Mechanical loading during growth is associated with plane-specific differences in vertebral geometry: A cross-sectional analysis comparing artistic gymnasts vs. non-gymnasts. Bone 49:1046-1054.

11. Eijkelkamp MF. 2002. On the Development of an Artificial Intervertebral Disc: University Library Groningen.

12. Faiz O, Moffat DB. 2002. Anatomy at a glance: Blackwell Science.

13. Friess W. 1998. Collagen--biomaterial for drug delivery. European Journal of Pharmaceutics and Biopharmaceutics 45:113-136.

14. Frobin W, Brinckmann P, Biggemann M, Tillotson M, Burton K. 1997. Precision measurement of disc height, vertebral height and sagittal plane displacement from lateral radiographic views of the lumbar spine. Clinical Biomechanics 12, Supplement 1:S1-S63.

15. Fujiwara A, An HS, Lim T-H, Haughton VM. 2001. Morphologic Changes in the Lumbar Intervertebral Foramen Due to Flexion-Extension, Lateral Bending, and Axial Rotation: An In Vitro Anatomic and Biomechanical Study. Spine 26:876-882.

16. Gormley J, Hussey J. 2005. Exercise Therapy: Prevention and Treatment of Disease: Wiley.

17. Grant JP, Oxland TR, Dvorak MF. 2001. Mapping the Structural Properties of the Lumbosacral Vertebral Endplates. Spine 26:889-896.

18. Grant JP, Oxland TR, Dvorak MF, Fisher CG. 2002. The effects of bone density and disc degeneration on the structural property distributions in the lower lumbar vertebral endplates. Journal of Orthopaedic Research 20:1115-1120.

19. Gruber HE, Hanley EN, Jr. 2002. Ultrastructure of the human intervertebral disc during aging and degeneration: comparison of surgical and control specimens. Spine 27:798-805.

20. Guerin HA, Elliott DM. 2006. Degeneration affects the fiber reorientation of human annulus fibrosus under tensile load. Journal of Biomechanics 39:1410-1418.

21. Hardman AE, Stensel DJ. 2009. Physical Activity and Health: The Evidence Explained: Routledge Chapman & Hall.

22. Harrison DE, Harrison DD, Cailliet R, Troyanovich SJ, Janik TJ, Holland B. 2000. Cobb method or Harrison posterior tangent method: which to choose for lateral cervical radiographic analysis. Spine 25:2072-2078.

23. Hauerstock D. 2000. Telemetric Measurement of Compressive Loads in the Sheep Lumbar Spine: McGill University.

24. Haughton V. 2004. Medical imaging of intervertebral disc degeneration: current status of imaging. Spine 29:2751-2756.

25. Houwen EB, Baron P, Veldhuizen AG, Burgerhof JGM, Ooijen PMA, Verkerke GJ. 2010. Geometry of the Intervertebral Volume and Vertebral Endplates of the Human Spine. Annals of Biomedical Engineering 38:33-40.

26. Keller TS, Colloca CJ, Harrison DE, Harrison DD, Janik TJ. 2005. Influence of spine morphology on intervertebral disc loads and stresses in asymptomatic adults: implications for the ideal spine. The Spine Journal 5:297-309.

27. Keller TS, Harrison DE, Colloca CJ, Harrison DD, Janik TJ. 2003. Prediction of osteoporotic spinal deformity. Spine 28:455-462.

28. Keller TS, Nathan M. 1999. Height Change Caused by Creep in Intervertebral Discs: A Sagittal Plane Model. Journal of Spinal Disorders 12:313-324.

29. Kjær M, Krogsgaard M, Magnusson P, Engebretsen L, Roos H, Takala T, Woo SL-Y. 2003. Textbook of Sports Medicine: Basic Science and Clinical Aspects of Sports Injury and Physical Activity. In: Blackwell Science.

30. Krag MH, Seroussi RE, Wilder DG, Pope MH. 1987. Internal displacement distribution from in vitro loading of human thoracic and lumbar spinal motion segments: experimental results and theoretical predictions. Spine 12:1001-1007.

31. Kurtz SM, Edidin A. 2006. Spine Technology Handbook: Elsevier Science.

32. Lee CK. 2003. Intervertebral Disk and Nucleus Prosthesis. In. USA.

33. McLain RF, Ferrara L, Kabins M. 2002. Pedicle Morphometry in the Upper Thoracic Spine: Limits to Safe Screw Placement in Older Patients. Spine 27:2467-2471.

34. Mizuno H, Roy AK, Vacanti CA, Kojima K, Ueda M, Bonassar LJ. 2004. Tissue-engineered composites of anulus fibrosus and nucleus pulposus for intervertebral disc replacement. Spine 29:1290-1297.

35. Mizuno H, Roy AK, Zaporojan V, Vacanti CA, Ueda M, Bonassar LJ. 2006. Biomechanical and biochemical characterization of composite tissue-engineered intervertebral discs. Biomaterials 27:362-370.

36. Panjabi MM, Duranceau J, Goel V, Oxland T, Takata K. 1991a. Cervical Human Vertebrae: Quantitative Three-Dimensional Anatomy of the Middle and Lower Regions. Spine 16:861-869.

37. Panjabi MM, Goel V, Oxland T, Takata K, Duranceau J, Krag M, Prize M. 1992. Human lumbar vertebrae—quantitative three-dimensional anatomy. Spine 17:299-306.

38. Panjabi MM, Takata K, Goel V, Federico D, Oxland T, Duranceau J, Krag M. 1991b. Thoracic human vertebrae: Quantitative three-dimensional anatomy. Spine 16:888-901.

39. Pećina M, Bojanić I. 2004. Overuse Injuries of the Musculoskeletal System: CRC Press.

40. Petit B, Masuda K, D'Souza AL, Otten L, Pietryla D, Hartmann DJ, Morris NP, Uebelhart D, Schmid TM, Thonar EJ. 1996. Characterization of crosslinked collagens synthesized by mature articular chondrocytes cultured in alginate beads: comparison of two distinct matrix compartments. Experimental Cell Research 225:151-161.

41. Roux J-P, Wegrzyn J, Arlot ME, Guyen O, Delmas PD, Chapurlat R, Bouxsein ML. 2010. Contribution of Trabecular and Cortical Components to Biomechanical Behavior of Human Vertebrae: An Ex Vivo Study. Journal of Bone and Mineral Research 25:356-361.

42. Seroussi RE, Krag MH, Muller DL, Pope MH. 1989. Internal deformations of intact and denucleated human lumbar discs subjected to compression, flexion, and extension loads. Journal of Orthopaedic Research 7:122-131.

43. Shankar H, Scarlett JA, Abram SE. 2009. Anatomy and pathophysiology of intervertebral disc disease. Techniques in Regional Anesthesia and Pain Management 13:67-75.

44. Schmidt H, Shirazi-Adl A, Galbusera F, Wilke H-J. 2010. Response analysis of the lumbar spine during regular daily activities—A finite element analysis. Journal of biomechanics 43:1849-56.

45. Singh K, Masuda K, Thonar EJ, An HS, Cs-Szabo G. 2009. Age-related changes in the extracellular matrix of nucleus pulposus and anulus fibrosus of human intervertebral disc. Spine 34:10-16.

46. Stokes IA, Gardner-Morse M, Churchill D, Laible JP. 2002. Measurement of a spinal motion segment stiffness matrix. Journal of biomechanics 35:517-521.

47. Tan SH, Teo EC, Chua HC. 2004. Quantitative three-dimensional anatomy of cervical, thoracic and lumbar vertebrae of Chinese Singaporeans. European Spine Journal 13:137-146.

48. Tanaka N, An HS, Lim T-H, Fujiwara A, Jeon C-H, Haughton VM. 2001. The relationship between disc degeneration and flexibility of the lumbar spine. The Spine Journal 1:47-56.

49. Thompson JP, Pearce RH, Schechter MT, Adams ME, Tsang IKY, Bishop PB. 1990. Preliminary Evaluation of a Scheme for Grading the Gross Morphology of the Human Intervertebral Disc. Spine 15:411-415.

50. Tsantrizos A, Ito K, Aebi M, Steffen T. 2005. Internal Strains in Healthy and Degenerated Lumbar Intervertebral Discs. Spine 30:2129-2137.

51. Zhang Z, Chan Q, Anthony M-P, Samartzis D, Cheung KMC, Khong P-L, Kim M. 2012. Age-related diffusion patterns in human lumbar intervertebral discs: a pilot study in asymptomatic subjects. Magnetic Resonance Imaging 30:181-188.

52. Zindrick MR, Wiltse LL, Doornik A, Widell EH, Knight GW, Patwardhan AG, Thomas JC, Rothman SL, Fields BT. 1987. Analysis of the Morphometric Characteristics of the Thoracic and Lumbar Pedicles. Spine 12:160-166.

Internet sources:

http. 1.   Handout on Health: Back Pain. Available on-line from
            http://www.niams.nih.gov/Health_Info/Back_Pain/default.asp (accessed
            01/08/13)

http. 2.   Fourier Transform. Available on-line from
            http://homepages.inf.ed.ac.uk/rbf/HIPR2/fourier.htm (accessed 28/07/13)

http. 3.   Flexuspine® Available on-line from
            http://www.flexuspine.com/functional, (accessed 22/07/13)

http. 4.   A Guide to Writing the Dissertation Literature Review. Available on-line
            from http://pareonline.net/pdf/v14n13.pdf (accessed 29 July 2013)

LIST OF ABBREVIATIONS

2-D	two-dimensional
3-D	three-dimensional
6-DOF	six degrees of freedom
AF	annulus fibrosus
AID	artificial intervertebral disc
CT	computed tomography
FE	finite element
FSU	functional spinal unit
i-AF	inner annulus fibrosus
IVD	intervertebral disc
MR	magnetic resonance
MRI	magnetic resonance imaging
NP	nucleus pulposus
o-AF	outer annulus fibrosus
PMMA	polymethylmethacrylate
TSSR	Total spine segment replacement
WA	wedge angle